

# GEMS & GEMOLOGY

WINTER 2013  
VOLUME XLIX

THE QUARTERLY JOURNAL OF THE GEMOLOGICAL INSTITUTE OF AMERICA



Advances in Understanding the  
Geology of Diamonds

Sapphire from Mogok, Myanmar

Gemstone Mining in Vietnam



pg. 195



pg. 223



pg. 239

## EDITORIAL

### 187 Looking Ahead to 2014

*Duncan Pay*

## FEATURE ARTICLES

### 188 Recent Advances in Understanding the Geology of Diamonds

*Steven B. Shirey and James E. Shigley*

Examines the last two decades' advances in analyzing and understanding the formation of natural diamonds, and their relation to the earth's formation.

### 223 Blue Sapphires from the Baw Mar Mine in Mogok

*Hpone-Phyo Kan-Nyunt, Stefanos Karampelas, Klemens Link, Kyaw Thu, Lore Kiefert, and Pierre Hardy*

Reports on the microscopic, chemical, and spectroscopic features that differentiate the high-quality Baw Mar sapphire from "classic" gem-quality Burmese sapphire.

### 233 Update on Gemstone Mining in Luc Yen, Vietnam

*Pham Van Long, Vincent Pardieu, and Gaston Giuliani*

Explores the emergence of the Luc Yen area as a producer of corundum, spinel, tourmaline, and other colored stones.

## NOTES AND NEW TECHNIQUES

### 246 Characteristics of Coated Jadeite Jade

*Jian Zhang, Taijin Lu, and Hua Chen*

Analyzes the effects of coating on green jadeite specimens using DiamondView imaging, microscopy, spectroscopy, and Raman spectrophotometry.



pg. 258

## REGULAR FEATURES

### 252 Lab Notes

Black diamond with unusual color origin • Silicon in natural type IIa and type IaB diamond • Stellate inclusions in vivid pink morganite • Spinel submitted as diamond • Large synthetic moissanite with silicon carbide polytypes

### 257 Gem News International

Demantoid garnet fossil pseudomorphs • "Gran Dama" brooch featuring large Melo pearl • Greenish blue spodumene • Bright yellow diamonds from Sierra Leone • Scheelite and hübnerite inclusions in quartz from China • Faceted wurtzite from Tanzania • Composite amber with an unusual structure • Conference report

## Editorial Staff

### Editor-in-Chief

Duncan Pay  
dpay@gia.edu

### Managing Editor

Justin Hunter  
justin.hunter@gia.edu

### Editor

Stuart D. Overlin  
soverlin@gia.edu

### Technical Editors

Tao Z. Hsu  
tao.hsu@gia.edu

Jennifer Stone-Sundberg

### Associate Editor

Jennifer-Lynn Archuleta  
jennifer.archuleta@gia.edu

## Production Staff

### Creative Director

Faizah Bhatti

### Image Specialist

Chris Cruz

### Illustrators

Peter Johnston  
Larry Lavitt

### Photographer

Robert Weldon

## Editorial Review Board

Ahmadjan Abduriyim  
Tokyo, Japan

Shigeru Akamatsu  
Tokyo, Japan

Edward W. Boehm  
Chattanooga, Tennessee

James E. Butler  
Washington, DC

Alan T. Collins  
London, UK

John L. Emmett  
Brush Prairie, Washington

Emmanuel Fritsch  
Nantes, France

Eloïse Gaillou  
Los Angeles, California

Jaroslav Hyršl  
Prague, Czech Republic

A.J.A. (Bram) Janse  
Perth, Australia

E. Alan Jobbins  
Caterham, UK

Mary L. Johnson  
San Diego, California

Anthony R. Kampf  
Los Angeles, California

Robert E. Kane  
Helena, Montana

Lore Kiefert  
Lucerne, Switzerland

Thomas M. Moses  
New York, New York

Mark Newton  
Coventry, UK

Nathan Renfro  
Carlsbad, California

George R. Rossman  
Pasadena, California

Kenneth Scarratt  
Bangkok, Thailand

Andy Shen  
Wuhan, China

Guanghai Shi  
Beijing, China

James E. Shigley  
Carlsbad, California

Wuyi Wang  
New York, New York

Christopher M. Welbourn  
Reading, UK

# GEMS & GEMOLOGY®

gia.edu/gems-gemology

### Subscriptions

Copies of the current issue may be purchased for \$29.95 plus shipping. Subscriptions are \$79.99 for one year (4 issues) in the U.S. and \$99.99 elsewhere. Canadian subscribers should add GST. Discounts are available for group subscriptions, GIA alumni, and current GIA students. For institutional rates, contact Customer Service.

To purchase print subscriptions, visit [store.gia.edu](http://store.gia.edu) or contact Customer Service.

### Database Coverage

*Gems & Gemology* is abstracted in Thomson Reuters products (Current Contents: Physical, Chemical & Earth Sciences and Science Citation Index—Expanded, including the Web of Knowledge) and other databases. For a complete list of sources abstracting *G&G*, go to [gia.edu/gems-gemology](http://gia.edu/gems-gemology).

### Manuscript Submissions

*Gems & Gemology* welcomes the submission of articles on all aspects of the field. Please see the Guidelines for Authors at [gia.edu/gandg](http://gia.edu/gandg) or contact the Managing Editor. Letters on articles published in *Gems & Gemology* are also welcome.

### Copyright and Reprint Permission

Abstracting is permitted with credit to the source. Libraries are permitted to photocopy beyond the limits of U.S. copyright law for private use of patrons. Instructors are permitted to photocopy isolated articles for noncommercial classroom use without fee. Copying of the photographs by any means other than traditional photocopying techniques (Xerox, etc.) is prohibited without the express permission of the photographer (where listed) or author of the article in which the photo appears (where no photographer is listed). For other copying, reprint, or republication permission, please contact the Managing Editor.

*Gems & Gemology* is published quarterly by the Gemological Institute of America, a nonprofit educational organization for the gem and jewelry industry.

Postmaster: Return undeliverable copies of *Gems & Gemology* to GIA, The Robert Mouawad Campus, 5345 Armada Drive, Carlsbad, CA 92008.

Our Canadian goods and service registration number is 126142892RT.

Any opinions expressed in signed articles are understood to be opinions of the authors and not of the publisher.

## About the Cover

The lead article in this issue discusses our evolving understanding of the geology of diamonds. The cover image, of diamond crystal in kimberlite matrix, was chosen to highlight the relevance of this gem material as part of the earth's makeup. The combined weight of the piece, retrieved from South Africa, is 314.47 carats. This specimen is part of the Oppenheimer Student Collection at the GIA Museum in Carlsbad. Photo by Robert Weldon.

Printing is by L+L Printers, Carlsbad, CA.

GIA World Headquarters The Robert Mouawad Campus 5345 Armada Drive Carlsbad, CA 92008 USA

© 2013 Gemological Institute of America

All rights reserved.

ISSN 0016-626X



## Looking Ahead to 2014



Welcome to the Winter 2013 *Gems & Gemology*. In this issue, we're privileged to present a significant paper reviewing the current state of knowledge about diamond geology. The article's lead author is Dr. Steven B. Shirey, a noted isotope geochemist from the Carnegie Institution of Washington and a leader in the field of inclusion-dating techniques as applied to diamond. Recent research in this area has helped date the oldest known diamonds back to 3.5 billion years—more than three-quarters the age of the earth. This article, which updates the landmark Spring 1991 *G&G* paper on the same topics by Melissa Kirkley et al., is co-authored by GIA's Dr. Jim Shigley.

We hope this is the first of many articles chronicling the new frontiers of diamond research from Carnegie's scientists. In the near future, we look to forge other active collaborations with institutions and researchers working in gem-related fields.

The Winter issue also includes excellent papers on blue sapphires from the Baw Mar area in Mogok, Myanmar; an update on gemstone mining in Luc Yen, Vietnam; and the characteristics of coated jadeite jade.

As always, we would be delighted to hear from our readers on any of the papers in this issue, or previous 2013 issues.

Now that we are on the cusp of *G&G*'s 80th anniversary in 2014, this is a fitting time to review some of the innovations we've brought to our readers during 2013.

*We look to forge more active collaboration with institutions and researchers working in gem-related fields...*

In April, we launched the Research & News section of the new GIA website and made every issue of *G&G*, from the current issue back to the journal's launch in 1934, free to all users as PDF downloads at <http://www.gia.edu/gems-gemology>.

In the Fall issue, we introduced a new *G&G* article category: the field report. In upcoming issues, we aim to bring our readers more of these "direct from the mine" articles, particularly from GIA's dedicated field gemologists, Vincent Pardieu and Andy Lucas.

With *G&G* now at the center of GIA's Research & News portal, we have the opportunity to complement our articles with supporting media. In our Fall issue, we supplemented the Cheapside Hoard and Oregon sunstone papers with video interviews, image slideshows, and additional articles. This is a trend we intend to expand on in 2014. In this issue, in fact, you'll notice a QR (quick response) code at the end of our lead article on diamond geology. This takes users with enabled smartphones and tablets directly to videos and related online content.

We also started integrating *G&G* into GIA's gemology curriculum, beginning with the Diamonds & Diamond Grading course. Students can now directly access and download relevant articles via links from their eLearning course assignments. In 2014, we will extend this initiative to the remaining gemology courses.

May I take this opportunity to wish all our contributors, subscribers, reviewers, and online readers the very best for 2014.



Duncan Pay | Editor-in-Chief | [dpay@gia.edu](mailto:dpay@gia.edu)

# RECENT ADVANCES IN UNDERSTANDING THE GEOLOGY OF DIAMONDS

Steven B. Shirey and James E. Shigley

It has been more than two decades since diamond ages have proven to be up to billions of years older than their host magmas of kimberlite or lamproite. Since then, there have been significant advances in the analysis of diamonds and their mineral inclusions, in the understanding of diamond-forming fluids in the mantle, and in the relationship of diamonds to the deep geology of the continents and the connecting mantle. The occurrence of natural diamonds is remarkable and important to earth studies. This article reviews current thinking of where, how, when, and why natural diamonds form.

Research into natural diamonds (figure 1) has emerged over the last two decades as one of the keys to understanding the deep earth. Analytical advances, improved geologic knowledge, and the emergence of new diamond-producing regions (such as the Slave craton of Canada) have all contributed to this change. The most prized specimens for research are flawed with visible inclusions (figure 2), for these carry actual samples of mantle minerals from depths as great as 800 km beneath the surface. Diamond provides the perfect container for mantle minerals, isolating them from the high pressure and temperature reactions within the earth for geologic time scales. Even low elemental concentrations and minute features in diamond can now be analyzed using instruments with higher sensitivity and resolution. As a result, study combining the inclusion and its diamond host is a powerful tool for geologic research, which itself has improved our understanding of diamond formation.

The purpose of this article is to describe our current understanding of where, how, when, and why natural diamonds have been formed. This article reviews currently accepted areas of knowledge, along with topics that are still the subject of ongoing research, where science does not yet have all the an-

swers. This basic subject was discussed more than two decades ago in *Gems & Gemology* (Kirkley et al., 1991); since then, there have been major advances in our understanding of diamond geology. Recent work of the research community (summarized in Pearson and Shirey, 1999; Cartigny, 2005; Harlow and Davies, 2005; Stachel et al., 2005, 2009; Stachel and Harris, 2008, 2009; Gurney et al., 2010; Shirey et al., 2013) has been of considerable interest to economic geologists searching for natural diamonds,

*Figure 1. Archean cratons in South Africa have yielded gem diamonds such as these specimens from the GIA Museum's Oppenheimer Student Collection. The loose crystals range from 1.24 to 22.32 ct. Photo by Orasa Weldon.*



See end of article for About the Authors and Acknowledgments.

GEMS & GEMOLOGY, Vol. 49, No. 4, pp. 188–222,  
<http://dx.doi.org/10.5741/GEMS.49.4.188>.

© 2013 Gemological Institute of America

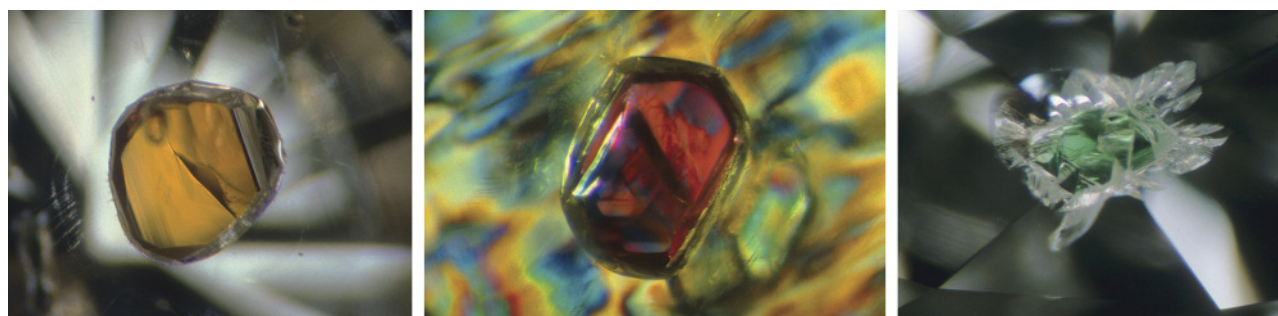


Figure 2. These photos show inclusions of silicate minerals in natural diamond whose background reflectivity has been enhanced by faceting: almandine (left), magnified 10 $\times$ ; pyrope (center), magnified 40 $\times$ ; and diopside (right), magnified 30 $\times$ . Photomicrographs by John Koivula.

guiding their models of how to explore for new occurrences. But it is also of importance to the practicing gemologist, since these are fundamental questions that a wearer of a beautiful diamond might ask. It is hoped that this article will give the gemologist a ready way to convey how nature first created the rough diamonds.

For the reader who is unfamiliar with geologic terms, a glossary is presented at the end of the article. Terms listed in the glossary are italicized on their first use in the text.

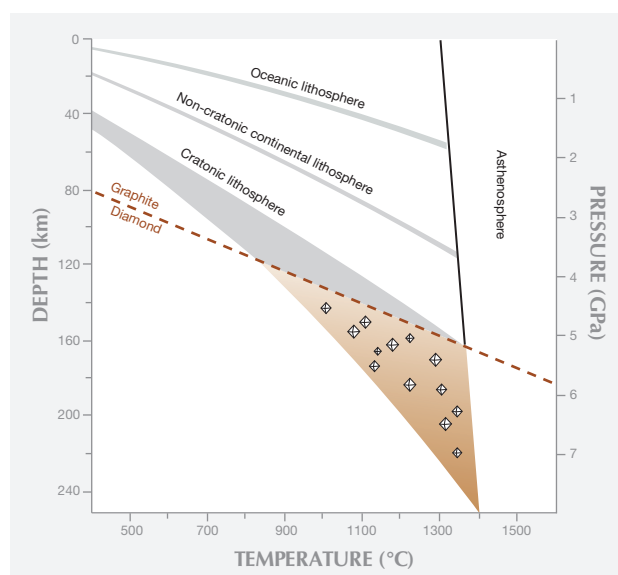
## GEOLOGY AND THE DISTRIBUTION OF DIAMONDS ON EARTH

**Carbon Abundance.** Carbon is widely dissolved in the earth's silicate minerals at part-per-million levels and lower. But whenever carbon occurs as a free species, diamonds have the potential to form. Carbon in the earth can occur in oxidized forms, such as when bound with oxygen in CO<sub>2</sub> or CO<sub>3</sub>, or in reduced forms such as diamond, graphite, or bound with hydrogen in methane and other organic molecules. The experimentally determined pressure-temperature conditions where diamond is stable (figure 3) dictate formation pressures higher than 40 thousand atmospheres (4 GPa) and temperatures of 950–1400°C. While these pressure-temperature conditions seem extreme, for a large rocky planet such as ours, they are not. Within the earth, temperature always rises with depth along a path known as the *geothermal gradient*, which is typically high enough for diamond growth at the necessary pressures. Thus, diamond can potentially form in any region of the earth where the depth of the *crust* or the *mantle* provides high enough pressure, because the temperature will also be high enough.

Most of the mantle is within the field of diamond stability. The crust, which is normally too thin (usually less than 40 km thick) to lie within this field,

can do so only if it has been thickened by the geologic processes related to *plate tectonics*. Yet diamonds are very rare because the mantle has a relatively low abundance of carbon. Furthermore, diamonds are far from evenly distributed throughout the earth—they are found in mineable quantities only in very unique geologic settings. Why is this so?

Figure 3. This graph depicts the rise of temperature with depth (the geothermal gradient) in the lithosphere. Diamonds are stable under the high pressure and temperature conditions that are only met at great depth in the earth's mantle. This phase diagram depicts the stability fields of graphite and diamond in relation to the convecting mantle (asthenosphere) and the lithospheric mantle. The graphite/diamond transition was recently revised to lower pressures (Day, 2012), providing for even greater storage of diamonds at shallower levels in the cratonic keel. Note that only the cratonic lithospheric keel is cold enough at high enough pressures to retain diamonds. Adapted from Tappert and Tappert (2011).



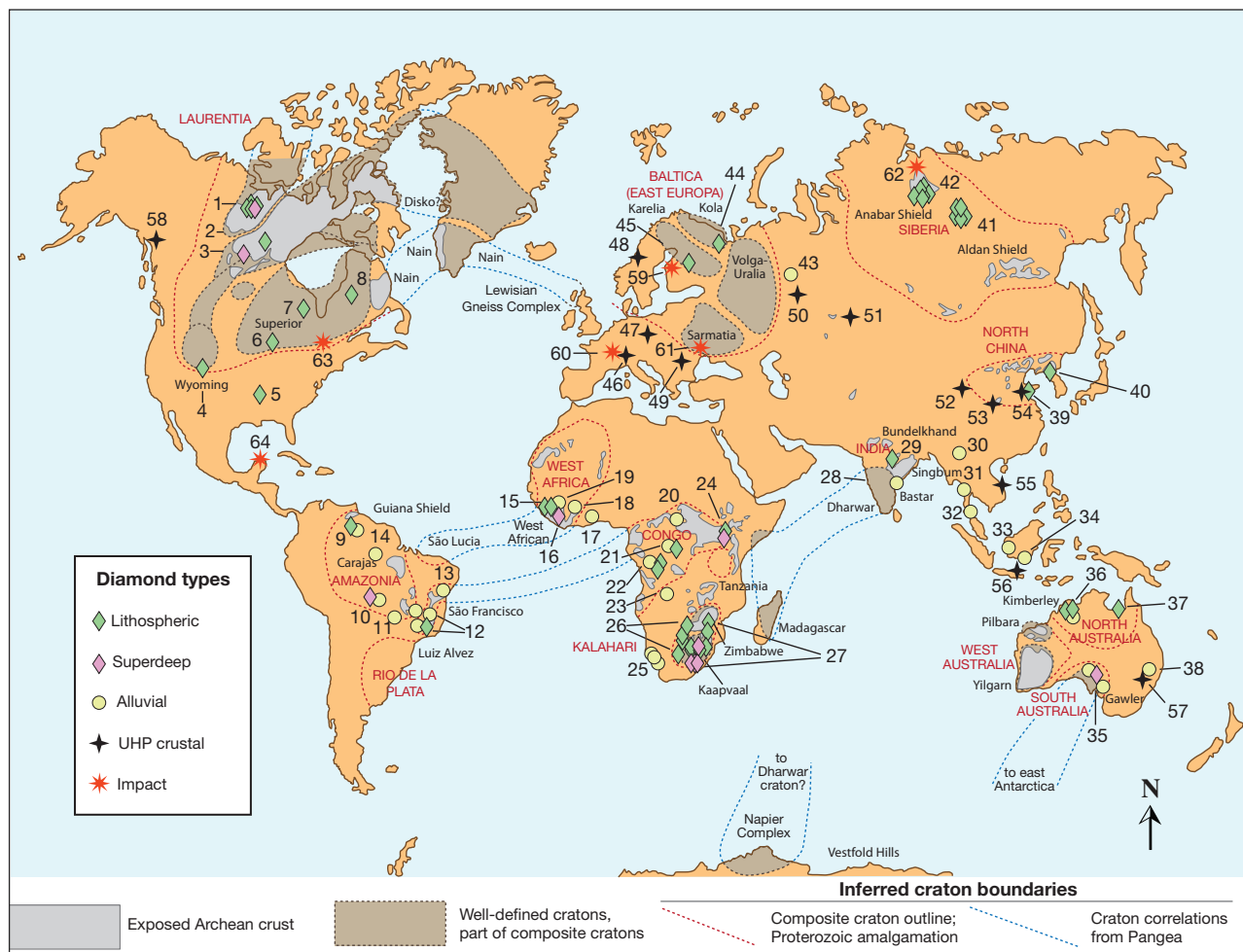


Figure 4. World diamond localities are shown here in relation to Archean cratons and classified as either kimberlite-hosted and from mantle keels (lithospheric), kimberlite-hosted and from the convecting mantle (superdeep), of surface origin (alluvial), from ultra-high-pressure crustal terranes (UHP crustal), or formed by the shock of meteorite impact (impact). Only a subset of these localities are rich enough to be mined for diamonds. The crustal age/craton basemap is from Pearson and Wittig (2008). Locality information is from Tappert et al. (2009), Harte (2010), Harte and Richardson (2011), Tappert and Tappert (2011), Dobrzhinetskaya (2012), and the authors.

Localities are as follows: (1) Diavik, Ekati, Snap Lake, Jericho, Gahcho Kue, DO-27; (2) Fort a la Corne; (3) Buffalo Hills; (4) State Line; (5) Prairie Creek; (6) Wawa; (7) Victor; (8) Renard; (9) Guaniamo; (10) Juina/Sao Luis; (11) Annapolis; (12) Coromandel, Abaete, Canasta; (13) Chapada Diamantina; (14) Boa Vista; (15) Koidu; (16) Kan Kan; (17) Akwatia; (18) Tortiya; (19) Aredor; (20) Bangui; (21) Mbuiji-Mayi; (22) Camafuca, Cuango, Catoca; (23) Masvingo; (24) Mwadui; (25) Luderitz, Oranjemund, Namaqualand; (26) Orapa/Damtshaa, Letlhakane, Jwaneng, Finsch; (27) Murowa, Venetia, The Oaks, Marsfontein, Premier, Dokolwayo, Roberts Victor, Letseng-la-Terae, Jagersfontein, Koffiefontein, Monastery, Kimberley (Bultfontein, Kimberley, De Beers, Dutoitspan, Kamfersdam, Wesselton); (28) Kollur; (29) Majhgawan/Panna; (30) Momeik; (31) Theindaw; (32) Phuket; (33) West Kalimantan; (34) South Kalimantan; (35) Springfield Basin, Eurelia/Orroroo, Echunga; (36) Argyle, Ellendale, Bow River; (37) Merlin; (38) Copetown/Bingara; (39) Mengyin; (40) Fuxian; (41) Mir, 23rd Party Congress, Dachnaya, Internatsionalskaya, Nyurbinskaya; (42) Aykhal, Yubileynaya, Udachnaya, Zarnitsa, Sytykansskaya, Komsomolskaya; (43) Ural Mts.; (44) Arkhangelsk; (45) Kaavi-Kuopio; (46) W Alps; (47) Moldanubian; (48) Norway; (49) Rhodope; (50) Urals; (51) Kokchetav; (52) Qinling; (53) Dabie; (54) Sulu; (55) Kontum; (56) Java; (57) New England Fold Belt; (58) Canadian Cordillera; (59) Lappajärvi; (60) Ries; (61) Zapadnaya; (62) Popigai; (63) Sudbury; and (64) Chixculub. Adapted from Shirey et al. (2013), with permission of the Mineralogical Society of America.

**Geologic Age of Continental Rocks.** Earth is special among the planets in that it has two crustal types,

continental and oceanic, that sit at two very different heights, approximately 840 meters above and

3,840 meters below sea level on average. This happens because the *continental crust* contains more of the lighter elements such as silicon and aluminum, and is underlain by a thickened *mantle keel* (described below), while the *oceanic crust* is composed of heavier elements such as iron and calcium and is not underlain by a thickened mantle keel. The continental crust is old—up to four billion years old. Its oldest parts, the ancient continental nuclei, or *cratons*, are isolated in the interior of the continent by belts of successively younger continental crust (figure 4). By comparison, oceanic crust is much younger and progresses regularly in age from zero (formation today) to the oldest known ocean floor, which is about 0.2 billion years old. This basic age distribution of rocks at the earth's surface (Hurley and Rand, 1969) became widely known within five years of the acceptance of plate tectonics theory in the mid-1960s, as naturally decaying radioactive elements (uranium, thorium, and rubidium) provided a quantitative way to measure the geologic age of exposed crustal rocks.

**Plate Tectonics and Diamonds.** Plate tectonics is the modern unifying theory that explains the earth's active geologic processes today, and is thought to have operated perhaps for as long as the latter half of the planet's history. No other planets in the solar system apparently have plate tectonics. The earth's upper surface is composed of rigid, lithospheric plates of crustal rock (too stiff to flow on geologic time scales, yet stiff enough to break and cause earthquakes) underlain by mantle rock. Surface deformation, volcanic activity, and earthquakes occur more readily at the margins of plates than at their interior. Two general types of *lithosphere* can occur on the same plate: continental and oceanic. Continental lithosphere is thickest where it is oldest. It can be more than twice the thickness of oceanic lithosphere, which is geologically younger. The latter is constantly being created at *mid-ocean ridges* where seafloor spreading occurs, and where oceanic crust is recycled back into the mantle by the process of *subduction*. The movement of the plates occurs on the mobile portion of the mantle known as the *asthenosphere*, and it is driven by deeper flow of the mantle, a process known as convection. The power for convection comes from the sinking of the oceanic lithospheric plates, the heat generated in the mantle by *radioactive decay*, and the return flow of warmer mantle. Plate tectonics is critical to diamond formation in two ways: It permits the recycling of surficial carbon, and it en-

ables mantle melting, both of which allow the creation of diamond-forming fluids/melts.

Continental regions that long ago ceased participating in active plate tectonic processes such as *rifting*, *mountain building*, or subduction are known as continental cratons. They are easily defined by an absence of earthquake activity. Such regions have been leveled by long-term weathering and erosion, though they may be relatively recently *uplifted*, as is the case for southern Africa. Most continents contain several cratons (again, see figure 4) joined by younger crust at times long after their creation. A craton always contains the oldest rocks within its host continent, and it typically has ages older than 2.5 billion years, from a geologic era known as the *Archean*. Common usage has evolved so that the term *craton* often implies the Archean portion. But strictly speaking, cra-

## In Brief

- Diamonds hold great value for understanding the earth, and knowing how they formed contributes to the discovery of new deposits.
- Diamonds contain the world's oldest and deepest mineral samples as inclusions.
- Diamonds were created by ancient processes often related to continent formation.
- Non-gem diamonds occur in a variety of geologic settings.

tons are not limited to the Archean era. Numerous younger terranes (e.g., 1 billion to 2.5 billion years old) now fit the requirement for long-term geologic stability. Thus, the plate tectonic process of continental assembly and breakup has led these younger terranes to be attached to the older cratonic core, so that they too can effectively be considered part of the craton. Both the Slave craton in Canada and the Kaapvaal craton in southern Africa are the Archean components of the larger Laurentia and Kalahari supercratons, respectively.

For economic geologists, the most important point is the striking correspondence between the oldest Archean portion of a craton and diamond occurrences, especially those hosted in *kimberlite*, the main carrier and hence "ore" of gem-quality diamond. This relationship, first formalized by Clifford (1966) and known as Clifford's Rule, implies that the diamondiferous kimberlites erupted through the oldest Archean portions of the cratons, whereas non-di-



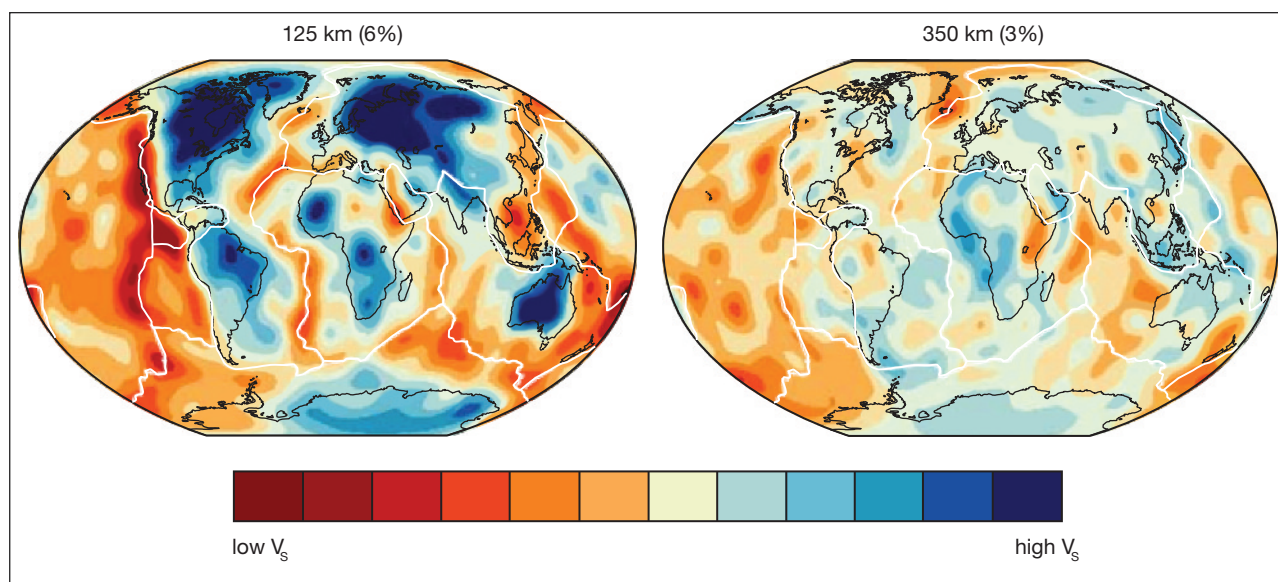


Figure 5. Seismic waves can illuminate the presence of mantle keels beneath most old continental regions (cratons). This global model of the velocity of seismic shear waves ( $V_s$ ) at 125 km depth and 350 km depth indicates a large range in shear wave velocity:  $\pm 6\%$  and  $\pm 3\%$  respectively. Note the high velocities (left) underneath the regions of ancient crust, which are not visible at 350 km depth (right). These regions have high velocity at 125 km because of a mantle keel attached down to 250 km depth, as depicted in figure 6. The blue regions indicate where lithospheric diamonds were stored for billions of years. Adapted from Ritsema et al. (2004) and Carlson et al. (2005), with permission of Wiley-Blackwell.

amondiferous kimberlites erupted through younger rocks. This relationship is nowhere more evident than the Kaapvaal craton, where all of the diamondiferous kimberlites are “on-craton” and all of the “off-craton” kimberlites are diamond-free. We will examine the geologic explanation for this below.

The erosion of ancient cratons has led to the weathering of surface exposures of kimberlite, and the release of diamonds to the *regolith*. Without crustal uplift, these diamonds remain trapped in geologic basins as in West Africa, Zimbabwe, and Brazil, where they can be panned for like gold. Where the craton has been uplifted, diamonds released from their host rocks have been transported by rivers (such as the Orange River in South Africa) and by *longshore currents* (such as the Benguela, along the continental shelf of the southern Atlantic Ocean). These *alluvial* diamonds are recovered by *placer* and marine mining techniques that are very different from hard-rock kimberlite mining. Although these specimens are found “off-craton,” they derive from “on-craton” kimberlites and are thus formed by those processes.

**Mantle Keels Under Continental Cratons.** Sitting beneath both oceanic and continental crust is rigid *peridotitic* mantle that, with the overlying crust, comprises the lithosphere. This region of rigid mantle

is known to exist because it can rupture to cause earthquakes; the resultant seismic waves travel faster through it than the convecting but still solid mantle just below. Beneath the cratons, the lithospheric mantle extends from about 40 km depth down to perhaps 250–300 km (figures 5 and 6). Under the oceans, it only extends down to about 110 km (Jordan, 1979). Because of its downward-protruding shape and its long-term attachment to the continental crust of the craton, this portion of mantle has taken the term *mantle keel*. The mantle keel is a major reason for some features we associate with continents: *tectonic stability*, elevation above the ocean floor, and the occurrence of diamonds. The kimberlite eruptions that transport diamonds to the surface also carry samples of lithospheric mantle rocks called *xenoliths*. From these samples, we know much about the mantle keel beneath the continents, such as the fact that it also contains about 5% of the high-pressure form of *basalt* known as *eclogite*. The mantle keel hosts nearly all of the world’s gem diamonds, and thus it deserves more than passing attention when considering the geologic origin of diamonds.

Naturally occurring radioactive elements present in small amounts in peridotite and eclogite allow geologists to measure the age of rock samples of the mantle keel (table 1). These include rhenium (Re), which decays over millions of years to osmium (Os),

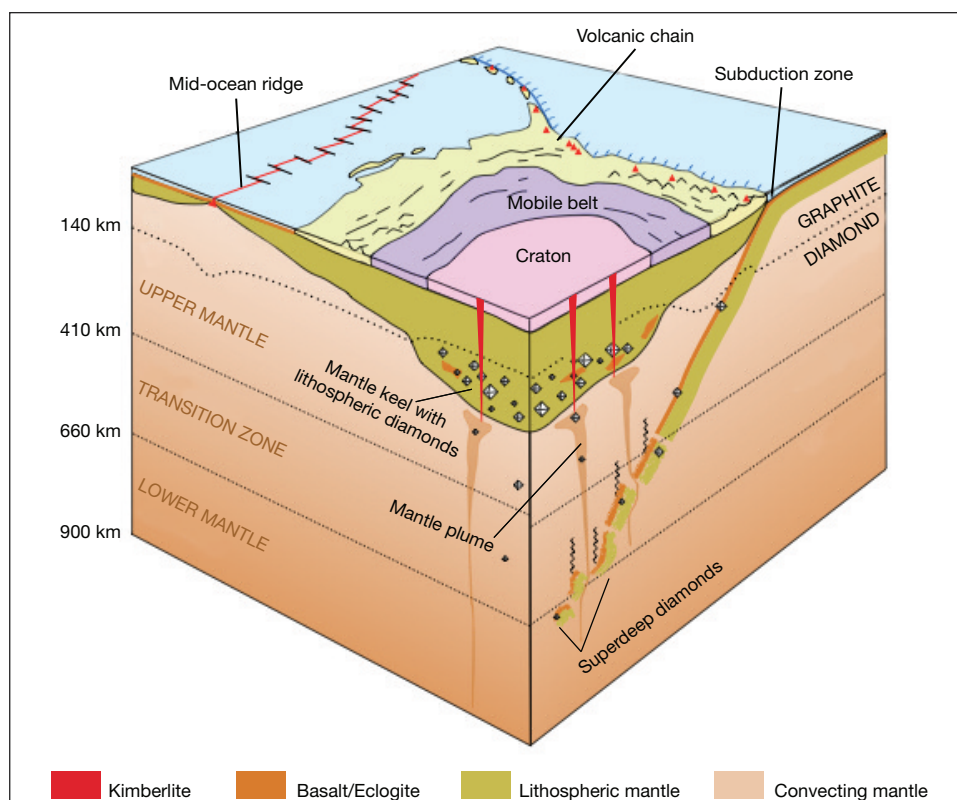


Figure 6. This block diagram depicts the basic relationship between a continental craton, its lithospheric mantle keel (the thick portion of the lithospheric mantle under the craton), and diamond stability regions in the keel and the convecting mantle. Under the right conditions of low oxidation, diamonds can form in the convecting mantle, the subducting slab, and the mantle keel. Adapted from Stachel et al. (2005), Tappert and Tappert (2011), and Shirey et al. (2013), with permission of the Mineralogical Society of America.

and samarium (Sm), which decays to neodymium (Nd). The age of the keel is the same (within uncertainties) as the geologic age of the overlying crust. Consequently, most geologists think that the crust and mantle keel of the continent were created together in a process of crust creation and craton stabilization. The duration of this process is poorly known, but may have taken many tens of millions

of years, starting with the formation of the oldest continental crust (nearly four billion years ago). The significance of this for diamond formation is that the bottom 100 km of the mantle keel under each old continental crustal region is at high enough pressure and comparatively low temperature to allow diamonds to crystallize whenever they receive fluids saturated in carbon from the underlying convecting

**TABLE 1.** Radioisotopic systems for diamond dating.

Isotope system	Parent isotope	Daughter isotope	Decay	Half-life (Ma)	Ratio measured	Inclusion minerals analyzed
Rb-Sr	$^{87}\text{Rb}$	$^{87}\text{Sr}$	$\beta$	48,800	$^{87}\text{Sr}/^{86}\text{Sr}$	Garnet, clinopyroxene
Sm-Nd	$^{147}\text{Sm}$	$^{143}\text{Nd}$	$\alpha$	106,000	$^{143}\text{Nd}/^{144}\text{Nd}$	Garnet, clinopyroxene
U-Pb	$^{238}\text{U}$ $^{235}\text{U}$	$^{206}\text{Pb}$ $^{207}\text{Pb}$	$\alpha, \beta$ $\alpha, \beta$	4,469 704	$^{206}\text{Pb}/^{204}\text{Pb}$ $^{207}\text{Pb}/^{204}\text{Pb}$	Sulfides, zircon, perovskite
Re-Os	$^{187}\text{Re}$	$^{187}\text{Os}$	$\beta$	41,600	$^{187}\text{Os}/^{188}\text{Os}$	Sulfides
Ar-Ar	$^{40}\text{K}$	$^{40}\text{Ar}$ $^{40}\text{Ca}$	$\beta$	1270	$^{40}\text{Ar}/^{39}\text{Ar}$	Clinopyroxene

Notes:  $\alpha$  = alpha decay,  $\beta$  = beta decay, and half-life is the average time taken for half of the parent radioisotope to decay. This is a constant and given here in millions of years (Ma). Note that for  $^{87}\text{Rb}$ ,  $^{147}\text{Sm}$ , and  $^{187}\text{Re}$  these times are much longer than the earth's age (~4,570 Ma).

mantle. Thus, the keel bottom can be viewed as an “ice box” (albeit with higher temperatures), available for billions of years to store diamonds and keep them from entering mantle circulation, yet ready to be sampled by a rising kimberlite *magma*. Both peridotite and eclogite contain diamonds, but intact peridotites erupted to the surface with their diamonds in place are rare, while eclogites with their diamonds in place are common. (For a detailed description of rock type, see Kirkley et al., 1991.) The mineralogical reason for this is a result of the way diamonds crystallize within the keel itself.

**Diamonds in Tectonically Active Areas.** Clifford’s Rule demonstrates the connection of the ancient stable mantle keel to gem-quality diamonds. Its corollary is that geologic activity related to plate tectonics such as volcanism, mountain-building, and intrusive magmatism near the earth’s surface typically destroys diamonds, because it occurs at pressures, temperatures, or oxidizing conditions where diamond cannot crystallize or remain stable. The typical slow mantle upwelling and resultant magmatism that occur beneath an ocean island such as Hawaii offers a good example. Nonetheless, a few exceptions to Clifford’s Rule do exist, where diamonds are found in non-kimberlitic rocks formed in tectonic areas that were once active.

A few localities are known where a non-kimberlitic, subduction-related magma type carries diamonds: young *microdiamonds* in the Japan *island arc* (Mizukami et al., 2008), and 2.7 billion-year-old *macrodiamonds* in the Wawa belt of the Superior geologic province of Canada (Stachel et al., 2006). In both cases, diamonds appear to have been created not by direct subduction magmas themselves, but rather by late-stage magmas that produced a rock called a *lamprophyre*. These magmas were intruded as *dikes* and transported diamonds to the surface that may have been created elsewhere in the mantle. At the world’s largest diamond producer by carat weight, Australia’s Argyle mine (Shigley et al., 2001), and its smaller and younger cousin, the nearby Ellendale mine, specimens were brought to the surface by another non-kimberlitic magma that produced a rock called *lamproite*. These diamonds are about 1.5 billion years old. The Australian geologic provinces in which they occur are known as *mobile belts*, which also contain metamorphic crustal rocks that are slightly older (1.8 billion years old). The *thermal pulse* revealed by the study of crustal rocks at the surface is thought to result from a tectonic process

that heated and recrystallized older lithospheric mantle while permitting the formation of diamonds at the same time (Smit et al., 2010).

More abundant than these examples are unique blocks of crustal rock known as ultra-high-pressure (UHP) metamorphic terranes. These were buried deep enough by crustal thickening, a process where portions of the crust override other portions and allow microdiamonds to crystallize, evenly distributed, throughout the buried crustal host rock with no apparent *magmatic* transport. Examples of this geologic setting occur in China, Germany, Norway, Russia, and Indonesia.

Perhaps the most prevalent example of diamonds formed by active geologic processes are those known as *superdeep* diamonds. These are usually not gem-quality macrodiamonds. Superdeep diamonds formed at great depths in freely convecting mantle beneath the continental lithosphere (again, see figure 6). They were brought up by the same kimberlitic volcanism that carried lithospheric diamonds, and therefore they are found in the same deposits. The high-pressure minerals they include show that they formed far below the 300 km approximate depths of kimberlite generation, perhaps as deep as 400–800 km (Harte, 2010). Thus, they must be carried into the depth of kimberlite generation by upwelling mantle convection in mantle *plumes*. Mantle plumes are thought to trigger kimberlite formation, because they bring hotter mantle to shallower depths where it begins to melt. Kimberlites form at the very first stages of mantle melting.

These examples of diamonds formed in actively convecting mantle are often subeconomic, lacking sufficient gem-quality stones. But they hold great scientific worth by preserving the record of dynamic geologic processes in the deep earth.

## EMPLACEMENT AND HOST ROCKS OF DIAMONDS

The kimberlitic volcanism that carried diamonds to the earth’s surface is unique and rare; in fact, no kimberlite eruption has ever been witnessed. The association of diamonds with ancient cratons makes it clear that kimberlitic volcanism occurs exclusively in these stable continental crustal environments. Because kimberlites are unknown in the oceanic mantle, the presence of mantle keels under the continents and the mechanical impediment provided by the rigid keel appears to be an important aspect of kimberlitic magma formation. The stiff lithosphere slows the rise of up-

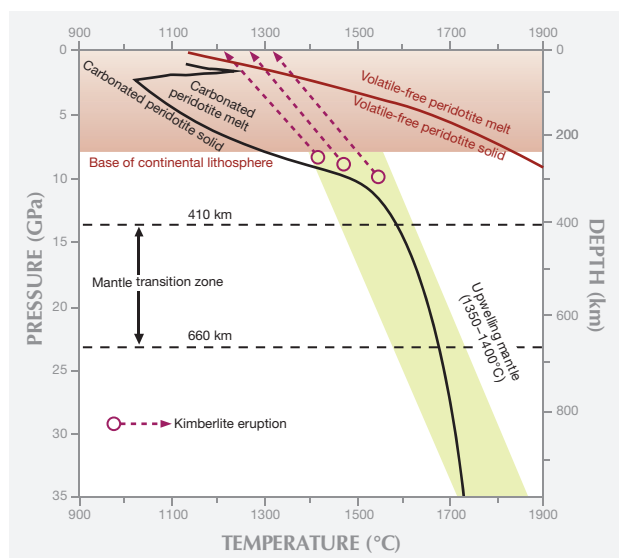


Figure 7. This pressure-temperature diagram compares the melting curve for mantle peridotite containing volatiles and carbonate (black) versus mantle peridotite that is dry and free of volatiles and carbon (red). Upwelling ambient mantle at the present day falls within the green band and may melt below 300 km. At depths shallower than 300 km, the carbonated mantle melting temperature drops drastically below 1400°C and melting occurs, producing carbonatitic liquids that will evolve to kimberlite. Note that there is just enough space below the base of the continental lithosphere for the melting to occur. Adapted from Dasgupta (2013).

welling mantle beneath it, at about the same depth where carbonate-bearing peridotite has been shown to begin to melt (figure 7). As melting begins, the first melts form in between the stiffer main silicate grains. These volatile-rich melts migrate rapidly through the silicate grains, separating a volatile-enriched kimberlite. Such an effect is missing under the oceans.

**Magma That Carry Diamonds.** Diamonds are known to be carried to the earth's surface in only three rare types of magmas: kimberlite, lamproite, and lamprophyre. Of the three types, kimberlites are by far the most important, with several hundred diamondiferous kimberlites known. Although the number of diamondiferous lamproites is much smaller, they do host the Argyle mine and notable subeconomic occurrences in the United States, India, and Australia. Lamprophyres are rarely diamondiferous; they are only of petrological interest as hosting the world's oldest erupted diamonds, which occur at Wawa in Ontario, Canada. In general, all three magma types are: (1) derived by small amounts of melting deep within the mantle; (2) relatively high

in volatile ( $H_2O$ ,  $CO_2$ , F, or Cl) contents; (3) MgO-rich; (4) marked by rapid eruption; and (5) less oxidizing than more common basaltic magma. These features work together to transport diamond crystals upward to the surface without enough resorption to dissolve them (figure 8)—something that is just not possible with other melts from the mantle, such as the far more abundant basalt and its alkalic varieties.

The classification of volcanic rocks by their textures, mineralogy, and chemical composition in a way that accounts for their genesis (Woolley et al., 1996) has historically been an inexact science. But such classification (table 2) is critical to finding and recognizing diamond-hosting rocks in the field—the essential first step to extracting gem diamonds. Kimberlites weather rapidly in the geologic sense, often forming exposures of low topographic relief, and even lakes. When exposed and fresh, they are dark bluish green to greenish gray rocks that rapidly turn brown and crumbly. Texturally, they are full of mineral grains and rock clasts ranging from the size of a watermelon down to small grain sizes that dominate the matrix (figure 9). These diamond-bearing rocks are distinguished from the related *carbonatites* by having an *igneous* carbonate mineral abundance of less than 50%. Experiments show that kimberlites and carbonatites can form a continuum in which carbonatites may beget kimberlites. Furthermore, carbonatites may be a ready source of diamond-forming fluids (e.g., Walter et al., 2008). But at the earth's surface, carbonatites are almost never diamond-bearing. The simple reason is that their carbon is locked up in the carbonate mineral calcite ( $CaCO_3$ ), which simply has too much oxygen to allow carbon to exist in the elemental form needed to stabilize diamond.

Figure 8. Comparison of natural diamond morphologies: a 15.96 ct euhedral octahedron (left) and a 4.82 ct rounded resorbed octahedron (right). Photos by Robert Weldon.



**TABLE 2.** Characteristics of known diamond-carrying magmas.

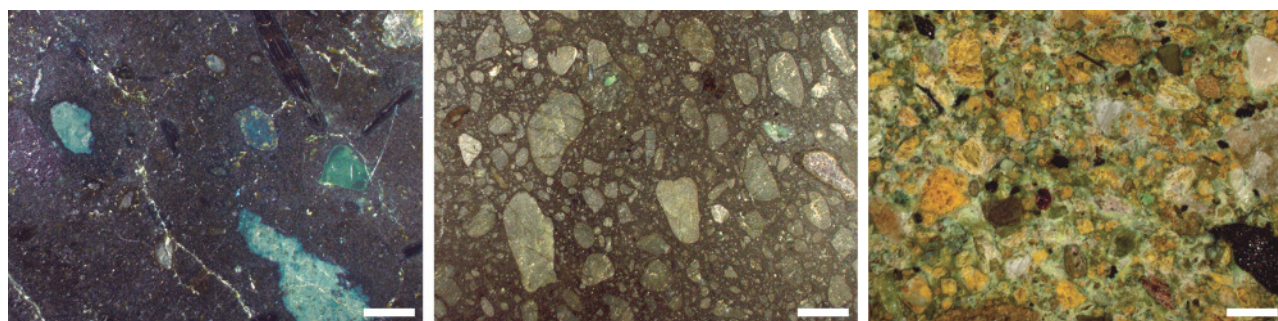
Characteristic	Kimberlite	Lamproite	Lamprophyre
Color of rock in outcrop	Green, dark bluish green	Dark gray, black	Dark gray, black
Volatiles	CO <sub>2</sub> >H <sub>2</sub> O, halogens (Cl, F)	H <sub>2</sub> O>CO <sub>2</sub> , halogens	H <sub>2</sub> O>CO <sub>2</sub> , halogens
Composition	Not peralkaline, hybrid, K <sub>2</sub> O>Na <sub>2</sub> O	Peralkaline, hybrid to magmatic	Peralkaline, magmatic
Setting	Cratonic	Mobile belt, craton margin	Subduction zone
Depth of origin	200–300 km mantle, can be sourced >400–700 km	>140 km, but probably not much deeper	>140 km, but probably not much deeper
Eruptive style	Explosive volcanic pipes, pyroclastic	Small volcanic pipes and cones	Dikes
Diagnostic phenocryst minerals	Olivine	Ti-phlogopite	Biotite, amphibole
Typical matrix mineralogy	Olivine, carbonate	Phlogopite	Feldspar
Diamond potential	Common, can range to high diamond grade	Rare, but can range to high diamond grade	Rare, few diamondiferous known

Notes: A hybrid composition is one that is substantially modified by incorporation of early-crystallizing minerals, xenoliths, and pieces of country rock so that determining a real magmatic composition is difficult; magmatic composition can be directly related to its igneous source.

These three diamond-carrying rocks all lack the minerals melilite (Ca-Na-Mg-Al-silicate) and kalsilite (KAlSiO<sub>4</sub>), whose presence would indicate a different clan of rocks (Woolley et al., 1996) that are never diamond-bearing. If the magma forms a minor-size intrusion, is not *peralkaline* (Na<sub>2</sub>O+K<sub>2</sub>O>Al<sub>2</sub>O<sub>3</sub>), and is dominated by ferro-magnesian (*mafic*) mineral *phenocrysts*—more of which are olivine compared to

lesser phenocrysts of magnesite, phlogopite, carbonate, or diopside—then the rock is a kimberlite (table 2). If these lesser phenocrysts dominate and the rock is peralkaline and contains obvious Ti-phlogopite, then it is a lamproite. If the rock is similar to a lamproite in being peralkaline but contains abundant biotite or amphibole, then it can be considered a lamprophyre. If this sounds confusing, you are not

Figure 9. These direct, incident-light photomicrographs of kimberlite slabs illustrate the variable appearance and texture of kimberlites when seen in hand specimens. Left: black, very fresh, fine-grained, massive, magmatic kimberlite with xenocrysts of ilmenite, garnet, olivine, and phlogopite (from the Monastery pipe, South Africa). Center: medium to fine-grained, dark gray to black, fresh, hypabyssal kimberlite with rounded grains of spinel, monticellite, serpentine, and carbonate (from the Grizzly pipe in the Ekati mine, Canada). Right: medium to coarse-grained, light green to buff-colored pyroclastic kimberlite composed nearly entirely of subrounded to angular xenocryst of altered olivine, garnet, and ilmenite. The sample has coarse to medium rounded peridotite, garnet peridotite, and limestone xenoliths (from the Victor North pipe, Canada). Note the progression in the three panels toward less-fresh kimberlite and toward a lower ratio of matrix to grains. Also, the left and center samples crystallized at much deeper levels in the kimberlite pipe (see figure 13), while the one on the right crystallized at the surface. Scale bar in all photos is 1 mm. Photos by Steven B. Shirey.



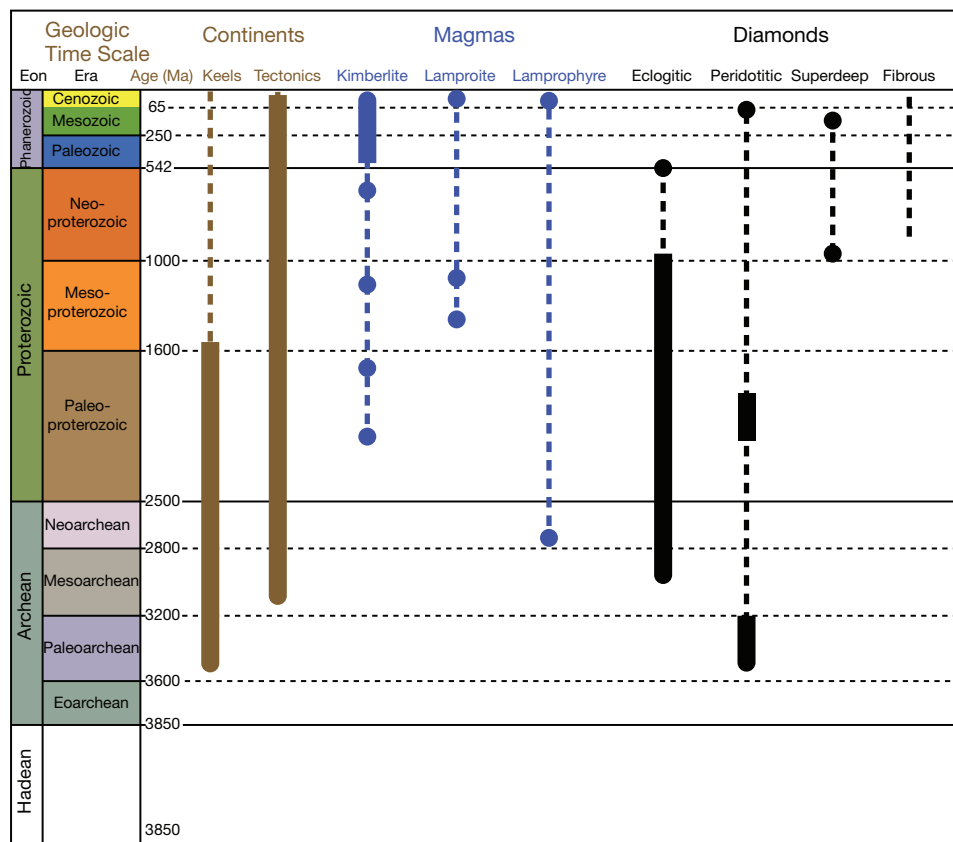


Figure 10. This diagram shows the ages of continental keels and their relationships with tectonic processes, diamond-hosting magmas, and different diamond types. Note the antiquity of mantle keels and lithospheric diamonds (>1 billion years) and the youth of most kimberlite eruptions (<550 million years). Solid vertical bars depict the duration of ongoing processes, magmas, or diamond-forming events, while solid dots indicate single known occurrences. Dashed lines connect known ages or indicate when these events might have occurred. Adapted from Gurney et al. (2010), with modifications.

alone; many papers (summarized in Woolley et al., 1996) have been written to ensure that geologists who study diamondiferous rocks use consistent criteria in the field and laboratory. The point is that volcanic rocks that carry diamonds have a specific chemical and mineral composition, and can be recognized in outcrop or drill core by their textural characteristics above (again, see figure 9). Recognizing kimberlite in the field is important because diamonds are always so scarce in kimberlite that they are never visible in outcrop. Starting with the right rock is the first step to finding diamonds.

Typically, the host rocks that carry diamonds are younger than the diamonds and the ancient continental cratons they intrude, as shown in figure 10. With only a few exceptions (Argyle, Premier, and Wawa), all known diamond-bearing kimberlites are less than about 550 Ma (million years old) and most of them less than 300 Ma, with abundant episodes of kimberlite eruption at less than 120 Ma in southern Africa and less than 80 Ma in North America. Kimberlites are very quickly weathered and eroded rocks, so quickly—years, in fact—that this degradation cannot explain the preponderance of young kimberlitic volcanism. Instead there are likely some unique changes in mantle volatiles and the relationship of plate tec-

tonic subduction to the mantle keels beneath cratons that account for this observation, but its explanation remains unknown.

**How Emplacement Occurs.** Kimberlites are difficult to interpret texturally, mineralogically, and chemically because of the high-energy mechanism of emplacement that breaks up the abundant extraneous materials they contain. Kimberlites are chaotic mixtures of xenoliths of crustal rocks and mantle, minerals released from the xenolith crumbling during eruption, phenocryst minerals, alteration minerals of these previous phases such as serpentine, and pieces of preexisting kimberlite. The texture of the host kimberlite and the relative proportions of these components (including diamonds) vary greatly with depth in the kimberlite pipe. The rock is a mixture consisting of preexisting materials and those that crystallized during the eruption. Geologists describe this as a *hybrid rock* (figure 11), which they do not consider a true representation of melt composition. Typical kimberlites and lamproites are hybrid rocks, and lamprophyres less so even though they may contain abundant xenoliths.

The volcanic emplacement of a kimberlite, though it has never actually been witnessed, is thought to be

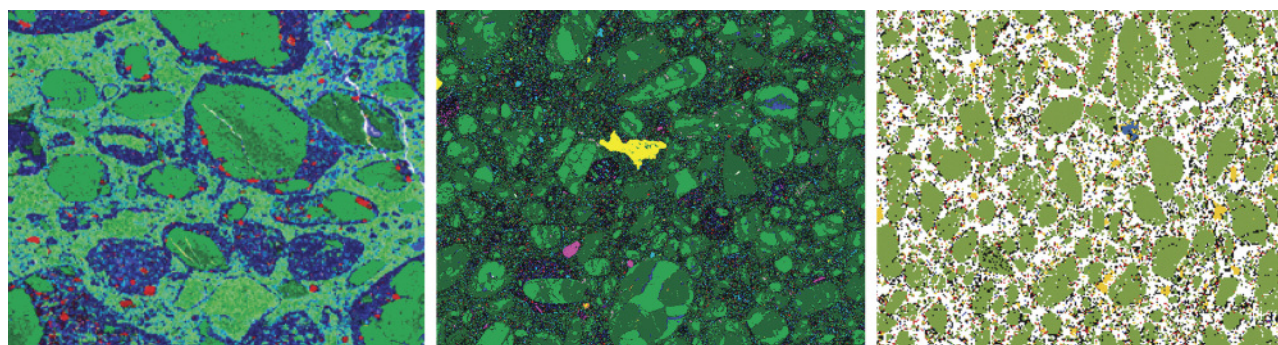


Figure 11. Kimberlites are complex mineralogically, texturally, and in their degree of alteration. These high-resolution images of the mineral composition of three different hypabyssal kimberlites (see definition in figure 13 caption) were made with a QEMScan, which uses X-rays to map the surface of thin slices of the kimberlite and can identify all minerals at all sizes in the rock. Such an unprecedented level of detail in the fine-grained matrix mineralogy will lead to a much better understanding of these important diamond host rocks. Dark green = olivine, medium green = serpentine, light green = chlorite, dark blue = pyroxene, light blue = dolomite, yellow = pyrite, red = Ti oxides, buff = phlogopite, and white = calcite. Note the variability in the alteration of the olivine, and its content in the matrix. Diamonds are too scarce to be visible in these sections. Left to right: Letseng kimberlite, Lesotho; unknown kimberlite, Alberta, Canada; Jos kimberlite, Nunavut, Canada. Scale bar in all photos is 1 mm. Left and center photos by Karin Olson; right photo adapted from Malarkey et al. (2010), with permission of Elsevier.

one of this planet's most dynamic volcanic processes. Kimberlites propagate upward through the lithosphere by hydraulically fracturing the overlying rock. They move at relatively high velocity for a magma (from 4 to 20 meters per second; Sparks et al., 2006), and the progressively lower pressure as they rise allows a vapor phase to *exsolve* from the system. This vapor phase keeps the components fluidized, and it supports a column of entrained material that becomes rounded and broken during transport. The evolution of the magma from its deep mantle source is a complex history of changing features such as the magma composition (siliceous or carbonaceous), the proportion of the system that is condensed (magma+rock and mineral fragments) versus gaseous ( $H_2O+CO_2$ ), and the ratio of  $CO_2$  to  $H_2O$ .

A kimberlite magma can start at depths as great as 200–300 km, but must be generated at least below the depths where diamonds are stable (>140 km) in order to pick them up from their lithospheric source. The source of kimberlite, either within or below the lithosphere, is a matter of active debate in the geologic community. Theory and field observation led Sparks et al. (2006) to propose a four-stage model of kimberlite eruption (figure 12):

- Stage I: Overpressured, explosive fissure eruption producing high vent velocities (>200 m/s)
- Stage II: Underpressured, erosive pipe formation causing *brecciation* near the surface
- Stage III: Waning, fluidized *pyroclastic* stage

producing volcanoclastic kimberlite ranging from massive to layered

- Stage IV: Post-eruptive hydrothermal *metamorphism* producing widespread serpentinization and crater fill

Fallback of volcanic material can occur once the eruption halts, but the kimberlitic rock formed during the latter three eruptive stages is typically well-preserved in the kimberlite pipe (figure 13). Their field interpretation by volcanologists, aside from being pivotal to understanding the nature of these eruptions, forms the basis for determining the distribution of diamonds in the kimberlite. This distribution is the essential step to evaluating the diamond *grade* of any kimberlite. Establishing diamond grade is a laborious process that combines bulk assay for diamonds in large amounts of exposed kimberlite (in some cases hundreds of tons) with core drilling of the unexposed kimberlite. The goal of this process is to accurately estimate the size of the kimberlite that could be mined (figure 14), the carats of diamond per hundred tons of rock, and the revenue per ton versus mining cost per ton.

The high-energy dynamics and changing conditions of a kimberlite eruption leave their textural imprint on the minerals and rock fragments carried by a kimberlitic magma. From these mineral clues and the textures described above, the geologist must deduce the nature of the eruption. Foreign rocks (xenoliths) of upper crust such as shale, dolomite, and

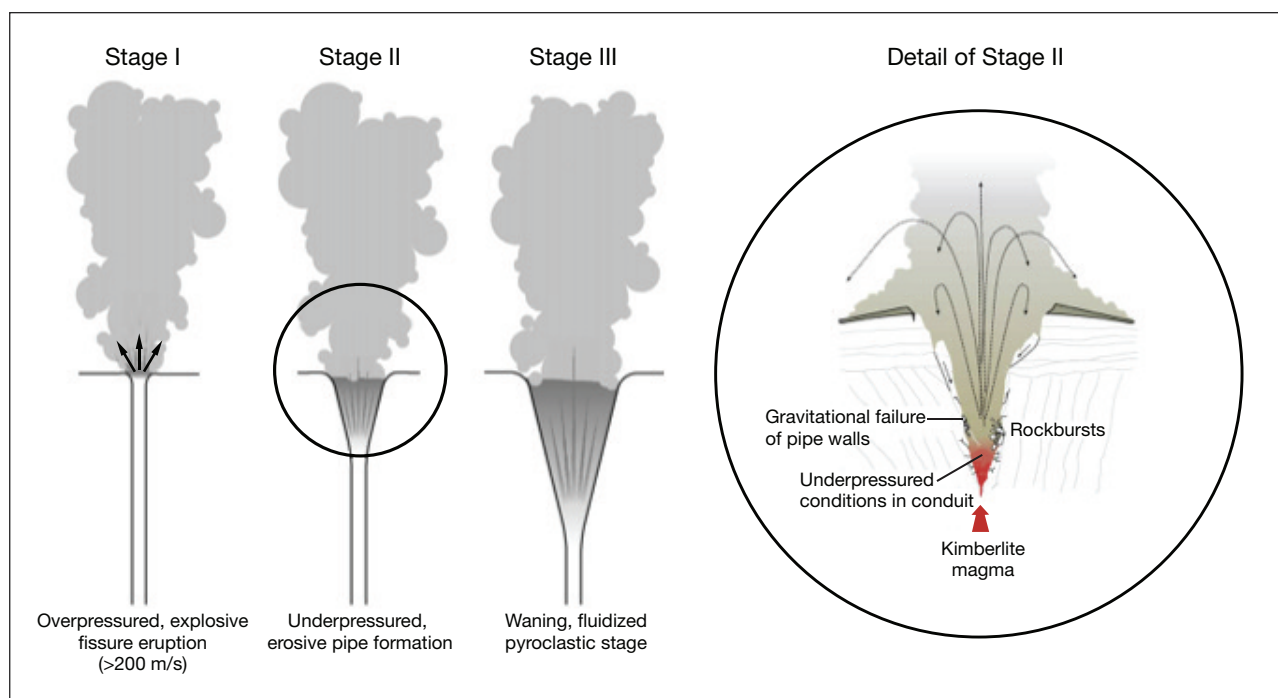


Figure 12. Stage I of a kimberlite eruption is overpressured, and eruption at this stage experiences the highest velocities. Stage II is underpressured, and during this stage significant wallrock erosion occurs. Stage III produces a kimberlite pipe in its final form, as shown in figure 10. Significant fallback of material can occur in Stage III. Stage IV (not shown) involves hydrothermal metamorphic alteration of the kimberlite pipe. Adapted from Sparks et al. (2006), with permission of Elsevier.

basalt, or of lower crust such as felsic and mafic granulite, are commonly found in the kimberlite pipe. Common too are xenoliths of mantle rocks such as harzburgite, lherzolite, websterite, and eclogite—the more fragile of which (e.g., magnesite-bearing harzburgite) are easier to break apart into their constituent minerals.

These foreign minerals, or *xenocrysts*, include olivine, clinopyroxene, orthopyroxene, garnet, ilmenite, and diamond itself, whose composition and relative abundance can reveal the makeup of the lithospheric mantle even in the absence of discrete rocks. As we will see below, such xenocrysts become the main prospecting tool for finding new diamondiferous kimberlites. Crystallizing directly out of the kimberlitic magma are phenocrysts of olivine, zircon, phlogopite, and groundmass perovskite. The latter three minerals can be used to determine the absolute geologic age and source composition of the kimberlite.

Very rarely, diamond can precipitate from the kimberlite. When it does, it can occur as overgrowths on monocrystalline diamond cores, as xenocrystic diamond hosts, and as microdiamonds. Any of these minerals, once formed or liberated, is subject to modification in the dynamic kimberlite eruption. Breakage, abrasion, and resorption may occur. Perhaps the most dra-

matic examples of resorption come from diamonds themselves (again, see figure 8), which display morphologies that range from simple etching to even teardrop shapes. There also is a noticeable difference between the perfect crystal morphology of type I diamonds and the cleavage fragments often seen in type II specimens.

**Finding New Diamonds.** Until the early 20th century, diamonds—even the famed Koh-i-Noor, Hope, and Cullinan—were typically found in alluvial or surface deposits, more or less by accident. The richness of the alluvial deposits of the Vaal and Orange Rivers of South Africa eventually led to the discovery of kimberlite and the famous workings around Kimberley, establishing kimberlite as the primary volcanic host of diamonds. From that point, exploration techniques centered on the best ways to find diamondiferous kimberlite using modern scientific methods. To the list of early alluvial diamond producers (e.g., South Africa, Namibia, India, Congo, and Brazil) have been added other hard ground or primary rock countries (namely Botswana, Russia, Australia, and Canada), which have greatly increased worldwide production.

As with other valuable ores, diamond exploration has become increasingly sophisticated and now in-



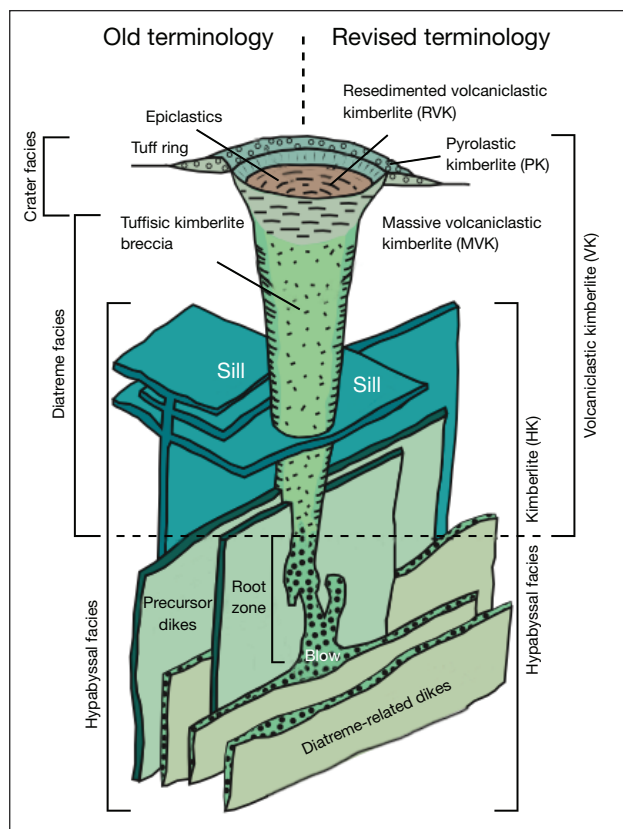


Figure 13. This perspective diagram of a kimberlite pipe with the surrounding country rock removed shows dikes and sills related to different levels of intrusion of kimberlitic magma and the kimberlite types exposed at different levels. Shown here is the terminology used by field geologists to understand what part of the kimberlite is exposed at the surface or sampled in drill core. Figures 9 and 11 show examples of shallower pyroclastic kimberlite (erupted into the air) versus deeper or hypabyssal kimberlite (crystallized several kilometers below the earth's surface). Diamonds can potentially be distributed through all the types of kimberlite shown here. Adapted from Kjarsgaard (2007), with permission from the Geological Association of Canada.

cludes some combination of different methods: geophysical techniques (airborne magnetic surveying, electrical resistivity, and gravity); geologic modeling (isotopic dating of ancient terranes and recognition of the history of their geologic modification); mineral analysis (garnet, ilmenite, and spinel *indicator minerals*); and geochemistry (surficial materials). Geophysical techniques and geologic modeling are useful for general narrowing of the exploration target area on a continental scale, whereas mineral analysis and geochemistry are applied on the ground when relatively close to the kimberlite.

Continental cratons are the first target for diamondiferous kimberlite exploration (see "Geology and the Distribution of Diamonds on Earth" and Clifford's Rule above). By definition, these regions are not orogenically active. They consist of flat or *peneplaned* surfaces that can be deeply weathered (Brazil and Australia), covered by desert sands (Botswana), uplifted and eroded (South Africa), or extensively glaciated (Russia and Canada). Locating diamondiferous kimberlites is challenging due to their small surface outcrop and their tendency to weather faster than the surrounding crystalline country rock, which means the pipes are often hidden beneath vegetation, unconsolidated surface deposits, or lakes (figure 15).

One very successful method for locating diamondiferous kimberlites employs a search in surficial deposits for actual fragments of the kimberlite, or for grain-sized indicator minerals weathered from these fragments (figure 16). These grains survive erosion, and their presence in sediments and soils is a predictor of whether a nearby kimberlite might contain diamonds. Indicator minerals range from single grains of silicate and oxide phases that have been released from mantle xenoliths broken up during sampling and transport by the kimberlite, to actual phenocryst phases in the kimberlite (Cookenboo and Grütter, 2010). In kimberlite, indicator minerals (figure 17) are

Figure 14. This aerial view shows the open pits containing the kimberlite pipes that comprise the bulk of the Diavik mine. The open pits outline the vertical geologic form of a typical kimberlite eruption, though the pit shape is wider than the actual kimberlite so that the pit walls do not collapse. The lines on the inside of the pit walls are benches along which massive 100-ton ore trucks are driven. Photo courtesy of Diavik Diamond Mine.



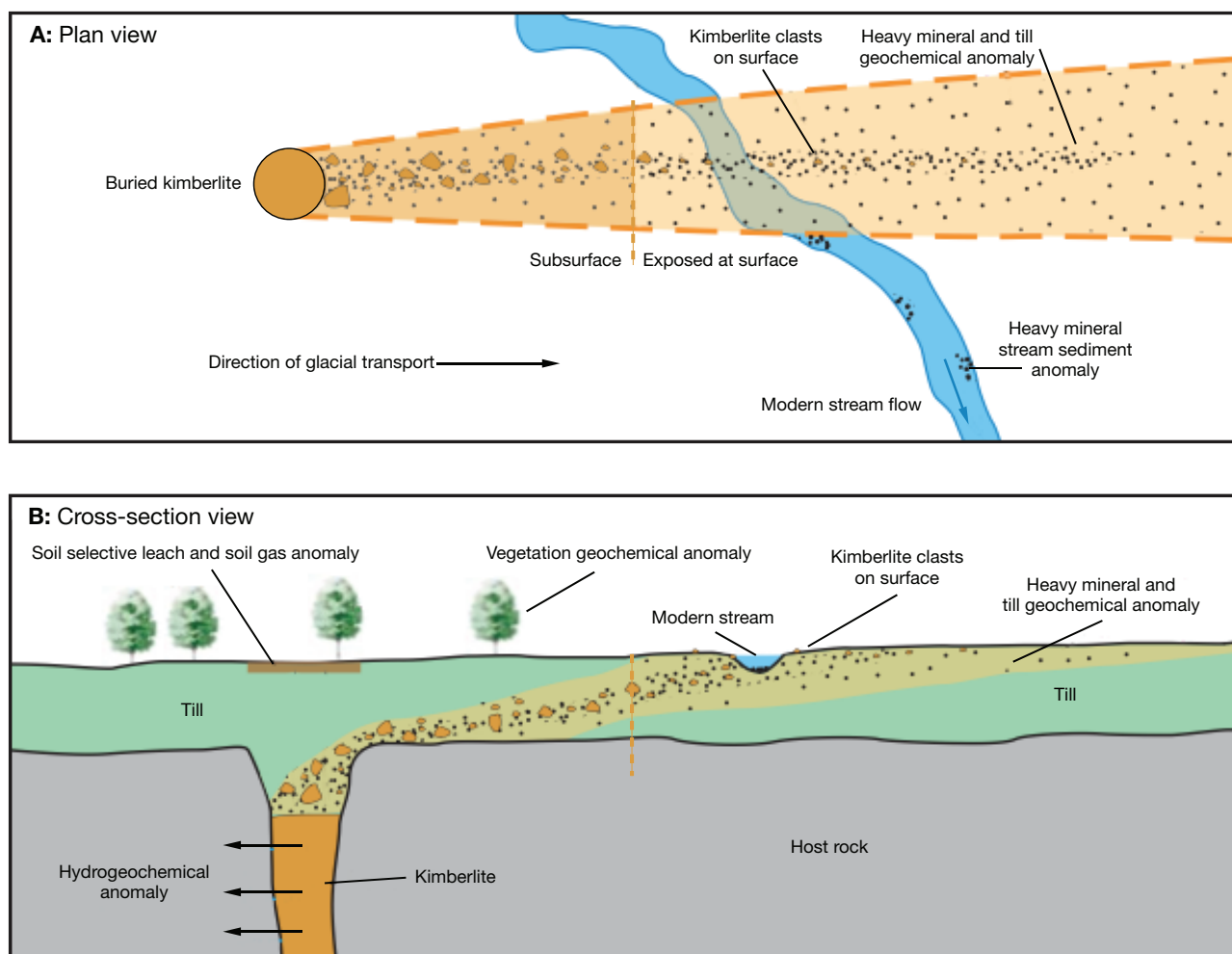


Figure 15. These illustrations show the mechanism for dispersal of indicator mineral grains from a buried kimberlite. Note the variety of techniques used to detect a kimberlite and the wide scattering of indicator minerals (see figure 16). Adapted from McClenaghan and Kjarsgaard (2007), with permission of the Geological Association of Canada.

much more abundant than diamonds, serving as markers for the chemically depleted mantle that can contain diamonds at depth. Furthermore, systematic mapping of the pattern of indicator minerals in surface deposits such as *till*, *glaciofluvial* sediments, or beach and stream sediments can point to the location of a kimberlite (McClenaghan and Kjarsgaard, 2007).

The key feature of the indicator mineral is its chemical composition as analyzed with the electron microprobe. A mineral is an indicator when its composition is characteristic of either the extreme *melt depletion* that typifies Archean continental mantle keels (peridotitic diamonds), or the high pressures found in subducted basaltic slabs (eclogitic diamonds). Indicators for peridotitic diamonds are so-called G10 pyrope garnets (high Cr and low Ca), chromite (high Cr + Mg and low Al + Ti), diopside

(high Cr + Al), and orthopyroxene (high Mg/Mg+Fe). For eclogitic diamonds, Cr-poor garnets (high Na + Ti) and diopside (high Na) are commonly used. Mg-rich ilmenite (picroilmenite) is a general kimberlite indicator. The relationship between indicator mineral composition and diamond can be imperfect, and a more sophisticated approach uses pressure and temperature relations (*geothermobarometers*) deduced from the composition of individual minerals as if they were in *equilibrium* with other coexisting mantle minerals (Cookenboo and Grütter, 2010). This approach can be applied to a wider range of mineral compositions, and it has provided more sensitivity in locating mantle lithosphere capable of hosting diamond.

Exploration tools based on indicator minerals and surficial geochemistry are tailored to the nature of

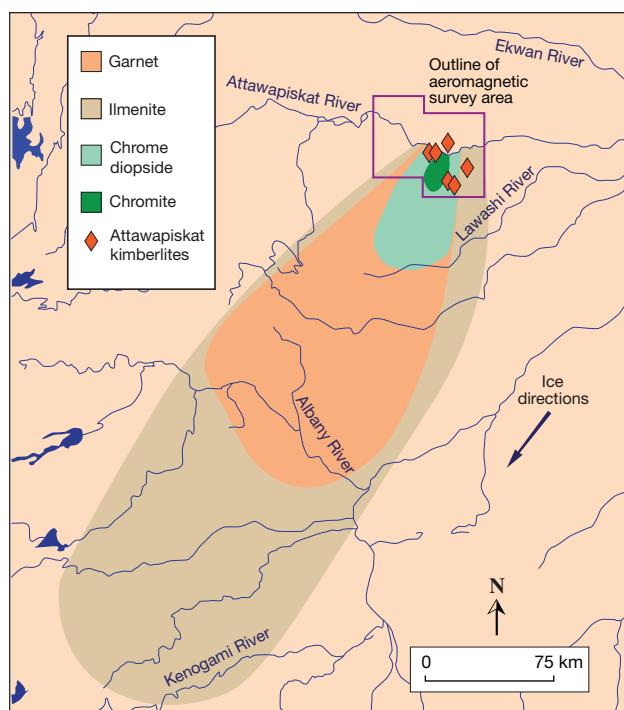


Figure 16. The indicator-mineral dispersion patterns for chromite, chrome diopside, pyrope garnet, and ilmenite are shown here for the Attawapiskat kimberlite in Canada. Dispersion of the ilmenite grains is detectable more than 300 km from the kimberlite source, whereas chromite and chrome diopside yield much smaller dispersion halos closer to the source because they are more easily weathered. The indicator minerals were collected from streams that were eroding glacial deposits. Adapted from Kjarsgaard and Levinson (2002), with permission of GIA.

the weathering process. In deeply weathered and arid climates, vegetation, termite mounds, and geochemical anomalies directly overlie kimberlites and streambeds that potentially hold diamond placer deposits. In heavily glaciated terranes, kimberlite indicators are dispersed for tens of kilometers in patterns that relate to ice-flow directions (figure 16; Kjarsgaard and Levinson, 2002). In glaciated settings, other indicators include geochemical analysis of till, soil, soil gas, biota, and groundwater (figure 15; McClenaghan and Kjarsgaard, 2007). Under these conditions, regional surveys have proven quite effective in locating kimberlitic targets.

The success of these exploration methods has led directly to the discovery of some of the world's most productive diamond mines, including Orapa and Jwaneng (Botswana's Zimbabwe/Kaapvaal craton) and Ekati and Diavik (Canada's Slave craton). As with all mined commodities, diamond exploration is highly dependent on price, global economic cycles, and rap-

idly changing mining company partnerships (to fund the costly exploration techniques). This search effort goes through boom and bust periods. Insightful case-study descriptions can be found on the Argyle deposit (Shigley et al., 2001) and occurrences in Canada (Kjarsgaard and Levinson, 2002).

The Argyle case study provides a perfect example of how long-known but sparse alluvial diamond occurrences in an arid and unglaciated terrain were combined with unconventional thinking, perseverance, and scientific methods to bring about the world's most productive deposit. Of all the aspects of the Argyle discovery, perhaps the most important is unconventional thinking, because the diamonds occur in lamproite (all other rich deposits are in kimberlite) and are located off-craton (not truly adhering to Clifford's Rule). The Canadian case illustrates exploration in heavily glaciated terrain. Here the diamonds were distributed far from their sources, and the most important discovery aspects were perseverance and scientific method.

In both cases, systematic exploration led to the discovery of many potential diamond host rocks (more than 80 kimberlite pipes in the Kimberley craton, and more than 300 in the Slave craton), only some of which were diamondiferous (10% and 50%, respectively). Even fewer were of sufficient diamond grade to mine (none in the Kimberley craton and <1% in the Slave craton). Taking into account how difficult it is to find just one kimberlite buried below surficial deposits and vegetation, these diminishing percentages illustrate just how special an economically viable deposit is. With the exception of the Canadian discoveries of the 1980s and 1990s (summarized in Kjarsgaard and Levinson, 2002), none of the producing countries have seen the discovery of a major diamond-bearing kimberlite pipe in recent decades. When this scarcity of discoveries is combined with the finite lifetime of existing mines, sometimes as brief as 25–30 years with modern mining techniques, a future shortage of rough diamond production could result.

## ORIGIN OF DIAMONDS

Since the summary by Kirkley et al. (1991) that appeared in this journal, there have been major advances in understanding the relationship between diamond types and their hosts, the pressure and temperature conditions for diamond formation, the sources of carbon, and how diamond growth relates to fluids in the mantle. Much of this new information has centered around:

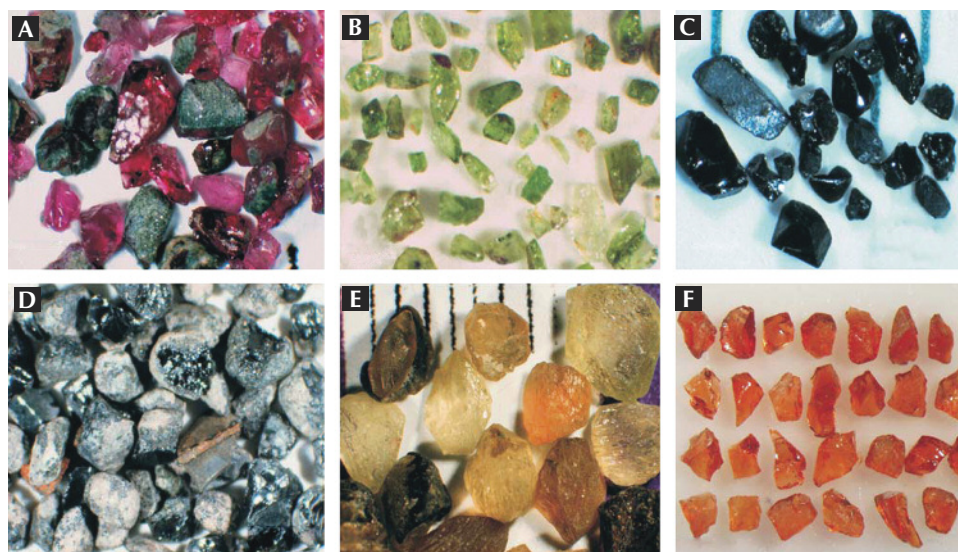


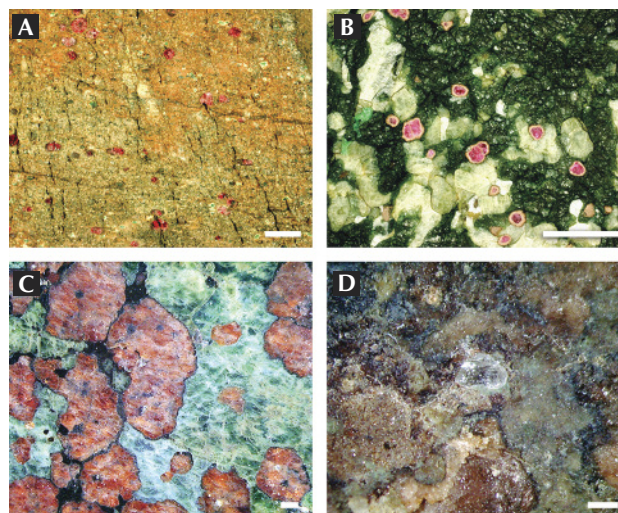
Figure 17. Examples of colors and surfaces of important kimberlite indicator minerals: (A) Cr-pyrope, (B) Cr-diopside, (C) Cr-spinel, (D) Mg-ilmenite, (E) Mg-olivine, and (F) pyrope-almandine garnet. Adapted from McClenaghan and Kjarsgaard (2007), with permission of the Geological Association of Canada.

- (1) Better geologic dating on the mineral inclusions in diamonds in relation to the ages of depletion/*metasomatic* processes in the mantle
- (2) Refined models for the partitioning of major elements between the main minerals in mantle rocks
- (3) Improved analytical sensitivity, permitting spatially resolved, spot-sized chemical analyses for stable isotopes and trace elements
- (4) Realistic laboratory simulations of the behavior of carbon-bearing fluids in the mantle
- (5) High-resolution imaging and analysis of nanophases in microscopically transparent diamonds

**Host Rocks for Diamond Crystallization and Diamond Types.** Eclogite and peridotite are the chief rocks in which diamonds grow in the mantle (figure 18). Single diamonds in kimberlite are thought to be released from eclogite or peridotite by mechanical disaggregation during eruptive transport (Kirkley et al., 1991; Harlow and Davies, 2005). Whereas eclogites, diamondiferous or otherwise, survive transport by kimberlite, nearly all peridotite xenoliths are diamond-free. Diamond within a few eclogites has been studied by computerized axial tomography (CAT-scan) techniques. There diamond is found in between the major silicate minerals along pathways where metasomatic fluids usually traveled (Keller et al., 1999; Anand et al., 2004), although it is unknown whether diamond always has this spatial relationship. Diamond in peridotite may have a similar textural relationship with its major silicates, but because CO<sub>2</sub>-rich diamond-forming fluids react with magnesian silicates to form *friable* magnesite

(MgCO<sub>3</sub>) along grain boundaries, diamondiferous peridotites disaggregate and release their diamonds, destroying the textural relationship with their host.

Figure 18. Incident-light photomicrographs of rock types that typically can host diamonds in the lithospheric mantle keel. A: Sheared garnet peridotite from Jagersfontein, South Africa. Shown is the typical buff color of the external surface of a rounded xenolith composed chiefly of olivine and orthopyroxene. Note the red garnets and green diopside. B: Garnet peridotite from Letlhakane, Botswana, Kaapvaal craton. Dark green = olivine, light green to white = orthopyroxene, bright green = clinopyroxene. C and D: Eclogites from Roberts Victor, South Africa (Kaapvaal craton). The garnet is red to reddish brown, while the clinopyroxene is green to blue green to pale brown. Note the diamond in the center of panel D. The scale bar in panel A is 1 cm; the scale bar in panels B, C, and D is 1 mm. Photomicrographs by Steven B. Shirey.



Little is known about where, texturally, superdeep diamonds reside in their mantle hosts. At the high pressures and temperatures of the mantle transition zone and below, and in a mantle that is mobile by solid-state convection, they are not likely to reside in open cracks. They could, however, form in anomalously fluid-rich regions of the deep mantle.

Diamonds that formed in the crust are restricted to terrains exposed by continental tectonic processes (again, see figure 4). They are found directly within their host lithologies, which are typically carbonate-bearing packages of rocks, including garnet-biotite gneisses and schists, which get reduced to form diamonds in place. Diamond also forms in the crust during the high pressures and temperatures produced when an extraterrestrial body strikes the earth's surface to form impact diamonds from carbon-rich targets (graphite to diamond solid-state transition) or impact melts. Crustal diamonds are either small or not of gem-quality, and useful only to the abrasives industry.

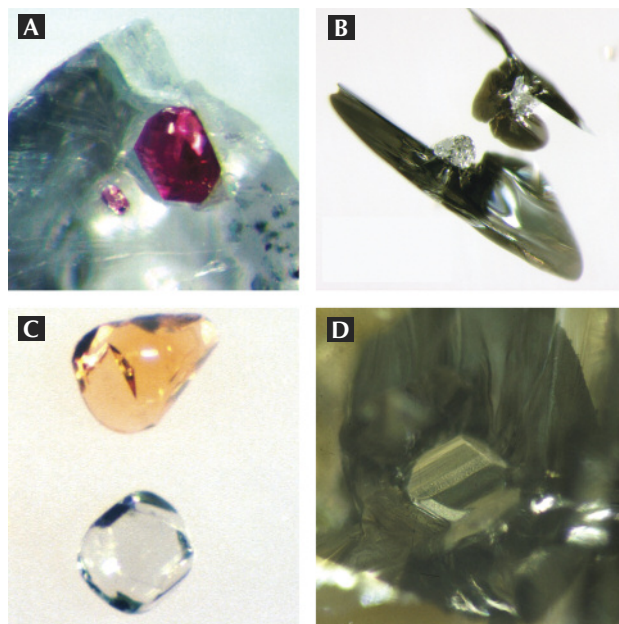
The gemologist is taught the basic "type" classification of diamonds by nitrogen content and aggregation (Breeding and Shigley, 2009). This is very useful for gemology, but not for understanding diamond in its geologic context. Some 95% of natural lithospheric diamonds are type Ia. With the exception of sublithospheric diamonds, which are mostly type II, the remaining 5% non-type Ia specimens are poorly correlated with geologic setting. The composition of mineral inclusions in diamonds, even though more than 95% of monocrystalline diamonds are devoid of them, provides a more useful scheme because inclusion mineralogy can be closely related to the host rock.

Inclusions of silicate minerals (garnet and pyroxene) in lithospheric diamonds allow gem diamonds to be classified into two dominant groups following their major eclogitic and peridotitic host rocks in the mantle (figure 19). Silicate minerals transmit light and their compositional differences produce striking color variations, making these inclusions an effective way to classify diamonds into types. Compositional parameters akin to those used for indicator minerals in exploration are used to make the classification. Peridotitic diamonds are known as "P-type" and eclogitic diamonds as "E-type." P-type specimens can be further subdivided into harzburgitic and lherzolithic in descending order of abundance that parallels the occurrence of these types of peridotites in the population of mantle xenoliths in diamondiferous kimberlites.

Sulfide mineral inclusions such as pyrrhotite and pentlandite (again, see figure 19) also allow diamonds to be subdivided into P- and E-types in a manner analogous to silicate inclusions. For sulfides, the distinction is based on Ni content. The higher-Ni sulfides occur in P-type diamonds, while the lower-Ni (and slightly higher-Cu) sulfides occur in E-type diamonds (Pearson and Shirey, 1999). Recent isotopic work using the platinum-group element osmium on single sulfides has yielded osmium abundance data that show the P- versus E-type distinction even more clearly (Pearson and Shirey, 1999). Unfortunately, the opacity of sulfides and their obscuration by internal fracturing renders this classification scheme useful only after breakage of the diamond and removal of the mineral inclusion.

Mineral inclusions in sublithospheric diamonds are less understood than in lithospheric diamonds be-

Figure 19. Peridotitic (P-type, A and B) and eclogitic (E-type, C and D) inclusions of silicate (A,C) and sulfide (B,D) mineral groups that have been successfully used for radioisotopic age dating (geochronology). A: harzburgitic garnet (high in Cr, low in Ca), used in Rb-Sr and Sm-Nd dating by Richardson et al. (1984). B: Ni-rich iron sulfide (pentlandite) used in Re-Os dating by Westerlund et al. (2006). C: orange garnet and colorless clinopyroxene used in Rb-Sr and Sm-Nd dating by Richardson (1986). D: Ni-poor iron sulfide (pyrrhotite) used in Re-Os dating (Pearson et al. 1998; Richardson et al., 2001). Grain size ranges from 50 to 300 microns. Photos courtesy of J.W. Harris, S.H. Richardson, and K. Westerlund.



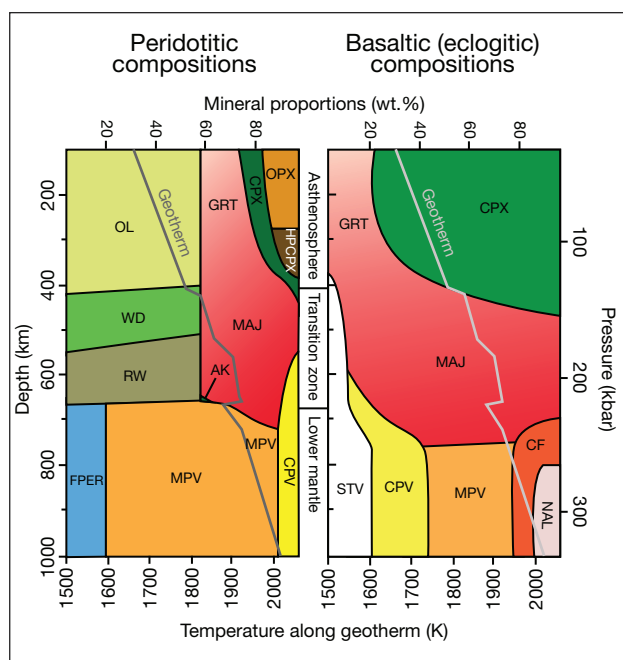


Figure 20. This diagram shows the mineralogy with depth for two different rock compositions that would be expected at great depth in the mantle. The peridotitic compositions on the left make up most of the mantle by volume. The compositions on the right are typical of basalt that would be subducted to high pressure and recycled into mantle peridotite. The basaltic composition is more  $\text{SiO}_2$ -rich, and therefore has much more clinopyroxene (CPX) and garnet (GRT) than the peridotitic composition. At 200 km depths, for example, the basaltic composition contains only clinopyroxene, and garnet, whereas the peridotitic composition has olivine (OL), garnet, clinopyroxene, and orthopyroxene (OPX). MAJ=majorite, WD=wadsleyite, RW=ringwoodite, FPER=ferroperricite, MPV=magnesium perovskite, CPV=calcium perovskite, STV=stishovite, CF=calcium ferrite, NAL = Na- and Al-bearing phase. Adapted from Harte (2010).

cause of the rarity of specimens, the small grain size of inclusions, and difficulties in recognizing original high-pressure minerals from their low-pressure forms. But the basic distinction (figure 20) between peridotitic diamonds is basically related to Mg-rich, *ultramafic* mineral assemblages (such as Mg-perovskite, ringwoodite, wadsleyite, and olivine with ferropericite, majorite, and Ca-perovskite); in eclogitic diamonds it is related to basaltic mineral assemblages (such as majorite, clinopyroxene, CaTi-perovskite, Ca-perovskite, Ca-ferrite, stishovite, and the Na- and Al-bearing phase). These distinctions, which seem to apply to the deepest diamonds (Pearson et al., 2003; Shirey et al., 2013) will be fundamental in understanding the source of recycled materials in the deep earth.

**Pressure-Temperature Conditions.** All diamonds at the earth's surface today exist outside the pressure and temperature regime for their growth. Yet we know the conditions under which they can form, based on experimental studies that simulate diamond-forming reactions, the mineral inclusion indicators of pressure and temperature (geothermobarometers), and the co-occurrence of diamonds in kimberlites with xenoliths whose pressure-temperature history can be studied. Basically, most gem diamonds are thought not to form directly from graphite. They can form at pressures and temperatures higher than the graphite-to-diamond phase transition under the right reducing conditions, and when there is enough free carbon to allow diamond to form. With depth below the surface, rocks reside at ever higher pressure and temperature along the geothermal gradient. This renders the entire mantle below about 140 km capable of forming diamond.

Pressure-temperature estimates for the formation of lithospheric, gem-quality diamonds can be calculated from analysis of their mineral inclusions. Review studies of more than 1,000 diamonds (e.g., Stachel and Harris, 2008) show that they formed at a temperature of 1150–1200°C and at a depth within the appropriate P–T range for diamond growth. Rather than reflecting a favored condition for formation, this may simply represent the most “probable” temperature range within the limits imposed by diamond stability and mantle conditions. Superdeep diamonds obviously form in a pressure-temperature regime much higher than what can be obtained in the lithospheric mantle, but one that can be estimated from the solid solution of silicon (the pyroxene or “majorite” component) into the garnet structure (Shirey et al., 2013), or some other estimate of minerals that have exsolved at low pressure from a higher pressure inclusion (e.g., Walter et al., 2011). Crustal diamonds have formation conditions best estimated from the metamorphic history of their enclosing host rocks, because they typically lack mineral inclusions that indicate pressure and temperature. Impact diamonds, forming directly at the earth's surface, can only be modeled from the heat and pressure effects generated by the transient shock wave of the impact.

**Sources of Carbon.** Major advances in understanding the sources of carbon that eventually turn into diamond have come from examining carbon's isotopic composition. Elemental carbon is composed of two stable isotopes:  $^{12}\text{C}$  (98.9%) and  $^{13}\text{C}$  (1.1%). The ratio

of  $^{13}\text{C}$  to  $^{12}\text{C}$ , measured easily with a gas-source mass spectrometer, varies with geologic process and the original source of carbon. Nitrogen, the second most abundant element in diamond, also has two isotopes,  $^{14}\text{N}$  (99.6%) and  $^{15}\text{N}$  (0.4%), and is amenable to the same kind of study; however, because nitrogen is a trace element in diamond and much more difficult to analyze accurately, it has been subjected to far less scrutiny and less is known (for a recent review, see Cartigny and Marty, 2013). In general, isotopic study remains a very active area of research, because of the potential for diamonds to trace the igneous rock aspects of the deep mantle portion of the carbon cycle. Earth's large solid volume relative to the atmosphere makes the mechanisms by which carbon contributes to the volcanic  $\text{CO}_2$  gas flux a critical factor that requires better understanding.

Carbon that becomes diamond has two sources in the earth: primordial and recycled. Primordial carbon is that which has resided in the mantle since the *accretion* of the planet. Recycled carbon has, at some stage, been released from the mantle to form  $\text{CO}_2$  in the atmosphere, or become incorporated in organic matter and formed carbonate, graphite, or other carbon-bearing minerals in sedimentary and metamorphic rocks. Carbon is a volatile element, and much of the original carbon available to be incorporated in the earth may have been lost during accretion (Marty et al., 2013). Thus, the amount of carbon in the mantle is not known (estimated at 500–1000 ppm; Marty et al., 2013), nor is the proportion of primordial to recycled carbon (given the large meteoritical range; Haggerty, 1999). We can say that carbon has a long residence time in the mantle (similar to the earth's lifetime), that it has a concentration that may be close to steady state (i.e., unchanged by addition from subduction or loss due to volcanism), and that it is an actively cycled element. It is remarkable that diamonds display a large range in their  $^{13}\text{C}/^{12}\text{C}$  isotope ratio despite the mantle mixing process of convection that might lead to isotope homogenization. In fact, diamonds retain compositional variability that is as large as the range induced by photosynthesis at the earth's surface (the largest range in  $^{13}\text{C}/^{12}\text{C}$  routinely measured).

The variability in carbon isotopic composition is not random; instead, it is related to the diamond type and presumably to the petrogenesis or igneous geologic history of the diamond (figure 21). P-type diamonds display a restricted range in carbon isotopic composition (given in the delta notation,  $\delta^{13}\text{C}$ , where  $^{13}\text{C}/^{12}\text{C}$  is referenced to a standard and expressed in ‰)

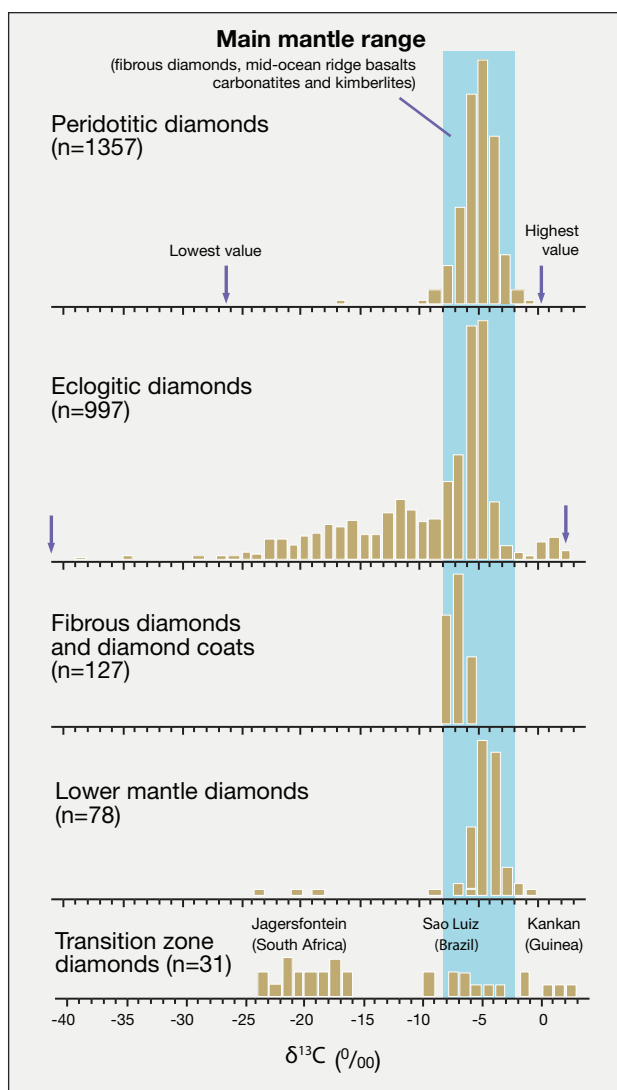


Figure 21. Carbon isotope content reflects the nature of the host diamond and tells us about its geologic history. This figure shows the difference between some of the main diamond types.  $\delta^{13}\text{C}$  is the  $^{13}\text{C}/^{12}\text{C}$  ratio measured against a reference standard and deviating from this standard by 0.1%. Note the negative scale and how eclogitic diamonds extend to much lower  $\delta^{13}\text{C}$  than peridotitic diamonds; n = number of analyses. Adapted from Cartigny (2005), with permission of the Mineralogical Society of America.

of  $-10$  to  $-2$   $\delta^{13}\text{C}$ , with more than 95% of P-type diamonds falling in the main mantle range of  $-8$  to  $-2$  (Cartigny, 2005). E-type diamonds show a very wide range in  $\delta^{13}\text{C}$ , from  $-42$  to  $+3$ , even though they too have a large percentage that fall within the main mantle range.

Superdeep diamonds from the top of the lower mantle have a carbon isotopic distribution similar to that of P-type diamonds, whereas superdeep dia-

monds from the mantle transition zone more closely resemble E-type diamonds (Pearson et al., 2003). Other unusual specimens such as fibrous, polycrystalline, and crustal metamorphic diamonds have their own unique compositional ranges (Cartigny, 2005). Carbon in meteorites has a very large range in  $^{13}\text{C}$  to  $^{12}\text{C}$  that was inherited from solar system sources (Haggerty, 1999) and is much greater than that of the average mantle. If the carbon isotopic variability were inherited from primordial carbon with compositions even close to the large range seen in meteorites, then it remains unexplained how groups of diamonds would retain different compositional distributions and not all reflect that large range. A more likely scenario is that the compositional differences have been created by active geologic processes such as those related to plate tectonics.

Active geodynamic processes create and bring to the surface the diamonds we have today, just as they have shaped the earth for 4.5 billion years. These processes formed the ancient continents with mantle keels ready to store diamonds. They also introduced, deep in the earth's interior, mobile substances such as water and carbon that were essential for the creation of diamonds and their sampling by kimberlitic volcanism. Oceanic lithospheric plates are eventually subducted, and when the oceanic lithosphere is created at the mid-ocean ridges by the decompression melting that occurs during spreading, hydrothermal circulation of seawater alters the primary minerals and deposits hydrous minerals in their place. Sedimentary carbonate minerals (high  $\delta^{13}\text{C}$ ) and organic compounds (very low  $\delta^{13}\text{C}$ ) collect in the oceanic lithosphere, along with volatile elements such as chlorine, fluorine, sulfur, and nitrogen. Since subduction must occur along the pressure-temperature path of the geothermal gradient, none of these volatile elements and compounds can be transported to the conditions of diamond growth as a fluid; otherwise, they would be driven off by the high temperatures reached. Rather, these elements must become locked, in solid form, in mineral structures (e.g., graphite, apatite, and biotite) or dissolved as trace elements within stable minerals (e.g., hollandite) that can be subducted to great depth.

One of the most active areas of current research is the distribution, speciation, and mineral hosts of volatile species in the oceanic lithosphere, and their transformations with pressure and temperature as the oceanic lithosphere is subducted. A goal for understanding diamond formation is to be able to predict the minerals involved and estimate their water- and

carbon-carrying capacity. This is challenging enough for the earth's current geodynamic regimes, where the present lithosphere can be sampled and geophysics can be used to form a picture of lithospheric plates and their rates and depths of subduction. But for understanding gem diamonds, most of which are billions of years old, an even greater challenge is whether current geodynamic processes are like those of the past. Despite these unknowns, the spatial association of old diamonds of different types with the rocks of known geologic history allows us to understand past processes at the basic level and to investigate the role of primordial versus recycled carbon.

Mantle convection, in which subduction plays a part, is the key process driving plate tectonics. Deep in the mantle, convection will trigger *adiabatic* or decompression melting, which occurs when the hotter mantle from below is convected upward too quickly to exchange heat with the surrounding mantle through which it moves (again, see figure 7). Due to the lower pressure of the shallower level it has reached, it is now hotter than its melting temperature at that pressure and will melt. Associated with mantle convection is the subduction of oceanic lithosphere. Subduction will enable the recycling of carbon as carbonate ( $\text{CO}_3$ ), leading to the creation of carbonated peridotite. Carbonated peridotite melts more easily than carbonate-free peridotite, and upon small degrees of melting will release a low-viscosity melt known as a carbonatite. Carbonatites are carbonate-rich igneous liquids that have too much oxygen to stably host a reduced carbon mineral such as diamond. They are, however, extremely mobile, and can move through parts of the mantle where they can be reduced and produce diamonds. Furthermore, carbonatitic liquids show compositional continuity with kimberlitic liquids (Gudfinnsson and Presnall, 2005), and it has been proposed that carbonatites will dissolve enough of the silicate mantle through which they pass to actually form a kimberlite (Russell et al., 2012). Thus, it is evident that the earth's active geodynamics are intimately associated with all facets of the diamond cycle, including creation of carbon-rich regions where diamonds form, production of carbonated peridotite that can melt, the generation of the mantle upwelling that leads to melting, and formation of the kimberlite.

**Fluids, Textures, and Diamond Growth in Mantle Rocks.** The marriage of imaging techniques that can reveal diamond growth patterns with small-spot-size analytical capabilities has led to new ideas about how they grow in the mantle. Some work at the



small scale borrows from the field of nanotechnology, and includes high-tech procedures at the cutting edge of resolution and sensitivity that involve laser ablation, secondary ion mass spectrometry, and focused ion beam fabrication and extraction of tiny diamond wafers.

Such analytical work starts with the internal textures. Gem diamonds that show no growth zoning in visible light may show it in polarized light, photoluminescence, and especially cathodoluminescence (CL), as shown in figure 22. Nitrogen, the major diamond impurity, activates CL in diamond; thus, CL can be applied to almost every sample. It is best accomplished on polished plates, which must be oriented perpendicular to one of the {110} axes and not parallel to {100} or {111} to cut across the growth zones and display them (Bulanova et al., 2005).

Irregular forms of lithospheric diamonds (macles, bort, and the like) exist, but many monocrystalline lithospheric diamonds have a roughly concentric internal structure. In gem-quality monocrystalline diamonds, the zoning patterns are characterized by two chief features: (1) extremely thin oscillations between stronger and weaker luminescence, and (2) alternating episodes of resorption and overgrowth on top of the resorption. Both features strongly support the idea that diamond grows from an aqueous fluid and/or low-viscosity melt with an aqueous component rather than from a solid medium such as graphite. Growth from graphite is not likely under the P-T conditions of the lithospheric mantle for monocrystalline diamonds (Stachel et al., 2009), and it would not produce the fine oscillations (e.g., rapid change in nitrogen content) or periods of resorption between periods of growth. Zoning patterns are extremely important to interpreting

carbon and nitrogen isotopic composition changes during growth and crystallization of individual mineral inclusions. Coated diamonds are a special case of monocrystalline diamond, where monocystals have been overgrown by a thick, cloudy, polycrystalline coat laden with microinclusions of fluid. If the coat is composed of rods or blades of diamond, it will exhibit a fibrous structure and be termed a “fibrous” diamond. These coats are believed to grow during transport in the kimberlite and therefore represent young, new diamond growth surrounding often ancient diamond (Shirey et al., 2013).

The textures revealed in sublithospheric diamonds are strikingly different, because they rarely form euhedral monocystals or (as seen with CL) display regular concentric zonation. Instead, these diamonds are characterized by multiple growth centers, non-concentric zonation of a blocky texture, and even what appears to be deformation texture; in short, they display almost polycrystalline internal structures. The major difference is that sublithospheric diamonds grow at much higher pressure and temperature and in a mantle that is actively convecting, whereas lithospheric diamonds grow in a mantle host that is not convecting. We can only speculate as to whether these textural differences are caused by the dramatic differences in the nature of the host mantle or by the possibility that some growth from solid graphite (Irifune et al., 2004) is favored by the much higher P-T conditions and deformation.

Diamond formation in the lithospheric mantle is considered a process whereby supercritical fluids or melts react with the mantle rocks through which they pass, a process known as metasomatism. A detailed discussion of this complicated topic is beyond

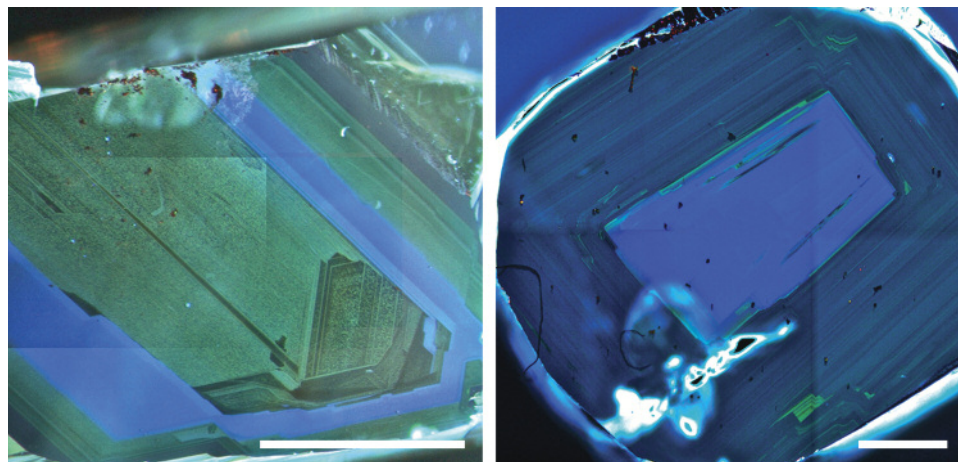


Figure 22. CL images of polished diamond plates from Orapa show the concentric growth zoning seen in lithospheric, gem-quality stones. The diamond on the left has a more complicated growth history, with multiple episodes of growth and resorption. A multistage history can be seen on the right; bright spots in the lower part are sulfide inclusions. Scale bars are 1 mm; composite photomicrographs by Steven B. Shirey.

the scope of this paper, but a brief review is necessary to understand general aspects of diamond growth. Diamond will crystallize when carbon is released from the fluid, either by the reduction of  $\text{CO}_2$  species or by the oxidation of methane ( $\text{CH}_4$ ) species. It becomes evident that the speciation of carbon and the formation of diamond will be intimately associated with the oxidation state of mantle rocks through which the fluids pass, which in turn is controlled by the mineralogy of the rocks and the type of reactions that ensue with the fluids/melts (Shirey et al., 2013). Thus, we can expect different diamond-forming reactions in peridotitic versus eclogitic host rocks. For example, a common reaction in peridotites involves enstatite and magnesite, which react to form olivine and diamond in the presence of a fluid. The mineralogy of an eclogite is different, so a comparable situation in an eclogite would involve dolomite and coesite to form diopside and diamond in the presence of a fluid. In both cases,  $\text{CO}_2$  is released by the system into the fluid, and diamond will only form if the oxidation state is low enough to allow it to be stable relative to  $\text{CO}_2$ . The oxidation conditions for these different reactions in eclogite versus peridotite do not overlap, so that fluids too oxidized to form diamonds in peridotites are reduced enough to form diamonds in eclogite. Diamond-free fluids could pass through peridotite into eclogite to crystallize diamond. This process could explain the common occurrence of eclogite xenoliths with diamonds in metasomatic veins (e.g., Shirey et al., 2013).

At pressures where diamond is stable, cratonic lithosphere is likely to have sufficient reducing conditions for carbon to exist as diamond. A modern approach to diamond formation includes a comprehensive view of mantle oxidation state, carbon speciation in peridotitic and eclogitic mantle rocks, and both experimental and theoretical mechanisms for growth.

## AGE OF DIAMONDS

Although some gemologists see beauty in mineral inclusions, a diamond with visible inclusions is of lesser value in the market. To the geologist or geochemist, a diamond with its mineral inclusion cargo is highly prized, because it preserves the oldest and deepest samples that can be obtained from the earth. Mineral inclusions are important for what they can tell us about the formation conditions (pressure + temperature), the host rock for growth, the source of diamond-forming fluids, and the age of a diamond.

**Inclusion Types for Dating and Diamond Ages.** Mineral inclusions can be classified as syngenetic, protogenetic, or epigenetic, according to when they crystallized with respect to their host diamond. Syngenetic inclusions crystallized simultaneously with the diamond, presumably in equilibrium with the diamond-forming fluid, and any geologic information extracted from the inclusion (e.g., P-T of formation, geochemical environment, and age) unequivocally applies to the host diamond. A protogenetic inclusion formed before the diamond and was encapsulated by it after some period that could vary from a geologically short to a very long time scale, and it could be related or unrelated to the diamond fluid. The maximum age obtained from a protogenetic inclusion might be close to the diamond's age, and a general age pattern of diamond growth in a region of lithospheric mantle might still be evident. Inclusions forming along fractures or made of alteration minerals that formed after syngenetic or protogenetic inclusions can be identified as epigenetic. They are viewed as being secondary, and data from them on diamond crystallization is suspect.

P- and E-type inclusions of syngenetic and protogenetic nature from gem-quality lithospheric diamonds have provided most diamond ages to date (again, see figure 19). (The dating of sublithospheric diamonds is in its infancy, hampered because the inclusions are small and have unfavorable mineralogy for the commonly used radioactive decay schemes.) There is a large age difference between the relatively young kimberlites and the old lithospheric diamonds they transport. Diamondiferous kimberlites older than 550 Ma are rare, and most are younger than 150 Ma; the diamonds they carry are older than 1,000 Ma and may be as old as 3,500 Ma (again, see figure 10). With few exceptions, this age difference clearly negates a genetic link between kimberlite and diamond (see Kirkley et al., 1991), making the timing and origin of the host irrelevant to the timing and origin of its diamond cargo. The diamond cargo is just an accidental sampling of the ancient mantle lithospheric keel in which the diamonds were stored for long periods. The antiquity of lithospheric diamonds does make them ideal for probing the geologic processes occurring in the mantle keel during continent formation.

**Inclusion Analysis Methods.** Age dating of diamonds through analysis of their mineral inclusions has been reviewed regularly over the past two decades (Pearson and Shirey, 1999; Gurney et al., 2010; Shirey et al.,

2013), and these reviews provide a source for the following discussion. Five isotopic decay schemes have been applied to the dating of these mineral inclusions (table 1): rubidium-strontium (Rb-Sr), samarium-neodymium (Sm-Nd), uranium-lead (U-Pb), argon-argon (Ar-Ar), and rhenium-osmium (Re-Os). All isotopic systems are classified as “long-lived” decay schemes, where the time it takes for the parent *nucleide* to decay to half its original amount is ideally suited to the old ages of diamonds.

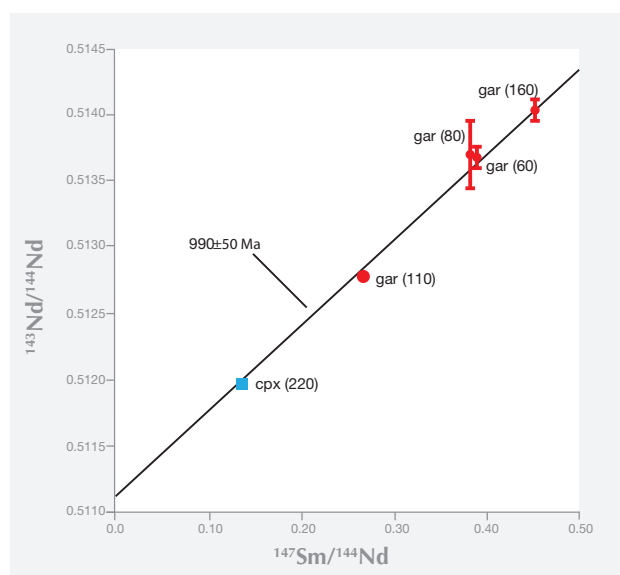
Not all methods can be applied to every mineral inclusion; minerals have different abundances of the elements, and the analytical procedures themselves have different sensitivities. Breakthrough dating studies were made using the uranium-lead method on sulfide inclusions by Kramers (1979), and the samarium-neodymium method on silicate inclusions by Richardson et al. (1984), by combining all the available grains (sometimes many hundreds of diamonds, each with a single inclusion) of similar mineral composition (figure 23). This work established the validity of the procedures and generally demonstrated an Archean age (more than 2.5 billion years old) for the most depleted (harzburgitic) garnet inclusions in diamonds from the mines in the Kimberley area and Finsch in the Kaapvaal craton.

The use of batches of inclusions derived from separate diamonds led to concerns about mixing diamonds of different ages and producing an average age that might not correlate with a specific geologic process (Navon, 1999; Pearson and Shirey, 1999). These uncertainties drove the need to perform chemical analyses on single inclusions. The argon-argon method on clinopyroxene inclusions was the first to be applied (Phillips et al., 1989; Burgess et al., 1992) because eclogitic omphacite (a sodium-bearing clinopyroxene) contains sufficient potassium to allow age determinations. Although argon-argon geochronologic studies of eclogitic pyroxenes generally confirm the results of the samarium-neodymium method, problems arose due to diffusion of argon out of the inclusion to the surface where the inclusion and diamond meet. Nonetheless, argon-argon studies indicated not only E-type formation from the Neoproterozoic (about 2,800 Ma) onward in southern Africa but also some unexpected old diamonds, highlighting the need for work on single diamonds.

Analysis of single inclusions is now chiefly carried out using the rhenium-osmium isotope system in sulfides (table 1). The relatively high sensitivity of mass spectrometry techniques for Re and Os, and their relatively high concentration in sulfides, makes single-

grain analysis possible. P-type sulfides weighing as little as a microgram (figure 24) can be analyzed due to their extraordinarily high osmium concentrations (Westerlund et al., 2006; Smit et al., 2010). But E-type sulfides have much lower concentrations (by as much as 1,000 times), and the focus on these mineral inclusions that are larger and easier to analyze has led to an apparent bias toward dating studies involving E-type diamonds (e.g., Pearson et al., 1998; Richardson et al., 2001; Richardson et al., 2004; Shirey et al., 2004a, b; Aulbach et al., 2009). Nonetheless, the single-inclusion work on sulfides by the rhenium-osmium method, with its ability to analyze a wide range of P-type and E-type sulfides, has led to important conclusions about the relationship of diamond growth episodes to processes that form and modify cratons (see below).

Figure 23. This diagram shows how the radioactive decay of  $^{147}\text{Sm}$  produces  $^{143}\text{Nd}$  (see table 1), resulting in a line, known as an isochron, whose slope increases directly with age and can be used to calculate the exact age. The five-point Sm-Nd isochron here is produced from silicate inclusions in diamonds from the Orapa mine (Richardson et al., 1990). The data were obtained by breaking apart 630 inclusion-bearing diamonds and grouping each set of inclusions as clinopyroxene (cpx) or garnet (gar). The number of inclusions combined together in one chemical dissolution procedure to produce one Sm-Nd data point is given by the numbers in parentheses. Based on the isochron here, the average age of these diamonds can be calculated to be 990 Ma, with an uncertainty of about 50 Ma.



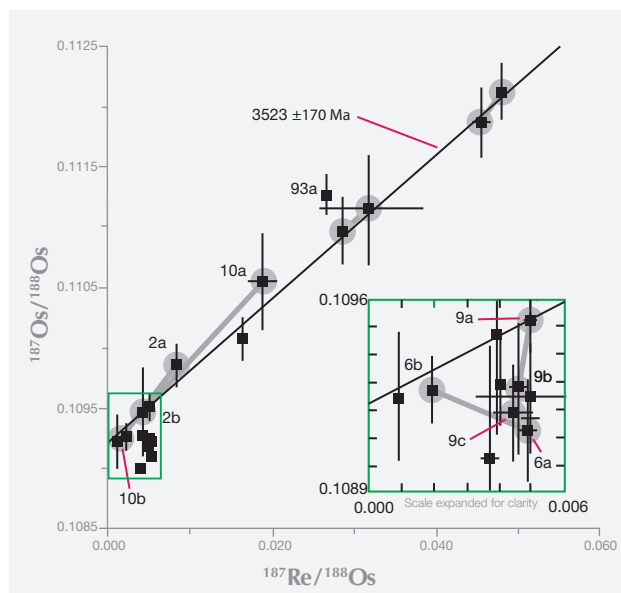


Figure 24. A 14-point Re-Os isochron on sulfide inclusions in diamonds from the Ekati mine, Canada. In this diagram, radioactive decay of  $^{187}\text{Re}$  produces  $^{187}\text{Os}$  (see table 1), resulting in a line whose slope increases directly with age. The isochron was produced by analyzing separately each sulfide from a diamond. Diamonds with multiple sulfides are numbered individually and shown connected by gray dumbbells between the “a” and “b” inclusions in each diamond. These serve as internal “mineral isochrons” and corroborate the age of the diamonds as 3,523 Ma. These are the oldest known diamonds whose age has been determined directly. At low  $^{187}\text{Re}/^{188}\text{Os}$ , some sulfides do not plot on the age isochron but are still connected by dumbbells. These connect two sulfides from the same diamond whose initial isotopic composition changed with diamond growth from core to rim (lower to higher  $^{187}\text{Os}/^{188}\text{Os}$ ). These types of isotopic changes can be correlated with specific geologic conditions of growth more than 3.5 billion years ago. The inset box on the right presents an expanded view of the data points. Adapted from Westerlund et al. (2006).

To date, only three age determinations have been made on inclusions from ultra-deep, sublithospheric diamonds, and all have come from the Brazilian craton. The uranium-lead method was used on one Ca-silicate perovskite inclusion (re-equilibrated to walstromite) from the Collier-4 kimberlite (Bulanova et al., 2010) and gave an age of 107 Ma, just slightly older than kimberlite eruption. A preliminary rhenium-osmium method was used on a sulfide inclusion from Juina and gave an early Proterozoic mantle model age around one billion years (Hutchison et al., 2012). Age inferences can be drawn from the Sr and Nd isotopic composition of majoritic garnets from Sao Luis that fall on the present oceanic mantle isotopic array (Harte and Richard-

son, 2011), which is known to often display Phanerozoic (e.g., 0–542 Ma) mixing ages. The point is that these ages are significantly younger than those of nearly all lithospheric diamonds.

### Diamonds of Multiple Ages from Some Kimberlites.

With the advent of widespread single-mineral inclusion analyses, it has become possible to see, with better resolution, if there is more than one episode of diamond formation at any one locality. Early work on E-type silicate inclusions clearly showed this possibility, but the need to combine many different grains from different diamonds always raised the possibility of combining formation ages as well. The general picture of lithospheric formation revealed by several generations of age dating, and the advent of the rhenium-osmium dating, is that there can be multiple diamond ages within the lithosphere sampled by any one kimberlite; perhaps this is the rule rather than the exception (Pearson et al., 1998; Richardson et al., 2004; Aulbach et al., 2009). For example, the Orapa and Jwaneng kimberlites carry three and four generations, respectively, of E-type sulfide-bearing diamonds, whereas the Diavik kimberlite carries Paleoproterozoic P-types and Paleoproterozoic E-types. The Ellendale kimberlite carries one P-type and three E-type generations. And of course, lithospheric diamonds are always found accompanying sublithospheric specimens because they are erupted in the same kimberlites, perhaps illustrating the greatest possible contrast in age and geologic setting.

**Residence Time in the Mantle.** Extensive samarium-neodymium studies by Richardson (summarized by Pearson and Shirey, 1999; Gurney et al., 2010) confirmed the general antiquity of lithospheric diamonds and their billion-year or longer residence in the lithospheric mantle, and established the Proterozoic as an important time of formation, at least for the Kaapvaal craton. Within the population of old lithospheric gem diamonds, some patterns emerge. The E-type sulfide-bearing diamonds analyzed thus far appear to have formed no earlier than three billion years ago (again, see figure 10). In contrast, diamonds containing P-type sulfides and silicates may be older or younger than three billion years. The geodynamic implications of these differences in residence time are discussed below.

This long lithospheric residence time for diamonds, as shown by all the mainstream studies with the samarium-neodymium and rhenium-osmium systems, contrasts sharply with a small number of stud-

ies in uranium-lead and argon-argon (e.g., Phillips et al., 1989; Burgess et al., 1992) on inclusions in lithospheric diamonds that have yielded relatively young formation ages due to analytical aspects of the particular system. Because the minerals analyzed can be related to proto-kimberlite melts, these ages are part of a growing body of evidence, supported by nitrogen-aggregation systematics, that a small proportion of lithospheric gem diamonds grew shortly before kimberlite eruption and occur mixed in with the much more abundant older diamonds in any one kimberlite.

The few sublithospheric specimens that have been analyzed are younger than most lithospheric diamonds. The uranium-lead on Ca-perovskite of 107 Ma was only slightly older than the age of kimberlite emplacement 93 million years ago, and was consistent with the highly aggregated nitrogen; this indicates a brief, hot residence time in the mantle (Bulanova et al., 2010). A model age of around 500 Ma, resolvably older than kimberlite ages but again much younger than lithospheric diamonds, was obtained with rhenium-osmium on a sulfide inclusion by Hutchison et al. (2012). This age is consistent with growth deep in the convecting oceanic mantle. Furthermore, neodymium and strontium isotopic analyses of a composite of majoritic garnets are also consistent with oceanic mantle compositions (Harte and Richardson, 2011), and support their derivation from the convecting mantle. The restricted age information on superdeep diamonds compared to lithospheric diamonds, and its potential for estimating deep mantle convection rates, means that this is an area of continuing research.

## MANTLE GEOLOGY AND DIAMONDS

A sustained focus over the years on diamonds and how they form has allowed researchers to turn the tables and use diamonds as indicators of geologic processes in the mantle rocks that host them. This type of research is standard fare in the fields of igneous/metamorphic petrology and meteoritics, where each rock's composition and the age relations of its constituent minerals may reveal an important story. Diamonds have always had unique potential because of their antiquity and depth of formation. But because they occurred as isolated xenocrysts in kimberlite, a detailed understanding of how they form was needed to realize their potential as a record of deep-mantle geologic processes.

**Imitating Diamond Fluids at Depth.** Perhaps one of the best ways that diamonds can be used to inform us about the deep earth is to simulate their growth

in realistic physicochemical models of their mantle host rocks. This field of endeavor, known as experimental petrology, has a core research goal of duplicating diamond formation in the laboratory (see Shirey et al., 2013) at the pressure, temperature, behavior, and composition of the various components involved in the natural setting. This experimental approach is an essential aspect of understanding mantle geology through diamonds, because in many of the world's diamond-forming regions the kimberlites have failed to expose samples of diamond host rocks.

Diamond is the likely mineral form of free carbon (not bound up in other silicates) within the lithospheric mantle, leading to many ways that it can form, as briefly discussed above. From an experimental perspective, formation in the lithosphere will be in the compositional system carbon-oxygen or carbon-oxygen-hydrogen which will produce fluids that contain mostly CO<sub>2</sub>, mixed CO<sub>2</sub> plus H<sub>2</sub>O, mostly H<sub>2</sub>O, and mostly CH<sub>4</sub> (figure 25). Specific experiments and their results are too numerous to quote here, but various combinations of these fluids with carbonate or graphite in the presence or absence of silica or alkali metals have been shown to be effective in forming diamond. Sulfides and native metals also have been shown experimentally to foster diamond growth. Sulfides are common inclusions in diamonds, and metals are at least known. In the end, fluid/melt composition is likely to be important in facilitating or inhibiting diamond nucleation and perhaps in determining growth mechanism and crystal form. Although simplified systems are an insightful starting point, fluids and melts in the lithospheric mantle will react with silicate minerals in peridotite or eclogite, which can lead to a wide range of chemically diverse compositions as seen, for example, in fibrous diamonds.

In the convecting mantle below the lithosphere, diamond again will be the likely mineral form of free carbon. This region, which comprises the whole mantle above the core, has a silicate mineralogy that accommodates progressively higher pressure with depth. The olivine + orthopyroxene + clinopyroxene + garnet mineralogy of the lithospheric upper mantle gives way to a mineralogy dominated by wadsleyite + majoritic garnet in the transition zone and eventually aluminous silicate perovskite in the lower mantle (Harte, 2010; see figure 20). Because of the challenges of high-pressure experiments on these minerals, much of our current understanding comes from theoretical studies. The essential results of these numerous studies show that with increasing

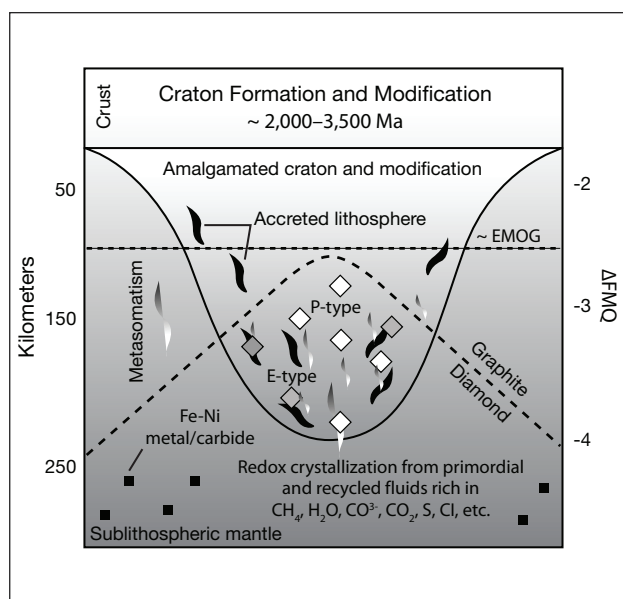


Figure 25. This model of diamond formation in the lithospheric mantle involves the introduction of volatile components from the deep mantle into the cratonic lithospheric mantle keel where diamonds can form. It was this type of process in the ancient past that led to widespread creation and storage of gem-quality diamonds that were subsequently sampled by much younger kimberlites.  $\Delta\text{FMQ}$  stands for the offset relative to the reduction-oxidation conditions specified by the fayalite-magnetite-quartz oxygen buffer, a measure of how strongly reducing or oxidizing a rock is. EMOG, an acronym for the reaction enstatite + magnesite = olivine + graphite, indicates a surface where, at lower pressure and higher oxidation than FMQ, diamonds cannot form in the mantle. Adapted from Shirey et al. (2013), with permission of the Mineralogical Society of America.

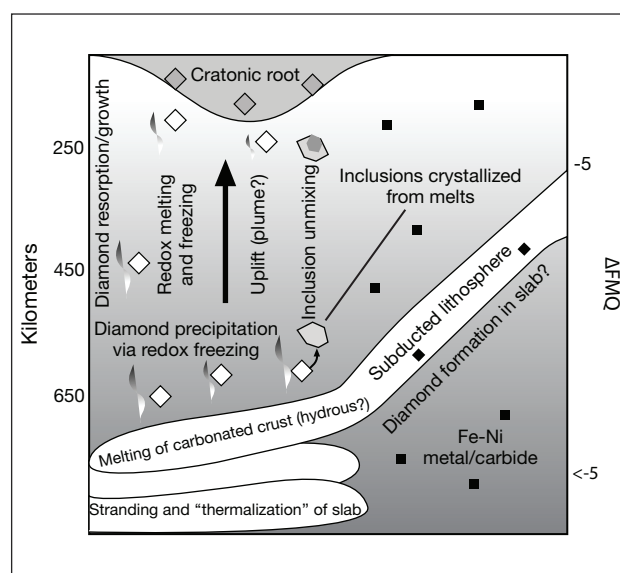
pressure,  $\text{Fe}_2\text{O}_3$  ( $\text{FeO}_{1.5}$ ) is stabilized in the structure of these minerals over FeO. The net effect is to bind oxygen more greatly within the silicate bulk mineralogy of the mantle, reducing the rest of the minerals. Thus, the deep upper mantle and the entirety of the transition zone and lower mantle are expected to be reducing, metal-saturated, and potentially diamond-forming—even more so than the lithospheric mantle.

As in the lithospheric mantle, diamond again will form in the compositional system carbon-oxygen-hydrogen from fluids that are  $\text{CH}_4$ - and  $\text{H}_2\text{O}$ -dominated in the transition zone and shallow lower mantle and will become  $\text{H}_2\text{O}$ -dominated in the deeper lower mantle (Frost and McCammon, 2008). At these incredibly high pressures, there is considerable storage capacity for hydrogen in the silicate minerals, which tends to suppress the existence of a free fluid and suggests that the carbon may be locked up in Fe(Ni) carbides (e.g.,

$\text{Fe}_3\text{C}$  and  $\text{Fe}_7\text{C}_3$ ; figure 26). These phases may be stable enough to accommodate the entire carbon budget of the deep mantle for normal mantle regions that are not anomalously carbon-rich. Rohrbach and Schmidt (2011) recently proposed that the subduction of carbonate or carbonated peridotite to transition zone depths and below are an important way to add carbon to the deep mantle. If this were to occur often enough, carbonate reduction via the mechanism just outlined would be a ready way to make diamond.

The thermodynamic and experimental observations described above permit a number of pathways for diamond crystallization, from a compositional range of fluids/melts. The compositional range of mineral and fluid inclusions found in diamonds likely attests to the importance of these pathways in nature, and perhaps involving both recycled and primordial carbon. What is clear from the range of mantle compositions is that diamond crystallization is an explicable and expected outcome of melt migration and mantle metasomatism. Future experiments will hopefully link sublithospheric inclusion mineralogy and trace-element composition to diamond fluid composition, deep mantle carbonate melt mi-

Figure 26. This model of superdeep diamond formation in the sublithospheric mantle involves introduction of volatile components into the deep mantle through subduction of carbonate-bearing, hydrated oceanic crust. The interaction of these fluids with the surrounding silicate mantle reduces the fluids and carbonate, triggering diamond formation. Adapted from Shirey et al. (2013), with permission of the Mineralogical Society of America.



gration, and mantle reducing/oxidizing conditions in a way that can be related to mantle convection patterns (e.g., Walter et al., 2008).

**Specific Mantle Geologic Settings.** From the data gathered on diamond ages within some cratons, patterns of age and mineral inclusion composition can be linked to broad-scale regional cratonic lithosphere evolution. The way diamonds form in the lithosphere is better understood if diamond formation pulses can be correlated with thermo-tectonic events for which there is independent evidence. The best examples where this correlation can be drawn are the Kaapvaal craton of southern Africa (box A) and the Slave craton of Canada. In both cases, suites of diamonds that form with initial craton stabilization can be distinguished from diamonds produced by later fluids added to the base of the mantle keel by underthrusting of oceanic slabs or upwelling plume magmatism.

**Correlation of Diamond Type with Geodynamic Processes.** The diamond record remains one of the prime ways to examine geodynamic processes on the broad scale from mantle depths while avoiding the later overprinting effects of magmatism and metasomatism. A compilation of all the ages determined on lithospheric diamonds to date (figure 27) shows a significant difference in age distribution between E- and P-types. As a result of the association of the E-type paragenesis with eclogite, this difference can be interpreted to record the first capture at three billion years of high-pressure basaltic rock in the mantle keel of the continents. This process would have been intimately associated with ocean basin closure and continental collision (a process of modern plate tectonics known as the Wilson Cycle), because the basalt would have been derived from the ocean floor as it was underthrust, and incorporated into a portion of the mantle keel that thickened during collision. The absence of E-type diamonds before this time suggests that the process did not occur earlier, and may mark a transition from a planet dominated by more vertical geodynamic processes of plumes, recycling, and poorer crustal preservation to one dominated by lateral tectonics, subduction, and more efficient crustal preservation. Independent evidence from geologic studies of exposed crustal rocks supports such a dramatic change.

This proposed change in geodynamics may have important implications for the nature of carbon-bearing fluids and their delivery to diamond-forming

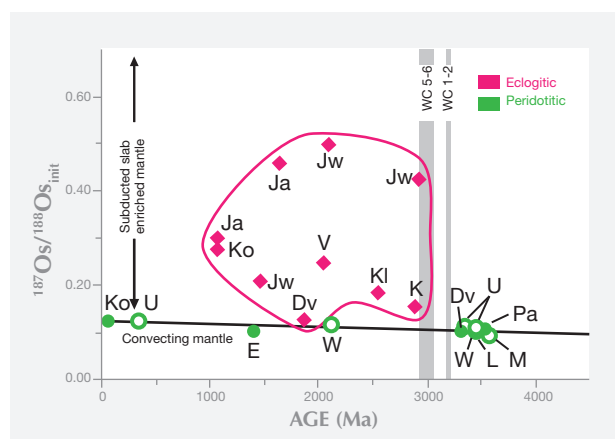


Figure 27. This figure illustrates the use of inclusions in diamonds to understand the onset of a global process. The absence of diamonds with E-type (eclogitic) inclusions in the oldest diamond populations suggests that something changed around 3,200 Ma to create and preserve diamonds with E-type inclusions. The letters refer to specific localities around the world (Pa = Panda, M = Murowa, L = Letseng, U = Udachnaya, W = Wellington, Dv = Diavik, K = Kimberley, Kl = Klip-springer, Jw = Jwaneng, V = Venetia, Ja = Jagersfontein, E = Ellendale, and Ko = Koffiefontein). Closed symbols are from many inclusion isochron ages, and open symbols are single inclusion model ages. Shirey and Richardson (2011) hypothesized that the change recorded was the onset of the major cycle of plate tectonics known as the Wilson Cycle (WC). The Wilson Cycle is comprised of the opening of an ocean basin (stages 1–2, thin gray band) and its closing (stages 5–6, thicker gray band), which culminates in continental collision. Global patterns in diamond composition, style of formation, and paragenesis hold great promise for understanding the earth's deep geologic processes. Adapted from Shirey and Richardson (2011), with permission of the American Association for the Advancement of Science.

depths in the mantle. Using subtle trends in the carbon isotopic composition of P-type diamonds, Stachel and Harris (2009) proposed that older specimens formed by methane oxidation and younger ones by carbonate reduction. If this observation is combined with the proposed onset of the Wilson Cycle, it could signify a change from the geodynamic processes that favor primary mantle devolatilization and/or the outgassing of recycled reduced fluids, to the geodynamic processes that favor carbonate recycling via slab subduction (Shirey et al., 2013).

Sublithospheric diamonds may be young enough to provide a unique way to follow the deepest parts of the mantle convection that drives current plate tectonics. Seismic studies, using a technique called

## BOX A: THE KAAPVAAL AND KIMBERLEY CRATONS

The Kaapvaal craton in southern Africa was assembled about three billion years ago from two independent continental blocks by continental collision that thrust oceanic lithosphere under the western block. Fluids and sulfur carried under the western block by the hydrated oceanic lithosphere percolated upward, triggering a major pulse of diamond formation at the time of collision. The surface distribution of diamond ages and types is a direct result of this process. Mines in the western block all contain three-billion-year-old E-type diamonds, which are absent in the eastern block.

Younger diamond formation in the Kaapvaal craton can be related to post-collisional events that modified the amalgamated cratonic block. In the center of the craton, igneous intrusion of the Bushveld Complex two billion years ago created the world's largest storehouse of chromium and platinum-group metals. The parental mafic-ultramafic melts, originating below the lithosphere, passed through it before filling the Bushveld magma chamber in the upper crust. As the melts passed through the lithosphere, they left behind basaltic components. These basaltic components (eclogitic at these pressures in the lithospheric mantle) can be detected at present through their lowered seismic velocities in the region of the lithospheric mantle below the Bushveld Complex. This region of the lithosphere correlates with a greater proportion of E- versus P-type silicate inclusions, a greater incidence of younger (Mesoproterozoic era) Sm-Nd inclusion ages, a greater proportion of diamonds with light carbon isotope compositions, and a larger proportion of higher nitrogen-containing diamonds. The likely explanation is that diamond-forming fluids equilibrated with the preexisting silicate mineralogy of the lithospheric mantle and incorporated the silicates as inclusions, retaining the mineralogical differences imparted by the sublithospheric magmatism of the Bushveld Complex. The ability of fluids to form diamonds under wider reducing/oxidizing conditions in eclogitic rocks explains the correspondence of E-type diamonds with the seismically slow region, because some fluids unable to form diamonds as they pass through peridotite can still form diamond once they encounter eclogite.

Subduction around the margin of the Kaapvaal craton was known to occur repeatedly (perhaps two to four times) throughout the Proterozoic era. Evidence for this is seen in the thermal and metamorphic history of rocks on the western and southern margins of the craton. The likely geometry of craton-margin subduction would have been to underthrust altered and thus fluid-rich oceanic lithosphere beneath the continental mantle lithosphere, allowing subduction-related fluids to invade the continental mantle lithosphere from below. Once these fluids encountered the reducing conditions of the continental mantle lithosphere, diamonds would form. Diamond mines in kimberlite that have penetrated such mantle lithosphere can sample multiple generations of diamonds.

In the rather small Archean craton on northern Australia known as the Kimberley craton, diamonds formed differently. Here, continental lithosphere did not remain stable, yet it was a good host for diamond formation. The Kimberley craton is surrounded by zones of deformed crustal rocks known as mobile belts. The deformation evident in the crustal rocks must extend through to the continental lithospheric mantle because the continental crust will have mantle keel attached. Many of the lamproites and kimberlites that penetrate these mobile belts are diamondiferous, including two lamproites rich enough to be economic, Ellendale and Argyle. Here, the timing of diamond formation matches some of the deformation in the mobile belts. Sulfide inclusions in Ellendale samples carry three-billion-year-old rhenium-osmium isotope signatures attesting to the presence of ancient continental mantle keel in the mobile belt and its ability to host diamond growth despite evident tectonic activity. Other examples of intra-cratonic domains of younger Proterozoic mobile belt or magmatic arc terrain containing diamonds must exist; the Yavapai-Mazatlal terrane southeast of the Wyoming craton, and the Buffalo Head terrane southeast of the Slave craton in North America, may be examples of the same phenomena. The idea that diamonds can form beneath the younger mobile belts surrounding the ancient cratonic nuclei opens up new tectonic settings for exploration and ties some diamond formation to deep continent-scale geologic processes.

mantle tomography, are able to image the subduction of oceanic lithospheric plates into the mantle transition zone (400–660 km depth), and in a few cases into the very top of the lower mantle (700–800 km). Mineral inclusions in sublithospheric diamonds from these depths can be grouped into those that have peridotite-like compositions, those that have basalt-like compositions (again, see figure 20), and those that are calcium-rich (Harte and Richardson, 2011).

The first two groups of inclusions are suggested to form in diamonds whose source fluids/melts may have been generated by dewatering the subducting oceanic lithospheric plate, whereas the third group is thought to be produced in association with carbonatitic melts generated from carbonated peridotite. In many cases, the basalt-like inclusions have compositions indicative of a surface origin and are housed in diamonds composed of a significant amount of re-



---

cycled carbon. The return of these minerals in kimberlite-erupted diamonds confirms the seismological evidence of subduction-recycling to the depth of the shallowest lower mantle (figure 26). Furthermore, association of some inclusions with carbonatite may suggest a connection between diamond formation in the deep mantle and the onset of plume initiation.

## SUMMARY OF THE GEOLOGY OF DIAMONDS

The past 25 years have seen scientific research answer many of the basic questions about gem-quality diamonds. For example, we now know that diamonds are old—in many cases nearly as old as the continental mantle keel in which they are stored. We can relate their age to the age of their hosts—in some cases distinguishing different generations of diamond-forming events.

We also know that diamonds form from fluids/melts whose composition and carbon speciation is controlled by the reduction-oxidation state of the rock through which they pass. We know that recycling of carbon may be essential, with the possibility that the recycled material may have changed through geologic time. Furthermore, the analytical tools exist to extend this knowledge and use diamonds as more sophisticated probes and tracers of deep mantle processes.

**New Perspectives on Diamond Geology.** Just as an enormous leap was made in the 1880s with the recognition that diamonds are found in kimberlite, recent advances have been made by putting together high-precision, high-resolution microanalyses of diamonds and their mineral inclusions, radiogenic and stable isotopes, geophysics, and the discovery of diamonds in unexpected new places. Clifford's Rule, the prospector's guideline that confines diamondiferous kimberlites to the Archean or oldest parts of the stable cratonic blocks of continental crust, worked well because of fortuitous geologic features. It is not only that the Archean was a special time to form diamonds—we have large numbers of samples formed in the Proterozoic. Rather, it is that in South Africa, the site of early geologically driven diamond prospecting, the craton was formed by an Archean continental collision that produced many diamonds at that time (figure 28). The collision made the mantle keel under the Archean crust deeper and more melt-depleted than the mantle keel under Proterozoic crust. Thus, it was just deep enough and reduced enough to receive much younger diamond-forming fluids created by subduction-related orogenic processes.

A new revelation, the result of dating both the diamonds and the depletion of their host mantle, is that diamond formation can appear associated with mobile belts, and that those intracratonic regions near Archean cratons may contain Archean mantle keel that was later *remobilized*. These could be ancient cratonic specimens that survived later tectonism in the mantle keel, or simply appear to be in a mobile belt because the latter was thrust onto the craton. A third possibility is that they could actually be younger diamonds formed from much older components. Indeed, the Argyle mine lies in just such a mobile belt, as do other very productive mines (e.g., Venetia) or diamond-rich localities (e.g., Sloan, Buffalo Head). Far from the simple correlation with just ancient crust, predicting where to look for diamonds must now include new thinking about the geologic evolution of the mantle lithosphere and the geologic sources of the diamond-forming fluids.

**Ubiquitous Diamonds.** Despite the rarity of gem-quality lithospheric diamonds in kimberlite and the rarity of kimberlite as a volcanic eruption, diamonds may not be as rare a mineral in deep sublithospheric mantle. The recent improvements in understanding the reduction-oxidation conditions of the deep mantle show that most of the mantle presents the right conditions for diamond to crystallize. In other words, diamonds should be ubiquitous. What typically keeps them from being more abundant is the lack of a geologic mechanism to put enough carbon in a free fluid/melt phase from which the diamond can crystallize. Where this can occur, diamonds will form. Another important aspect is that only a kimberlite (or lamproite) can bring them to the surface, so they may not be easily sampled from such depths. Diamonds may not be capable of surviving slow-ascending mantle plumes, and they certainly will be dissolved in the oxidizing magmas of basalt, alkali basalt, nepehelinite, and carbonatite that might be derived from them.

**Tracing the Carbon Cycle.** Diamond is recognized as the only material sampling the very deep mantle to depths exceeding 800 km, as shown in figures 25 and 26. Diamond is less useful at revealing deep carbon flux (the amount of carbon in motion) because it can provide only a small, variably distributed sample that is usually not directly related to its kimberlite host. Since we recognize diamond as deriving from a mobile carbon-bearing fluid/melt, it takes on new importance in tracking carbon mobility in the deep mantle via these fluids/melts. At the same time, di-

amond can be used to reveal mantle mineralogy and mantle reduction-oxidation state—actually exposing and preserving very tiny mantle minerals from these great depths. Through these mineral inclusions and the composition of the diamond, we have the unique ability to follow the path and history of the carbon from which it formed. Thus, diamond truly occupies a unique position in any discussion of the igneous and metamorphic aspects of the earth's carbon cycle.

## FUTURE RESEARCH

The advances of the last two decades have led to new conclusions about how diamonds crystallize and are stored in the mantle. We now know that they form from C-O-H-S fluids that flow through deep mantle rocks, especially in the lithosphere. These fluids transform the rocks by metasomatism while precipitating diamond. The reduction-oxidation state of the host rocks controls the diamond-forming reactions and can tie, locally and globally, geologic processes and mineral inclusion compositions to specific diamonds. Diamond has an internal growth morphology that records the chemical effects of this process and incorporates minerals during growth; this morphology can be used to study the deep mantle. Throughout the earth's history, diamonds formed by a multiplicity of reactions, rather than just one. Diamonds are potentially widespread in the mantle, as opposed to their scarcity in kimberlites and indeed the scarcity of kimberlites themselves. Formation could have taken place in recent geologic times, and may even be occurring now. The study of diamond provides a way to study deep mantle convection related to plate tectonics.

As scientists, we want to know the source of the carbon from which diamond is composed. Is it primordial or recycled? If the carbon is recycled, how does it get into the pressure and temperature regime of diamond growth from a low-T, perhaps even mobile phase? If the carbon is primordial, what does its presence and distribution tell us about how it was accreted into the earth and stored since the earliest times?

Nitrogen is the most abundant element in diamond after carbon. What is its chemical nature, and how is it partitioned between the diamond and its fluid during growth? When a diamond grows, is the isotopic composition of the carbon and nitrogen maintained or changed? Herein lies the key to using the isotopic composition of these two elements as important tracers of a diamond's geologic history.

Diamonds have long been grown by industrial processes, but we are just now capable of conducting geologically realistic growth experiments. How will the conditions of diamond growth relate to external morphological features or the incorporation of mineral components on the atomic scale, or the molecular makeup of the components in diamond-forming fluids?

In the deepest mantle, it is just now being understood that diamond formation may be related to highly mobile carbonatitic (CO<sub>3</sub>-dominant) magmas and regions where metal formation can remove the oxygen to leave reduced carbon ready for diamond crystallization. Could it be that diamond is an essential mineral link, not just an occasional participant in this aspect of the carbon cycle?

Diamond has a unique position as one of the earth's oldest preserved minerals. How have all these processes, especially the nature of diamond-forming reactions, changed with time? The answers to these questions await the discoveries of the next decade.

*Figure 28. Gem diamonds such as these, ranging in weight from 3.00 to 22.33 ct, result from unique geologic processes, adding to their desirability among today's jewelry consumers. Photo by Robert Weldon.*



## GLOSSARY

**Note:** Some of the definitions here are adapted from Neuendorf et al.'s *Glossary of Geology*, 5th edition (American Geological Institute, 2011).

**Accretion:** the process by which two continental masses collide and weld together, resulting in a larger continent.

**Adiabatic melting:** the melting of upward-moving mantle rocks as a result of depressurization, which leads to the formation of magmas.

**Alluvial:** a sorted or semi-sorted sediment deposited during comparatively recent geologic time by a stream or other moving body of water, and which occasionally contains concentrations of valuable minerals.

**Archean:** the earliest of the four principal divisions of geologic time, extending from 2.5 to about 3.8 billion years ago.

**Asthenosphere:** a part of the upper mantle below the lithosphere that is weak and capable of mobility, convection, and melting.

**Basalt:** a dark-colored, fine-grained igneous rock, composed mainly of plagioclase feldspar and pyroxene, that is formed by the solidification of magma near the earth's surface.

**Breccia:** a coarse-grained rock of sedimentary or igneous origin that is composed of angular rock fragments held together by a mineral cement or fine-grained matrix. *Brecciation* is the process of forming a breccia or the magma that crystallizes such a rock.

**Carbonatite:** a carbonate rock of magmatic origin.

**Continental crust:** the portion of the earth's crust that underlies the continents and continental shelves, ranging from about 35 to 60 km thick.

**Craton:** a large, ancient, and geologically stable portion of the continental lithosphere that has been little deformed for a prolonged period of geologic time. In diamond geology, a craton is the Archean portion of a much larger cratonic block, in which diamondiferous kimberlites are located on-craton. Non-diamondiferous kimberlites are located off-craton.

**Crust:** the earth's outermost layer or shell, consisting of the thicker continental crust and thinner oceanic crust.

**Dike:** a tabular intrusion of igneous rock that cuts across the bedding or structure of preexisting rocks.

**Eclogite:** a granular, ultramafic rock composed mainly of almandine-pyrope garnet and omphacite pyroxene that is formed by the metamorphism of basalts from the oceanic crust that have been subducted into the mantle.

**Emplacement:** referring to igneous rocks that intrude into a host rock or country rock, usually higher in the crust.

**Equilibrium:** a thermodynamic state where two minerals or components will not undergo further change at a given pressure and temperature.

**Exsolved:** when a mineral is crystallized directly in a solid host mineral, usually due to a decrease in pressure or temperature or both.

**Friable:** easily crumbled, as with a strongly weathered rock.

**Geothermal gradient:** the rate of increase of temperature with depth in the earth, with an average value of approximately 25°C per km.

**Geothermobarometer:** a pair of minerals whose chemical composition is temperature and pressure dependent, and which can be used to estimate the conditions under which the minerals formed.

**Glaciofluvial:** deposited by the streams or rivers flowing from glaciers.

**Grade:** a general term for ore content, in this case diamond abundance.

**Hybrid:** an igneous rock whose chemical composition results from assimilation of the country rock into a magma.

**Igneous:** a rock that solidified from molten or partially molten magma (the term is also applied to the geologic processes leading to or related to the formation of igneous rocks).

**Indicator minerals:** minerals that are geologically associated with diamonds but much more abundant, and which can be used to explore for diamond deposits.

**Island arc:** a curved chain of islands arising from the deep-sea floor that is the volcanic product of subduction.

**Kimberlite:** a hybrid, volatile-rich potassic ultramafic igneous rock composed principally of olivine, along with lesser amounts of phlogopite mica, diopside pyroxene, serpentine, calcite, garnet, ilmenite, and spinel. It can contain foreign rock fragments (xenoliths such as peridotite and eclogite) and crystals such as diamond (xenocrysts). Kimberlite is the chief host rock for commercial diamond mining.

**Lamproite:** a group of related dark-colored intrusive or extrusive igneous rocks that are rich in potassium and magnesium and characterized by minerals, including leucite, phlogopite, and feldspars. Diamondiferous varieties carry dominant olivine and lack feldspar.

**Lamprophyre:** a group of dark-colored intrusive igneous rocks characterized by a high percentage of mafic minerals (such as biotite mica, hornblende, and pyroxene) as larger crystals, set in a fine-grained groundmass composed of the same minerals plus feldspars or feldspathoids.

**Lithosphere:** the solid outer portion of the earth, consisting of the crust and upper mantle, that is approximately 100 km thick.

**Longshore (or littoral) current:** an ocean current caused by the approach of waves to a coastline at an angle so that it flows parallel and near to the shore.

**Macrodiamond:** a rough diamond that is more than 0.5 mm in diameter.

**Mafic:** a dark-colored igneous rock chiefly composed of iron- and magnesium-rich minerals.

**Magma:** molten material generated with the crust or upper mantle from which igneous rocks are derived by solidification, and that is capable of intrusion at depths in the crust or extrusion at the surface as lava or a pyroclastic ash flow.

**Magmatic:** related to or derived from magma.

**Mantle:** the zone between the earth's crust and core, consisting of a rigid lithosphere and an underlying asthenosphere of plastically flowing rock.

**Mantle keel:** the downward-protruding, thickened portion of the lithospheric mantle that resides under the continental crust of the craton, and which has had an extended period of attachment to the craton.

**Melt depletion:** an igneous process by which melt is removed, leaving a residual rock that is more refractory than the original starting composition.

**Metamorphism:** the process that causes mineralogical, chemical, or structural changes in solid rocks by exposing them to new pressure and temperature conditions by burial within the crust or mantle.

**Metasomatic:** formed by metasomatism, a geologic process that produces new minerals in an existing rock by replacement.

**Microdiamond:** a rough diamond less than 0.5 mm in diameter.

**Mid-ocean ridge:** a continuous chain of underwater mountains along the sea floor that mark the volcanic centers from which new oceanic crust is formed from magma being brought up by convection from the mantle. The solidified magma forms basalt, which spreads away along both sides of the ridge to form new oceanic crust.

**Mobile belt:** a long, relatively narrow crustal region of former tectonic activity.

**Mountain building (or orogeny):** the processes by which geologic structures in mountainous regions are formed. These processes include thrusting, folding, faulting, and (at depth) metamorphism and igneous intrusions.

**NAL:** Na- and Al-bearing mineral that occurs in basaltic-composition rocks subjected to pressures and temperatures equivalent to the top of the lower mantle (Harte, 2010).

**Nuclide:** a species of atom characterized by certain number of protons and neutrons in its nucleus.

**Oceanic crust:** the portion of the earth's crust that underlies the ocean basins, and that ranges in thickness from about 5 to 10 km.

**Peneplaned:** leveled to a quite flat surface by the sum of erosional geologic processes.

**Peralkaline:** a chemical classification of igneous rocks in which the molecular proportion of aluminum oxide is less than sodium and potassium oxides combined.

**Peridotite:** an ultramafic igneous rock composed of

olivine, orthopyroxene, clinopyroxene, and perhaps garnet, that is thought to be the most common and abundant rock type in the mantle.

**Phenocryst:** the large, conspicuous crystals set in a fine-grained groundmass in a porphyritic igneous rock.

**Placer:** a surface deposit consisting of valuable minerals that have been weathered out and then mechanically concentrated (normally by flowing water) in alluvial sediments.

**Plate tectonics:** a theory in which the lithosphere is divided into a number of thin, rigid crustal plates which move across the earth's surface and interact with one another at their boundaries along zones of tectonic and seismic activity.

**Plume:** an upwelling of molten rock that originates near the core-mantle boundary, and then rises upward through the mantle.

**Pyroclastic:** an igneous rock composed of angular rock fragments that originate from a volcanic explosion.

**Radioactive decay:** the spontaneous disintegration of the atoms of certain nuclides into other nuclides, which may be stable or undergo further decay until a stable nuclide is created.

**Regolith:** the fragmental and unconsolidated rock material which nearly everywhere forms the surface of the land and overlies the bedrock.

**Remobilized:** a once-molten igneous rock that has been remelted.

**Rifting:** a plate tectonic process that creates a zone where the lithosphere has ruptured due to extension.

**Subduction:** the process where one lithospheric plate descends beneath another plate.

**Superdeep:** an unusual type of diamond that originates at depths well below the base of the lithospheric mantle keel from within the convecting mantle.

**Surficial:** occurring at the earth's surface.

**Tectonic stability:** a region of the earth that is not undergoing active geologic processes such as volcanism, mountain building, subduction, faulting, or rifting. These regions have no or very few earthquakes.

**Thermal pulse:** a wave of heat passing through the crust carried by fluids or magma from below.

**Till:** an unsorted glacial deposit usually composed of finely ground rock flour, which may also contain dispersed, rounded cobbles or boulders.

**Ultramafic:** an igneous rock composed mainly of mafic minerals.

**Uplift:** a structurally high area in the crust that was produced by the raising or uplifting of rocks.

**Xenocryst:** a large crystal in an igneous rock that is foreign to the rock in which it occurs.

**Xenolith:** an inclusion of a foreign rock in an igneous rock.

## ABOUT THE AUTHORS

Dr. Shirey is a senior scientist in the Department of Terrestrial Magnetism of the Carnegie Institution in Washington, DC. He is one of the world's leading diamond geoscientists. Dr. Shigley is a distinguished research fellow at GIA in Carlsbad.

## ACKNOWLEDGMENTS

The authors are grateful for the advice and support of Duncan Pay, to John Koivula for the use of figure 2, and to three anonymous peer reviewers whose constructive criticism improved the manuscript.

## REFERENCES

- Anand M., Taylor L.A., Misra K.C., Carlson W.D., Sobolev N.V. (2004) Nature of diamonds in Yakutian eclogites: Views from eclogite tomography and mineral inclusions in diamonds. *Lithos*, Vol. 77, No. 1–4, pp. 333–348, <http://dx.doi.org/10.1016/j.lithos.2004.03.026>.
- Aulbach S., Shirey S.B., Stachel, T., Creighton S., Muehlenbachs K., Harris J.W. (2009) Diamond formation episodes at the southern margin of the Kaapvaal Craton: Re-Os systematics of sulfide inclusions from the Jagersfontein Mine. *Contributions to Mineralogy and Petrology*, Vol. 157, No. 4, pp. 525–540, <http://dx.doi.org/10.1007/s00410-008-0350-9>.
- Breeding C.M., Shigley J.E. (2009) The “type” classification system of diamonds and its importance in gemology. *G&G*, Vol. 45, No. 2, pp. 96–111, <http://dx.doi.org/10.5741/GEMS.45.2.96>.
- Bulanova G.P., Varshavsky A.V., Kotegov V.A. (2005) A venture into the interior of natural diamond; genetic information and implications for the gem industry. *Journal of Gemmology*, Vol. 29, No. 7–8, pp. 377–386.
- Bulanova G.P., Walter M.J., Smith C.B., Kohn S.C., Armstrong L.S., Blundy J., Gobbo L. (2010) Mineral inclusions in sublithospheric diamonds from Collier 4 kimberlite pipe, Juina, Brazil: subducted protoliths, carbonated melts and primary kimberlite magmatism. *Contributions to Mineralogy and Petrology*, Vol. 160, No. 4, pp. 489–510, <http://dx.doi.org/10.1007/s00410-010-0490-6>.
- Burgess R., Turner G., Harris J.W. (1992) <sup>40</sup>Ar–<sup>39</sup>Ar laser probe studies of clinopyroxene inclusions in eclogitic diamonds. *Geochimica et Cosmochimica Acta*, Vol. 56, No. 1, pp. 389–402, [http://dx.doi.org/10.1016/0016-7037\(92\)90140-E](http://dx.doi.org/10.1016/0016-7037(92)90140-E).
- Carlson R.W., Pearson D.G., James, D.E. (2005) Physical, chemical, and chronological characteristics of continental mantle. *Reviews of Geophysics*, Vol. 43, No. 1, p. 1001, <http://dx.doi.org/10.1029/2004RG000156>.
- Cartigny P. (2005) Stable isotopes and the origin of diamond. *Elements*, Vol. 1, No. 2, pp. 79–84, <http://dx.doi.org/10.2113/gselements.1.2.79>.
- Cartigny P., Marty B. (2013) Nitrogen isotopes and mantle geodynamics: The emergence of life and the atmosphere–crust–mantle connection. *Elements*, Vol. 9, No. 5, pp. 359–366, <http://dx.doi.org/10.2113/gselements.9.5.359>.
- Clifford T.N. (1966) Tectono-metallogenic units and metallogenic provinces of Africa. *Earth and Planetary Science Letters*, Vol. 1, pp. 421–434.
- Cookenboo H., Grütter H. (2010) Mantle-derived indicator mineral compositions as applied to diamond exploration. *Geochemistry: Exploration, Environment, Analysis*, Vol. 10, No. 1, pp. 81–95, <http://dx.doi.org/10.1144/1467-7873/09-220>.
- Dasgupta R. (2013) Ingassing, storage, and outgassing of terrestrial carbon through geologic time. *Reviews in Mineralogy and Geochemistry*, Vol. 75, No. 1, pp. 183–229, <http://dx.doi.org/10.2138/rmg.2013.75.7>.
- Day H.W. (2012) A revised diamond-graphite transition curve. *American Mineralogist*, Vol. 97, No. 1, pp. 52–62, <http://dx.doi.org/10.2138/am.2011.3763>.
- Dobrzhinetskaya L.F. (2012) Microdiamonds—Frontier of ultra-high-pressure metamorphism: A review. *Gondwana Research*, Vol. 21, No. 1, pp. 207–223, <http://dx.doi.org/10.1016/j.gr.2011.07.014>.
- Frost D.J., McCammon C.A. (2008) The redox state of Earth's mantle. *Annual Reviews of Earth Planetary Science*, Vol. 36, No. 1, pp. 389–420, <http://dx.doi.org/10.1146/annurev.earth.36.031207.124322>.
- Gudfinnsson G.H., Presnall D.C. (2005) Continuous gradations among primary carbonatitic, kimberlitic, melilititic, basaltic, picritic, and komatiitic melts in equilibrium with garnet lherzolite at 3–8 GPa. *Journal of Petrology*, Vol. 46, No. 8, pp. 1645–1659, <http://dx.doi.org/10.1093/petrology/egi029>.
- Gurney J.J., Helmstaedt H.H., Richardson S.H., Shirey S.B. (2010) Diamonds through time. *Economic Geology and the Bulletin of the Society of Economic Geologists*, Vol. 105, No. 3, pp. 689–712, <http://dx.doi.org/10.1093/petrology/egi029>.
- Haggerty S.E. (1999) A diamond trilogy; superplumes, supercontinents, and supernovae. *Science*, Vol. 285, No. 5429, pp. 851–860, <http://dx.doi.org/10.1126/science.285.5429.851>.
- Harlow G.E., Davies R.M. (2005) Diamonds. *Elements*, Vol. 1, No. 2, pp. 67–70, <http://dx.doi.org/10.2113/gselements.1.2.67>.
- Harte B. (2010) Diamond formation in the deep mantle; the record of mineral inclusions and their distribution in relation to mantle dehydration zones. *Mineralogical Magazine*, Vol. 74, No. 2, pp. 189–215, <http://dx.doi.org/10.1180/minmag.2010.074.2.189>.
- Harte B., Richardson S.H. (2011) Mineral inclusions in diamonds track the evolution of a Mesozoic subducted slab beneath West Gondwanaland. *Gondwana Research*, Vol. 21, No. 1, pp. 236–245, <http://dx.doi.org/10.1016/j.jgr.2011.07.001>.
- Hurley P., Rand J. (1969) Pre-drift continental nuclei. *Science*, Vol. 164, No. 3885, pp. 1229–1242, <http://dx.doi.org/10.1126/science.164.3885.1229>.
- Hutchison M.T., Dale C.W., Nowell G.M., Laiginhas F.A., Pearson D.G. (2012) Age constraints on ultra-deep mantle petrology shown by Juina diamonds. *10th International Kimberlite Conference, Bangalore*.
- Irifune T., Kurio A., Sakamoto S., Inoue T., Sumiya H., Funakoshi K.I. (2004) Formation of pure polycrystalline diamond by direct conversion of graphite at high pressure and high temperature. *Physics of the Earth and Planetary Interiors*, Vol. 143–144, pp. 593–600, <http://dx.doi.org/10.1016/j.pepi.2003.06.004>.
- Jordan T.H. (1979) The deep structure of the continents. *Scientific American*, Vol. 240, No. 1, pp. 92–107, <http://dx.doi.org/10.1038/scientificamerican0179-92>.
- Keller R.A., Taylor L.A., Snyder G.A., Sobolev V.N., Carlson W.D., Bezborodov S.M., Sobolev N.V. (1999) Detailed pull-apart of a diamondiferous eclogite xenolith: implications for mantle

- processes during diamond genesis. *Proceedings of the 7th International Kimberlite Conference*, Vol. 1, pp. 397–402.
- Kirkley M.B., Gurney J.J., Levinson A. (1991) Age, origin, and emplacement of diamonds. *G&G*, Vol. 27, No. 1, pp. 2–25, <http://dx.doi.org/10.5741/GEMS.27.1.2>.
- Kjarsgaard B.A. (2007) Kimberlite diamond deposits. In W.D. Goodfellow, Ed., *Mineral Deposits from Canada: A Synthesis of Major Deposit-Types, District Metallogeny, the Evolution of Geological Provinces, and Exploration Methods*. Geological Association of Canada, Special Publication No. 5, pp. 245–272.
- Kjarsgaard B.A., Levinson A. (2002) Diamonds in Canada. *G&G*, Vol. 38, No. 3, pp. 1–31, <http://dx.doi.org/10.5741/GEMS.38.3.208>.
- Kramers J.D. (1979) Lead, uranium, strontium, potassium and rubidium in inclusion-bearing diamonds and mantle-derived xenoliths from southern Africa. *Earth and Planetary Science Letters*, Vol. 42, No. 1, pp. 58–70, [http://dx.doi.org/10.1016/0012-821X\(79\)90190-0](http://dx.doi.org/10.1016/0012-821X(79)90190-0).
- Malarkey J., Pearson D.G., Kjarsgaard B.A., Davidson J.P., Nowell G.M., Ottley C.J., Stammer J. (2010) From source to crust: Tracing magmatic evolution in a kimberlite and a melilitite using microsample geochemistry. *Earth and Planetary Science Letters*, Vol. 299, No. 1–2, pp. 80–90, <http://dx.doi.org/10.1016/j.epsl.2010.08.020>.
- McClenaghan M.B., Kjarsgaard B.A. (2007) Indicator mineral and surficial geochemical exploration methods for kimberlite in glaciated terrain: Examples from Canada. In W.D. Goodfellow, Ed., *Mineral Deposits from Canada: A Synthesis of Major Deposit-Types, District Metallogeny, the Evolution of Geological Provinces, and Exploration Methods*. Geological Association of Canada, Special Publication No. 5, pp. 983–1006.
- Marty B., Alexander C.M.O., Raymond S.N. (2013) Primordial origins of Earth's carbon. *Reviews in Mineralogy and Geochemistry*, Vol. 75, No. 1, pp. 149–181, <http://dx.doi.org/10.2138/rmg.2013.75.6>.
- Mizukami T., Wallis S., Enami M., Kagi H. (2008) Forearc diamond from Japan. *Geology*, Vol. 36, No. 3, p. 219, <http://dx.doi.org/10.1130/G24350A.1>
- Navon O. (1999) Diamond formation in the earth's mantle. *Proceedings of the International Kimberlite Conference 7*, Vol. 2, pp. 584–604.
- Pearson D.G., Shirey S.B. (1999) Isotopic dating of diamonds. In D.D. Lambert and J. Ruiz, Eds., *Reviews in Economic Geology: Application of Radiogenic Isotopes to Ore Deposit Research and Exploration*. Society of Economic Geologists, pp. 143–171.
- Pearson D.G., Wittig N. (2008) Formation of Archaean continental lithosphere and its diamonds: the root of the problem. *Journal of the Geological Society of London*, Vol. 165, No. 5, pp. 895–914, <http://dx.doi.org/10.1144/0016-76492008-003>.
- Pearson D.G., Shirey S.B., Harris J.W., Carlson R.W. (1998) Sulphide inclusions in diamonds from the Koffiefontein kimberlite, S Africa; constraints on diamond ages and mantle Re-Os systematics. *Earth and Planetary Science Letters*, Vol. 160, Nos. 3/4, pp. 311–326, [http://dx.doi.org/10.1016/S0012-821X\(98\)00092-2](http://dx.doi.org/10.1016/S0012-821X(98)00092-2).
- Pearson D.G., Canil D., Shirey S.B. (2003) Mantle samples included in volcanic rocks: xenoliths and diamonds. In R.W. Carlson, Ed., *Treatise on Geochemistry: Vol. 2, The Mantle*. Elsevier, New York, pp. 171–277.
- Phillips D., Onstott T.C., Harris J.W. (1989) <sup>40</sup>Ar/<sup>39</sup>Ar laser-probe dating of diamond inclusions from Premier kimberlite. *Nature*, Vol. 340, No. 6233, pp. 460–462, <http://dx.doi.org/10.1038/340460a0>.
- Richardson S.H. (1986) Latter-day origin of diamonds of eclogitic paragenesis. *Nature*, Vol. 322, No. 6080, pp. 623–626, <http://dx.doi.org/10.1038/322623a0>.
- Richardson S.H., Gurney J.J., Erlank A.J., Harris J.W. (1984) Origin of diamonds in old enriched mantle. *Nature*, Vol. 310, No. 5974, pp. 198–202, <http://dx.doi.org/10.1038/310198a0>.
- Richardson S.H., Erlank A.J., Harris J.W., Hart S.R. (1990) Eclogitic diamonds of Proterozoic age from Cretaceous kimberlites. *Nature*, Vol. 346, No. 6279, pp. 54–56, <http://dx.doi.org/10.1038/346054a0>.
- Richardson S.H., Shirey S.B., Harris J.W., Carlson R.W. (2001) Archean subduction recorded by Re-Os isotopes in eclogitic sulfide inclusions in Kimberley diamonds. *Earth and Planetary Science Letters*, Vol. 191, No. 3–4, pp. 257–266, [http://dx.doi.org/10.1016/S0012-821X\(01\)00419-8](http://dx.doi.org/10.1016/S0012-821X(01)00419-8).
- Richardson S.H., Shirey S.B., Harris J.W. (2004) Episodic diamond genesis at Jwaneng, Botswana, and implications for Kaapvaal Craton evolution. *Lithos*, Vol. 77, Nos. 1–4, pp. 143–154, <http://dx.doi.org/10.1016/j.lithos.2004.04.027>.
- Ritsema J., van Heijst H., Woodhouse J. (2004) Global transition zone tomography. *Journal of Geophysical Research: Solid Earth*, Vol. 109, No. B2, 14 pp., <http://dx.doi.org/10.1029/2003JB002610>.
- Rohrbach A., Schmidt M.W. (2011) Redox freezing and melting in the earth's deep mantle resulting from carbon-iron redox coupling. *Nature*, Vol. 472, No. 7342, pp. 209–214, <http://dx.doi.org/10.1038/nature09899>.
- Russell J.K., Porritt L.A., Lavallée Y., Dingwell D.B. (2012) Kimberlite ascent by assimilation-fuelled buoyancy. *Nature*, Vol. 481, No. 7381, pp. 352–356, <http://dx.doi.org/10.1038/nature10740>.
- Shigley J.E., Chapman J., Ellison R. (2001) Discovery and mining of the Argyle diamond deposit, Australia. *G&G*, Vol. 37, No. 1, pp. 26–41, <http://dx.doi.org/10.5741/GEMS.37.1.26>.
- Shirey S.B., Richardson S.H. (2011) Start of the Wilson cycle at 3 Ga shown by diamonds from subcontinental mantle. *Science*, Vol. 333, No. 6041, pp. 434–436, <http://dx.doi.org/10.1126/science.1206275>.
- Shirey S.B., Richardson S.H., Harris J.W. (2004a) Age, paragenesis and composition of diamonds and evolution of the Precambrian mantle lithosphere of Southern Africa. *South African Journal of Geology*, Vol. 107, No. 1–2, pp. 91–106, <http://dx.doi.org/10.2113/107.1-2.91>.
- Shirey S.B., Richardson S.H., Harris J.W. (2004b) Integrated models of diamond formation and craton evolution. *Lithos*, Vol. 77, No. 1–4, pp. 923–944, <http://dx.doi.org/10.1016/j.lithos.2004.04.018>.
- Shirey S.B., Cartigny P., Frost D.J., Keshav S., Nestola F., Nimis P., Pearson D.G., Sobolev N.V., Walter M.J. (2013) Diamonds and the geology of mantle carbon. *Reviews in Mineralogy and Geochemistry*, Vol. 75, No. 1, pp. 355–421, <http://dx.doi.org/10.2138/rmg.2013.75.12>.
- Smit K.V., Shirey S.B., Richardson S.H., le Roex A.P., Gurney J.J. (2010) Re/Os isotopic composition of peridotitic sulphide inclusions in diamonds from Ellendale, Australia: Age constraints on Kimberley cratonic lithosphere. *Geochimica et Cosmochimica Acta*, Vol. 74, No. 11, pp. 3292–3306, <http://dx.doi.org/10.1016/j.gca.2010.03.001>.
- Sparks R.S.J., Baker L., Brown R.J., Field M., Schumacher J., Stripp G., Walters A. (2006) Dynamical constraints on kimberlite volcanism. *Journal of Volcanology and Geothermal Research*, Vol. 155, No. 1–2, pp. 18–48, <http://dx.doi.org/10.1016/j.jvolgeores.2006.02.010>.
- Stachel T., Harris J.W. (2008) The origin of cratonic diamonds, constraints from mineral inclusions. *Ore Geology Reviews*, Vol. 34, Nos. 1/2, pp. 5–32, <http://dx.doi.org/10.1016/j.oregeorev.2007.05.002>.
- (2009) Formation of diamond in the earth's mantle. *Journal of Physics: Condensed Matter*, Vol. 21, No. 36, 364206, <http://dx.doi.org/10.1088/0953-8984/21/36/364206>.
- Stachel T., Brey G.P., Harris J.W. (2005) Inclusions in sublithospheric diamonds: Glimpses of deep earth. *Elements*, Vol. 1, No. 2, pp. 73–78, <http://dx.doi.org/10.2113/gselements.1.2.73>.
- Stachel T., Banas A., Muehlenbachs K., Kurszlaukis S., Walker E.C. (2006) Archean diamonds from Wawa (Canada): Samples from deep cratonic roots predating cratonization of the Superior Province. *Contributions to Mineralogy and Petrology*, Vol. 151, No. 6, pp. 737–750, <http://dx.doi.org/10.1007/s00410-006-0090-7>.

Stachel T., Harris J.W., Muehlenbachs K. (2009) Sources of carbon in inclusion bearing diamonds. *Lithos*, Vol. 112, Supp. 2, pp. 625–637, <http://dx.doi.org/10.1016/j.lithos.2009.04.017>.

Tappert, R. Tappert, M.C. (2011) *Diamonds in Nature: A Guide to Rough Diamonds*. Springer Verlag, Heidelberg, Germany.

Tappert R., Foden J., Stachel T., Muehlenbachs K., Tappert M., Wills K. (2009) Deep mantle diamonds from South Australia: A record of Pacific subduction at the Gondwanan margin. *Geology*, Vol. 37, No. 1, pp. 43–46, <http://dx.doi.org/10.1130/G25055A.1>.

Walter M.J., Bulanova G.P., Armstrong L.S., Keshav S., Blundy J.D., Gudfinsson G., Lord O.T., Lennie A.R., Clark S.M., Smith C.B., Gobbo L. (2008) Primary carbonatite melt from deeply subducted oceanic crust. *Nature*, Vol. 454, No. 7204, pp. 622–625, <http://dx.doi.org/10.1038/nature07132>.

Walter M.J., Kohn S.C., Araujo D., Bulanova G.P., Smith C.B.,

Gaillou E., Wang J., Steele A., Shirey S.B. (2011) Deep mantle cycling of oceanic crust; evidence from diamonds and their mineral inclusions. *Science*, Vol. 334, No. 6052, pp. 54–57, <http://dx.doi.org/10.1126/science.1209300>.

Westerlund K.J., Shirey S.B., Richardson S.H., Carlson R.W., Gurney J.J., Harris J.W. (2006) A subduction wedge origin for Paleoproterozoic peridotitic diamonds and harzburgites from the Panda Kimberlite, Slave Craton: evidence from Re-Os isotope systematics. *Contributions to Mineralogy and Petrology*, Vol. 152, No. 3, pp. 275–294, <http://dx.doi.org/10.1007/s00410-006-0101-8>.

Woolley A.R., Bergman S.C., Edgar A.D., Le Bas M.J., Mitchell R.H., Rock N.M.S., Scott Smith B.H. (1996) Classification of lamprophyres, lamproites, kimberlites, and the kalsilitic, melilitic, and leucitic rocks. *The Canadian Mineralogist*, Vol. 34, pp. 175–186.



**For More on Diamond Geology**

Discover more about the fascinating world of diamond-related research at the Carnegie Institution of Washington, DC. *G&G's* exclusive online content gives you access to articles and video interviews, providing a rare view inside one of the world's leading geoscience research institutions.

Visit [www.gia.edu/gems-gemology](http://www.gia.edu/gems-gemology), or scan the QR code on the right.



# BLUE SAPPHIRES FROM THE BAW MAR MINE IN MOGOK

Hpone-Phyo Kan-Nyunt, Stefanos Karampelas, Klemens Link, Kyaw Thu, Lore Kiefert, and Pierre Hardy

In the last five years, fine Burmese blue sapphires from the Baw Mar area of Mogok have reached the market. The faceted stones typically show a strong pleochroism from greenish to violetish blue when viewed perpendicular and parallel to the *c*-axis, respectively, with medium to strong saturation and medium to dark tone. Most of the samples were relatively clean under the microscope, showing multiple twinning with whitish needle-like inclusions (presumably boehmite) at the intersections. Often, these inclusions were associated with stress tension fissures. Needles, most likely rutile, were found only occasionally, but small platelets and needle-like particles, probably ilmenite, appeared more frequently. Most of the stones contained surface-reaching open and healed fissures, but crystal inclusions of K-feldspar and mica (identified by Raman) were occasionally encountered. The sapphires also had a relatively high iron content, low gallium, and very low titanium. Their Ga/Mg ratio varied from 0.6 to 17. Their UV-Vis-NIR spectra displayed intense iron-related absorptions, and the FTIR absorption spectra presented mainly boehmite- and mica-related bands. Based on careful microscopic observations, combined with spectroscopic and chemical analysis, the sapphire from Baw Mar can, in most cases, be distinguished from the blue sapphire of other localities.

For several centuries, Burmese blue sapphires have been prized in the gemstone trade. Virtually all gem-quality blue sapphires from Burma (now Myanmar) have occurred in alluvial deposits along the Mogok Stone Tract. The previously described sapphires were mostly found at the Kyat Pyin area at Kyauk-Pyat-That, Kabaing, and Thurein-Taung (all west of Mogok) and at Chaung Gye in the north of Mogok (Gübelin and Koivula, 1986; Kiefert, 1987; Hughes, 1997; Themelis, 2008; Smith, 2010). In the last five years, blue sapphires with properties different from the “classic” Burmese sapphires, reportedly from the Baw Mar area of Mogok, have reached the market (figure 1).

The Baw Mar mining area is situated in the Kyat Pyin area, west of Mogok township (figure 2). In the past, the area yielded mostly low-quality sapphire from small-scale operations. Although several joint venture mines were reportedly operating in 1994, they did not produce enough quality material to stay open for any



Figure 1. The sapphires in this necklace, ranging in size from 2.4 to 6.7 ct, were reportedly produced in Baw Mar. This is one of the pieces that recently made its way to the Gübelin Gem Lab; some of the Baw Mar stones studied in the lab reached sizes up to 15 ct. Photo by Beryl Huber.

length of time. Only since 2008 has the area produced larger amounts of gem-quality blue sapphires.

See end of article for About the Authors and Acknowledgments.

GEMS & GEMOLOGY, Vol. 49, No. 4, pp. 223–232,

<http://dx.doi.org/10.5741/GEMS.49.4.223>.

© 2013 Gemological Institute of America



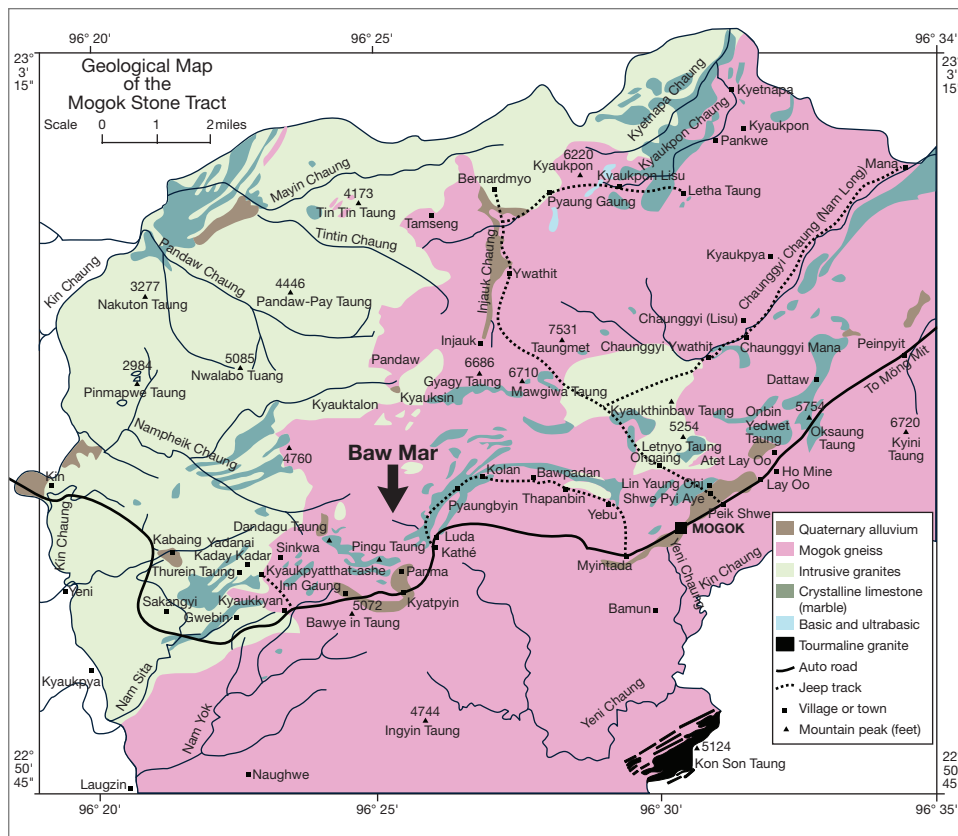


Figure 2. In this geological map of the Mogok Stone Tract, the black arrow marks the location of the Baw Mar mine. Adapted from Iyer (1953) and Hughes (1997).

In late 2012, one of the authors visited Mogok to collect stones directly from Baw Mar and other mines for the Gübelin Gem Lab (GGL) reference collection. After the recent opening of Mogok to foreigners, a larger group of GGL staff visited the area again in July 2013 to gain a better picture of the situation

Figure 3. Leucogranite (bottom) and a granitic pegmatite vein (coarser material in center) are seen in contact with weathered gneiss (top right). The width is approximately 1.2 meters. Photo by Kyaw Thu.



and to collect additional samples directly from the source. In August, November, and December 2013, another author revisited Mogok and the Baw Mar mine, and observed the rapid changes taking place. This paper gives a brief overview of the local geology of the Baw Mar area, describes the mining methods currently used, and presents the microscopic, chemical, and spectroscopic features of its blue sapphire.

### GEOLOGY AND CURRENT MINING METHODS

The Baw Mar mining site is situated in the northwest of Kyat Pyin township, 12 miles west of Mogok, at 22°54'37.60"N, 96°24'55.02"E. Similar to the rest of the Mogok Stone Tract, the area has a complex geology (figure 2). It is mainly composed of high-grade regionally metamorphosed rocks, garnet-biotite gneiss, calc-silicate rocks, and graphite marble (Kyaw Thu, 2007). Non-sapphire-bearing leucogranite dikes and granitic pegmatite veins intruded into weathered gneiss, which can be seen at ground level in exposed rock surfaces (figure 3). The recently mined area also shows exposed leucogranite in contact with syenite boulders. The high-quality blue sapphire is retrieved from this syenite, which, like the pegmatite, has intruded into weathered gneiss, as well as from pockets formed at the exposed leucogranite. These last sapphires are embed-

ded in clay lenses (feldspar altered to kaolinite) and are surrounded by biotite mica and chlorite (figure 4). Prospecting is done by local geologists.

The Baw Mar mine (figure 5), equipped with heavy machinery and an in-house sorting and cutting plant, is a more efficient producer than other private operations within the Mogok mining area. The Baw Mar mine combines open-pit mining, as in figure 5 (top), with tunneling. A 10–20 meter layer of overburden is removed by bulldozers and excavators (figure 6, left). Laborers work the exposed gemstone-

## In Brief

- Blue sapphire recently mined from the Baw Mar area in Mogok, Myanmar, exhibited chemical composition that differed from “classic” Burmese blue sapphire.
- Unlike traditional Burmese blue sapphire, the Baw Mar samples were relatively free of inclusions, occasionally displaying whitish needle-like inclusions of boehmite.
- The Baw Mar sapphire showed impurity contents comparatively high in iron, relatively low in gallium, very low in titanium, and wide-ranging Ga/Mg ratios that reflect the geological conditions of the area.

bearing layer of gravel, called *byone*, which is about 2 to 3 meters thick. The gravel is then transported by water to the washing plant (figure 6, right).

At the end of the tunnels, which can reach a depth of 80 meters (figure 7), miners use a drill to bore small holes in the rock face, and then crack the weathered






































*Figure 4. A sapphire-bearing clay pocket in a highly weathered and brecciated skarn zone. The pocket is approximately 60 cm long. Photo by Kyaw Thu.*



*Figure 5. Top: A panoramic view of the Baw Mar mine in August 2013. The small huts mark the entrance to the underground shafts. Bottom: In November 2013, the shafts were closed and the rock largely removed in order to reach lower sapphire-bearing levels. Photos by Kyaw Thu.*

rock in between the holes with a jackhammer to collect the material. The rock is relayed in bags to other miners. The material is hoisted to the surface, then transported down to the washing plant. Water pumps powered by generators simultaneously keep the tunnels from flooding and supply the washing operation. At the washing plant (figure 8), the collected gem-bearing gravels are packed into drums and transported to the sorting plant, where the gem-quality sapphires are sorted using sieves with different mesh sizes. Afterward, cutters trim off the non-gem-quality parts. The sapphires are then cut and polished onsite (figure 9). The polished sapphire sizes range up to 15 carats. The entire operation, including mining, sorting, and cutting, employs about 300 miners and workers.

**TABLE 1.** Weight, shape, and photos of the studied samples.<sup>a</sup>

Sample number	Weight (ct)	Shape		Sample number	Weight (ct)	Shape	
SABUM161	1.630	Cushion		SABUM180	0.447	Round	
SABUM162	1.270	Oval		SABUM184	0.325	Oval	
SABUM163	1.037	Cushion		SABUM191	0.306	Cushion	
SABUM164	0.863	Oval		SABUM192	0.330	Round	
SABUM165	0.716	Oval		SABUM194	0.288	Oval	
SABUM166	0.547	Cushion		SABUM195	0.308	Oval	
SABUM167	0.531	Cushion		SABUM196	0.289	Oval	
SABUM168	0.565	Cushion		SABUM197	0.257	Oval	
SABUM169	0.453	Cushion		SABUM198	0.199	Oval	
SABUM170	0.443	Round		SABUM200	0.305	Oval	
SABUM171	1.038	Cushion		SABUM204	0.892	Triangular	
SABUM172	0.431	Oval		SABUM282	7.323	Cushion, cabochon	
SABUM173	0.332	Oval		SABUM284	1.294	Cushion	
SABUM174	0.708	Oval		SABUM285	0.897	Cushion	
SABUM175	0.448	Oval		SABUM286_1	0.162	Rough	
SABUM176	0.480	Oval		SABUM286_2	0.240	Rough	
SABUM177	0.314	Oval		SABUM286_3	0.403	Rough	
SABUM178	0.321	Oval		SABUM287	0.847	Rough	
SABUM179	0.452	Oval					

<sup>a</sup>“SABUM” is the Gübelin Gem Lab’s acronym for “Sapphire BURma Mogok.”



Figure 6. Left: Miners use excavators to remove gem-bearing overburden gravels. Right: The gravels are transported downstream to the washing plant using water supplied by the pipes. Photos by Hpone-Phyo Kan-Nyunt.

## MATERIALS AND METHODS

For the initial study, 30 unheated and faceted blue sapphires, ranging in size from 0.20 to 1.63 ct, were analyzed (table 1). One of the authors obtained the faceted samples directly from the miners at the source. Additional samples, including two faceted sapphires (SABUM284 and SABUM285), a 7.32 ct cabochon (SABUM282), and a rough sapphire lot, were collected from the mining operation for confirmation of the initial data. The rough material was gathered directly

from the washing plant by the authors. Four rough sapphires were ultimately used in this study, ranging in size from 0.16 to 0.84 ct (SABUM286\_1, SABUM286\_2, SABUM286\_3, and SABUM287).

Standard gemological instruments were used to observe the samples' long- and short-wave UV fluorescence reactions (6W lamps emitting at 365 and 254 nm, respectively) and to measure their refractive index, birefringence, and pleochroism. Specific gravity was determined hydrostatically with an electronic balance.



Figure 7. These photos show part of the shaft system of the Baw Mar mine (left) and horizontal development of the tunnel (right). Photos by Hpone-Phyo Kan-Nyunt.



Figure 8. In this washing plant, gem gravel is concentrated and placed in drums. Photo by Daniel Nyfeler.

Internal features were examined using various gemological microscopes.

Energy-dispersive X-ray fluorescence (EDXRF) analyses were carried out at GGL with a Thermo Scientific ARL Quant'X. Sample holders with an aperture of 5 mm diameter were used, and specific sets of

parameters were optimized for the most accurate analysis of corundum. Various conditions were used for filters and voltage (no filter/4 kV, cellulose/8kV, aluminum/12kV, thin palladium/16 kV, medium palladium/20kV, thick palladium/28kV, and thick copper/50kV), with an acquisition time of about 40 minutes for each sample. Twelve samples were analyzed by laser ablation-inductively coupled plasma-mass spectrometry (LA-ICP-MS). All analyses were performed on a Perkin Elmer ELAN DRC-e single collector quadrupole mass spectrometer combined with a 193 nm ESI Excimer gas laser ablation system. A set of three single-spot analyses (120  $\mu\text{m}$  diameter) was collected on each sample using a laser frequency of 10 Hz and an ablation time of 50 seconds at a laser energy of 6.2 J/cm<sup>2</sup>. The mass spectrometer performance was optimized to maximum intensities at U/Th ratios of ~1 and ThO/Th < 0.3 using 16.25 liters per minute (L/min) Ar plasma gas, 0.88 L/min argon as nebulizer gas and 1 L/min helium as sample gas. Multi-element NIST610 was the glass standard used for external calibration; internal calibration was done by normalizing to 100% cations of stoichiometric corundum. The data reduction was carried out using an in-house spreadsheet following Longrich et al. (1996).



Figure 9. Top left: The sapphires from Baw Mar are sorted into different sizes and qualities. Some of the larger pieces can reach over 20 cm in length. Top right: The non-gem-quality portion of the rough is clipped off. Bottom left: After clipping, stones like the one here are left for faceting. Bottom right: Performing sapphire from Baw Mar. Photos by Lore Kiefert (top left), Daniel Nyfeler (bottom left), and Hpone-Phyo Kan-Nyunt (top and bottom right).

Polarized absorption spectra in the 200–1500 nm range were recorded using a Cary 5000 ultraviolet/visible/near-infrared (UV-Vis-NIR) spectrometer with diffraction grating polarizers. The data sampling interval and spectral bandwidth of each measurement were set at 0.5 nm and a scan rate of 150 nm/min. FTIR absorption spectra were acquired between 6000 and 400  $\text{cm}^{-1}$ , using a Varian 640 FTIR spectrometer with 4  $\text{cm}^{-1}$  resolution and 64 scans (background spectra were collected using the same parameters). A Renishaw Raman System 1000 spectrometer, coupled with a Leica DMLM optical microscope, was used to characterize accessible inclusions. Unpolarized and unoriented spectra were recorded using 514 nm argon ion laser excitation at 10 mW in standard mode (with 20 $\times$  magnification), from 200 to 2000  $\text{cm}^{-1}$  (three cycles with an acquisition time of 30 seconds) at approximately 1.5  $\text{cm}^{-1}$  resolution. Rayleigh scattering was blocked by a holographic notch filter; the backscattered light was dispersed on an 1800 groove/mm holographic grating with the slit width set at 50  $\mu\text{m}$ .

## RESULTS AND DISCUSSION

Most of the samples were pleochroic, from greenish to violetish blue, with medium to strong saturation and medium to dark tone. With the exception of the less saturated sapphires, the samples exhibited their deeper blue pleochroic color parallel to the c-axis (o-ray). Consistent gemological properties included RI ( $n_o=1.760\text{--}1.764$ ,  $n_e=1.768\text{--}1.772$ ), birefringence (0.008), and SG (3.96–4.01). All samples were inert to long- and short-wave UV radiation.

Figure 10. Strong polysynthetic twinning in SABUM 163, causing color zoning. Photomicrograph by Hpone-Phyo Kan-Nyunt; magnified 30 $\times$ .

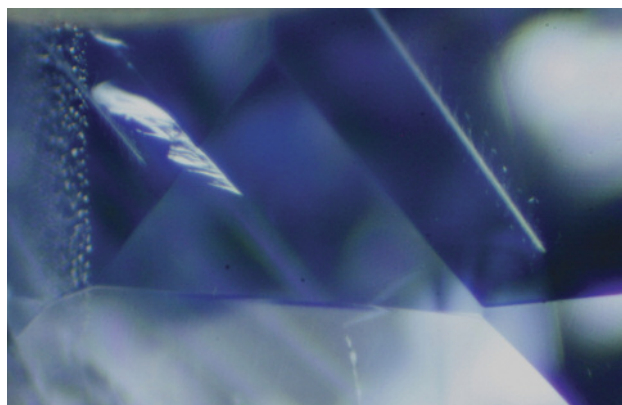
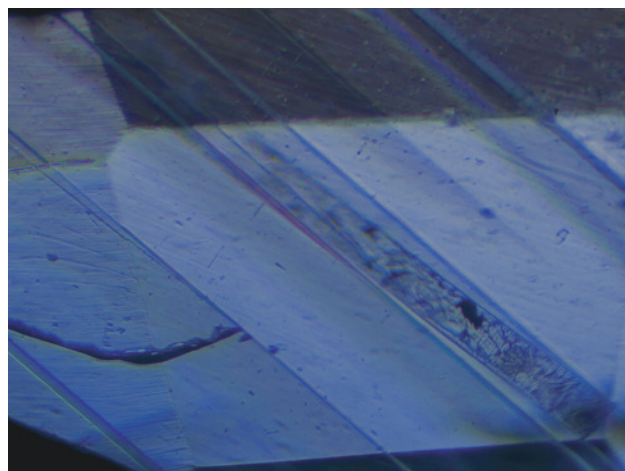


Figure 11. Needles, presumably of boehmite, associated with stressed tension fissures at the intersection of twin planes in SABUM163. Photomicrograph by Hpone-Phyo Kan-Nyunt; magnified 25 $\times$ .

Microscopic observation demonstrated that the samples were relatively free of inclusions, occasionally showing strong polysynthetic twinning (as in figure 10), in two or three directions parallel to the rhombohedral face  $r$   $\{10\bar{1}1\}$ . The twinning is associated with parallel “needle-like” deposits, presumably of boehmite, at the intersections of two sets of twin planes, or in three directions nearly perpendicular to each other when three sets of twin planes were present, often associated with small fissures along these “needles” (figure 11). Also observed were even color zoning; healed fissures consisting of fine negative crystals that can be seen in figure 12; fine reflective platelets (figure 13); brownish irregular needles, as in figures 14 and 15, that are presumably ilmenite; and only rarely a few short needles, exhibited in figure 15,

Figure 12. Healed fissure consisting of negative crystals in SABUM169. Photomicrograph by Hpone-Phyo Kan-Nyunt; magnified 25 $\times$ .



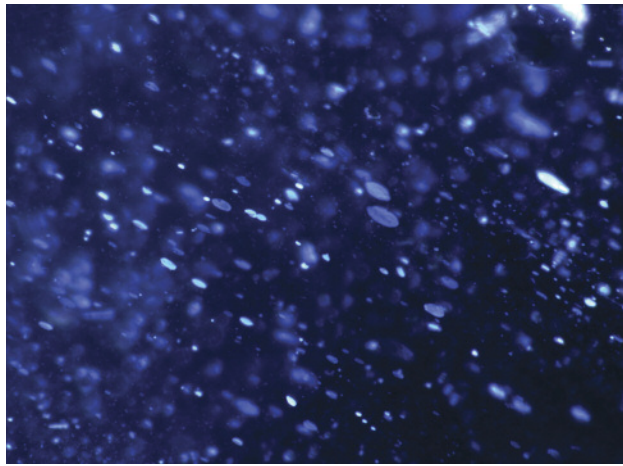


Figure 13. Reflective minute particles and platelets in SABUM161. Photomicrograph by Pierre Hardy; magnified 120x.

that are most likely rutile. Seldom were crystal inclusions observed; sample SABUM285, shown in figure 16, is such an example. The samples often showed reflective open fissures as well as open fissures with epigenetic material, as seen in figure 17. Unlike Mogok sapphires described in the past, where rutile needles and crystal inclusions such as zircons, apatite, plagioclase, and phlogopite mica are often encountered (Gübelin and Koivula, 1986; Kiefert, 1987; Hughes, 1997; Themelis, 2008; Smith, 2010), only a few samples from Baw Mar contained short rutile needles and crystal inclusions. Using Raman spectroscopy, these inclusions were identified as mica and K-feldspar (see Tlili et al., 1989 and Freeman et al., 2008, respectively).

Figure 14. Irregular needle-like particles in SABUM284, probably ilmenite. Photomicrograph by Pierre Hardy; magnified 60x.

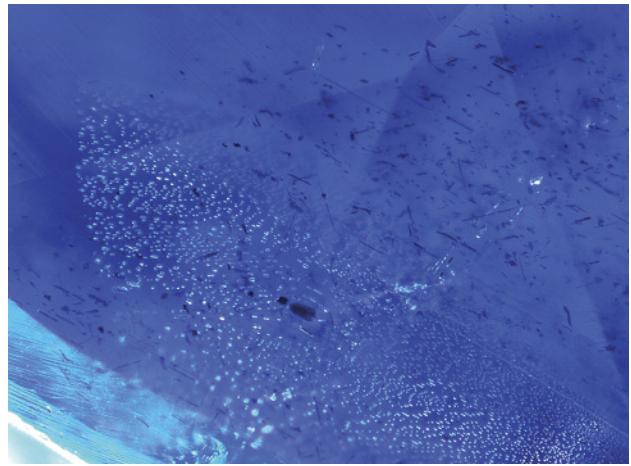
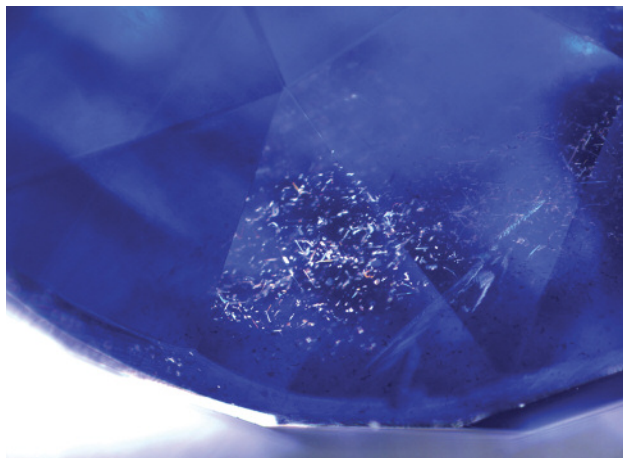
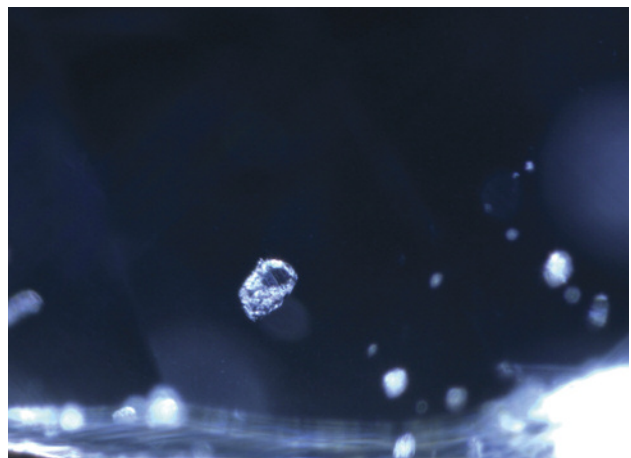


Figure 15. Short needles, probably rutile, and some irregular needles, most likely ilmenite, in SABUM 166. Photomicrograph by Pierre Hardy; field of view: 2 mm.

EDXRF chemical analysis of the major and minor elements of 30 samples revealed Fe between 1000 and 6800 ppmw, with an average of 4400 ppmw. Ga ranged between 45 and 180 ppmw, with an average of 110 ppmw. The Ti values were relatively low, from below EDXRF's detection limit (in nine samples) to 140 ppmw, with an average of 30 ppmw. All other measured elements (V, Cr, Mg, Mn, Nb, Zr, Sn, and Pb) were below detection limit (bdl). LA-ICP-MS analysis of 12 samples revealed  $^{57}\text{Fe}$  from 900 to 4500 ppmw,  $^{71}\text{Ga}$  from 35 to 115 ppmw,  $^{49}\text{Ti}$  from 15 to 115 ppmw,  $^{25}\text{Mg}$  from 5 to 80 ppmw, and  $^{51}\text{V}$  from 0.5 to 50 ppmw. All the other measured elements ( $^7\text{Li}$ ,  $^8\text{Be}$ ,  $^{44}\text{Ca}$ ,  $^{45}\text{Sc}$ ,  $^{59}\text{Co}$ ,  $^{62}\text{Ni}$ ,  $^{65}\text{Cu}$ ,  $^{66}\text{Zn}$ ,  $^{73}\text{Ge}$ ,  $^{85}\text{Rb}$ ,  $^{88}\text{Sr}$ ,  $^{89}\text{Y}$ ,  $^{90}\text{Zr}$ ,  $^{93}\text{Nb}$ ,  $^{118}\text{Sn}$ ,  $^{133}\text{Cs}$ ,  $^{137}\text{Ba}$ ,  $^{139}\text{La}$ ,  $^{140}\text{Ce}$ ,  $^{181}\text{Ta}$ ,  $^{182}\text{W}$ ,  $^{195}\text{Pt}$ , and

Figure 16. K-feldspar crystal in SABUM285 identified by Raman spectroscopy. Photomicrograph by Pierre Hardy; magnified 100x.



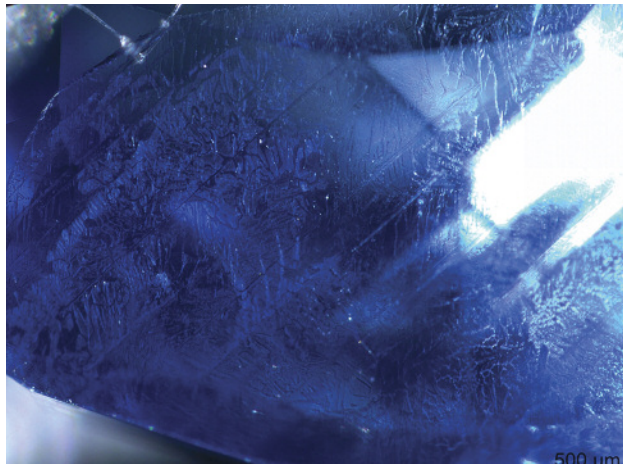


Figure 17. Epigenetic material on an open fissure in SABUM179. Photomicrograph by Pierre Hardy; magnified 60x.

$^{232}\text{Th}$ ) were bdl. The  $^{53}\text{Cr}$ ,  $^{55}\text{Mn}$ ,  $^{23}\text{Na}$ , and  $^{208}\text{Pb}$  levels were also generally bdl and rarely slightly above. The Ga/Mg ratio was used to differentiate blue sapphires of different geological origin. For example, Ga/Mg > 10 suggests “magmatic” origin, whereas Ga/Mg < 10 suggests “metamorphic” origin (Peucat et al., 2007). Within the studied samples, the Ga/Mg ratio varied from 0.6 to 17; this further confirms the complicated geological origin of the blue sapphires from this area. Slight differences between the element concentrations measured with EDXRF and LA-ICP-MS are probably due to different measurement areas (smaller for LA-ICP-MS), different detection limits (much lower detection limit for LA-ICP-MS), as well as some inclusion effects.

Figure 18 shows polarized UV-Vis-NIR spectra in the 250–1000 nm range for sample SABUM282. Most other samples presented very similar spectra. We observed the  $\text{Fe}^{3+}$ -related series of bands in the violet and blue areas of the spectrum, between 370 and 490 nm, which had relatively high intensity (Ferguson and Fielding, 1971; Eigenmann et al., 1972; Schmetzer, 1987). A cutoff above 300 nm and an intense shoulder in the UV region at around 340 nm were also observed. The larger samples showed a cutoff at around 340 nm, because the iron-related feature there saturated the spectrophotometer detector due to the longer beam path. The large bands absorbing from green to the near-infrared were due to  $\text{Fe}^{2+}\text{-Ti}^{4+}$  and  $\text{Fe}^{2+}\text{-Fe}^{3+}$  pairs (Ferguson and Fielding, 1971; Schmetzer, 1987). All the samples showed similar spectra. Unlike classic Burmese sapphires, the samples from Baw Mar contain high  $\text{Fe}^{3+}$  UV-Vis absorption peaks in the violet and blue; most also show an intense shoulder in the UV region at ~340 nm, as seen in fig-

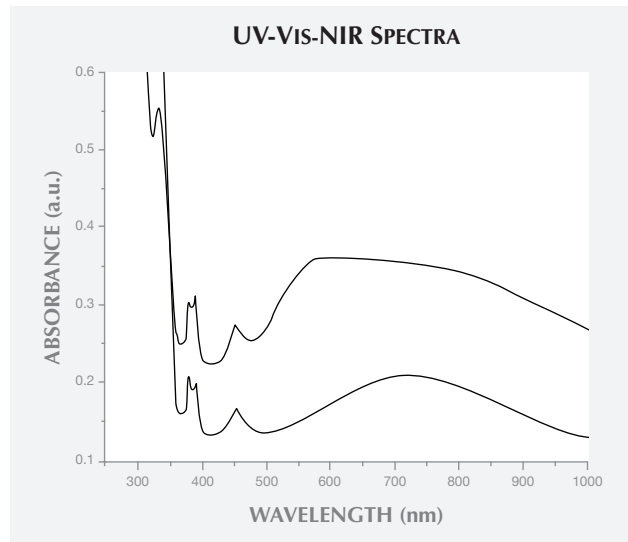
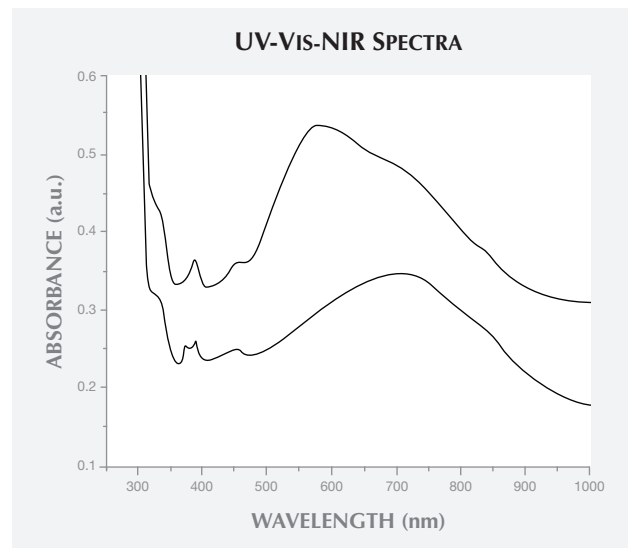


Figure 18. The polarized UV-Vis-NIR spectra from 250 to 1000 nm of sample SABUM282 show pronounced bands related to Fe (in the violet and blue) and a  $\text{Fe}^{2+}/\text{Fe}^{3+}$  pair (in the near infrared), as well as less-intense bands (in the green) due to  $\text{Fe}^{2+}/\text{Ti}^{4+}$  pairs. The spectra are normalized to a millimeter thickness. The top spectrum (o-ray) is offset by 0.1 absorbance units for clarity.

ure 19 (Hänni, 1994). The intensity of  $\text{Fe}^{2+}/\text{Fe}^{3+}$  bands situated in the near-infrared area varies greatly, and can in some cases be mistaken for the spectra of basaltic sapphires (Kiefert, 1987).

Figure 19. The polarized UV-Vis-NIR spectra from 250 to 1000 nm of a “classic” Burmese blue sapphire are different from those of Baw Mar blue sapphire. The spectra are normalized to a millimeter thickness. The top spectrum (o-ray) is offset of 0.1 absorbance unit for clarity.





Unpolarized FTIR spectra of some samples present multiple series of bands above 3000 cm<sup>-1</sup>, probably due to hydrous mineral inclusions such as mica and boehmite (Smith, 1995; Beran and Rossman, 2006). Many of the samples we studied did not show bands in this region, however. Raman spectra of the few rare crystal inclusions observed were consistent with mica and K-feldspar.

## CONCLUSION

Blue sapphires collected from the Baw Mar mine in Mogok showed properties distinctly different from those associated with “classic” Mogok blue sapphires. The Baw Mar samples, which are formed in syenite which intruded into weathered gneiss, as well as from pockets formed at the exposed leucogranite, typically exhibit greenish to violetish blue colors. They are often free of inclusions, sometimes with twinning in multiple directions and needles (most likely boehmite) at the intersections of the twin planes. They also exhibit

small platelets, healed and open fissures, irregular needles that are most likely ilmenite and, rarely, short needles that are probably rutile. The few crystal inclusions were identified as K-feldspar and mica by micro-Raman analysis. Their UV-Vis-NIR spectra are different from the inclusions of classic Mogok blue sapphires, with high iron-related bands; as a result, they are sometimes confused with basaltic blue sapphires. Chemical analysis also shows relatively high iron, low gallium, very low titanium contents, and Ga/Mg ratios that strongly vary from sample to sample. The presence of boehmite and mica bands is confirmed by FTIR. Additional research is underway on the Baw Mar sapphire geological formation, as well as on classic Burmese blue sapphires and similar-looking material from other mines worldwide. This research will shed further light on the positive identification of samples from this mine, as well as increase understanding of the differences observed in blue sapphire from other localities.

### ABOUT THE AUTHORS

*Hpone-Phyo Kan-Nyunt (hpone.phyo@gubelingemlab.com)* is lab manager at the Gübelin Gem Lab in Hong Kong. *Dr. Karampelas (stefanos.karampelas@gubelingemlab.com)* is a scientific researcher. *Mr. Link* is a research analyst, *Dr. Kiefert* the chief gemologist, and *Mr. Hardy* a gemologist at the Gübelin Gem Lab in Lucerne, Switzerland. *Kyaw Thu* is a gemologist at Macle Gem Lab, Yangon, Myanmar.

### ACKNOWLEDGMENTS

*We would like to express our deep gratitude to the people of Mogok for their guidance and constructive criticism in the field. In particular, the authors are grateful to Mr. Kyaw Swar from AGGL Gem Lab in Yangon for his assistance and sharing insightful knowledge during the field trip, as well as to the local contact, Mr. Yae Myo Aung, for his support and arrangements throughout the visit.*

## REFERENCES

- Beran A., Rossman G.R. (2006) OH in naturally occurring corundum. *European Journal of Mineralogy*, Vol. 18, No. 4, pp. 441–448, <http://dx.doi.org/10.1127/0935-1221/2006/0018-0441>.
- Eigenmann K., Kunz K., Günthard H. (1972) The optical spectrum of  $\alpha$ -Al<sub>2</sub>O<sub>3</sub>:Fe<sup>3+</sup>. *Chemical Physics Letters*, Vol. 13, No. 1, pp. 54–57, [http://dx.doi.org/10.1016/0009-2614\(72\)80041-1](http://dx.doi.org/10.1016/0009-2614(72)80041-1).
- Ferguson J., Fielding P.E. (1971) The origins of the colours of natural yellow, green, and blue sapphires. *Chemical Physics Letters*, Vol. 10, No. 3, pp. 262–265, [http://dx.doi.org/10.1016/0009-2614\(71\)80282-8](http://dx.doi.org/10.1016/0009-2614(71)80282-8).
- Freeman J.J., Wang A., Kuebler K.E., Jolliff B.L., Haskin L.A. (2008) Characterization of natural feldspars by Raman spectroscopy for future planetary exploration. *The Canadian Mineralogist*, Vol. 46, No. 6, pp. 1477–1500, <http://dx.doi.org/10.3749/canmin.46.6.1477>.
- Gübelin E.J., Koivula J.I. (1986) *Photoatlas of Inclusions in Gemstones*, Opinio Verlag, Basel, Switzerland, 532 pp.
- Hänni H.A. (1994) Origin determination for gemstones: Possibilities, restrictions, and reliability. *Journal of Gemmology*, Vol. 24, No. 3, pp. 139–148.
- Hughes R.W. (1997) *Ruby & Sapphire*. RWH Publishing, Boulder, CO, 512 pp.
- Iyer L.A.N. (1953) The geology and gemstones of the Mogok Stone Tract, Burma. *Memoirs of the Geological Survey of India*, Vol. 82, 100 pp.
- Kiefert L. (1987) Mineralogical investigations for the characterization and differentiation of natural and synthetic sapphires. MSc thesis, Mineralogic-Petrographic Institut of the University of Heidelberg, 203 pp.
- Kyaw Thu (2007) The igneous rocks of the Mogok Stone Tract: Their distribution, petrography, petrochemistry, sequence, geochronology and economic geology. Ph.D. thesis, Yangon University, Yangon, Myanmar, 139 pp.
- Longerich P.H., Jackson E.S., Günther D. (1996) Inter-laboratory note. Laser ablation inductively coupled plasma mass spectrometric transient signal data acquisition and analyte concentration calculation. *Journal of Analytical Atomic Spectrometry*, Vol. 11, No. 9, pp. 899–904, <http://dx.doi.org/10.1039/ja9961100899>.
- Peucat J.-J., Ruffault P., Fritsch E., Simonet C., Lasnier B. (2007) Ga/Mg ratio as a new geochemical tool to differentiate magmatic from metamorphic blue sapphires. *Lithos*, Vol. 98, No. 1–4, pp. 261–274, <http://dx.doi.org/10.1016/j.lithos.2007.05.001>.
- Schmetzer K. (1987) Zur Deutung der Farbausache blauer Saphire—eine Diskussion. *Neues Jahrbuch für Mineralogie, Monatshefte*, Vol. 8, pp. 337–343.
- Smith C.P. (1995) A contribution to understanding the infrared spectra of rubies from Mong Hsu Myanmar. *Journal of Gemmology*, Vol. 24, No. 5, pp. 321–335.
- (2010) Inside sapphires. *Rapaport Diamond Report*, pp. 123–132.
- Tlili A., Smith D.C., Beny J.M., Boyer H. (1989) A Raman microprobe study of natural micas. *Mineralogical Magazine*, Vol. 53, No. 2, pp. 165–179, <http://dx.doi.org/10.1180/minmag.1989.053.370.04>
- Themelis T. (2008) *Gem and Mine*. A&T Publications, 352 pp.

# UPDATE ON GEMSTONE MINING IN LUC YEN, VIETNAM

Pham Van Long, Vincent Pardieu, and Gaston Giuliani

In 1987, gems were discovered in the Luc Yen area of Vietnam's Yen Bai province. Ruby, sapphire, and spinel from primary and secondary deposits are the most valuable of these; tourmaline, gem-quality feldspar, pargasite, and humite are also mined there. As a result of this discovery, the Luc Yen district has become Vietnam's most important gemstone-trading center over the past 30 years. The markets of Yen The, the capital of Luc Yen, offer an additional assortment of natural gems from Vietnam and elsewhere (including peridot, beryl, aquamarine, topaz, and quartz); synthetic gems are also found in these markets.

Marble-hosted ruby and spinel deposits represent the foremost source of colored gems in Central and Southeast Asia (Garnier et al., 2008). They are contained in a series of platform carbonates that underwent amphibolite facies metamorphism to form crystalline marbles during the Cenozoic continental collision between the Indian and Eurasian plates about 21–23 million years ago (Garnier et al., 2006). These deposits occur in Afghanistan, Pakistan, Azad Kashmir, Tajikistan, Nepal, Burma (Myanmar), China, and central and northern Vietnam (Hughes, 1997). In northern Vietnam, the deposits are located in the Yen Bai province (figure 1). The city of Yen Bai, the regional administrative capital, is located some 200 km northwest of Hanoi, about halfway to the Chinese border. It was an important local gem trading center during the 1990s (Kane et al., 1991; Kammerling et al., 1994), though most of the dealers have since relocated to Hanoi. Luc Yen, on the other hand, is a mountainous district located in the north of Yen Bai province. Its main city, Yen The, is also known as Luc Yen, the name given to the ruby and spinel mining district described in the gemological literature (e.g., Kane et al., 1991; Pham et al., 2004a).



Figure 1. This map of northern Vietnam shows the location of the gem-rich Luc Yen district.

The aim of this paper is to present the state of gem mining activities in the Luc Yen district within their geological framework, and to provide insight into the local gem trade. The paper will show the evolution of Luc Yen's gem industry since 1987, with an eye toward the future.

## HISTORY OF THE LUC YEN MINING DISTRICT

The Luc Yen district mainly consists of jungle-covered karsts separated by several narrow valleys where paddy fields and traditional villages are located, as shown in figure 2. It is bordered on the west, south, and east by Thac Ba Lake (figure 3). The lake was cre-

See end of article for About the Authors and Acknowledgments.

GEMS & GEMOLOGY, Vol. 49, No. 4, pp. 233–245,  
<http://dx.doi.org/10.5741/GEMS.49.4.233>.

© 2013 Gemological Institute of America



Figure 2. A view over Yen The, the quiet capital of Luc Yen district. The town is surrounded by paddy fields and jungle-covered, karst-type mountains. Photo by Vincent Pardieu, © GIA.

ated in 1970 by the construction of a dam for Vietnam's first hydroelectric power plant. Thac Ba Lake is 80 km long, with a maximum width of 10 km, and contains more than a thousand islands. Covering the expanse between Tan Huong and the Luc Yen peninsula, it has submerged a potentially gem-rich area.

The initial discovery of high-quality Vietnamese rubies occurred in the Luc Yen district in late 1987, after farmers recovered the stones from placers. The ruby was found in colluvial and alluvial sediments, and the primary source was believed to be marble. Gem exploitation began in earnest in June 1988, with

the establishment of VINAGEMCO (Vietnam Gemstones Company), a state-owned company for exploration, mining, processing, and trading. Mining activity began that September, with a joint venture between VINAGEMCO and B.H. Mining Company of Thailand to work the Khoan Thong Valley placer. From November 1989 to March 1990, 244 kg of gem-quality rubies and sapphires were mined from Khoan Thong, most of them sold and cut in Bangkok (Kane et al., 1991; Garnier et al., 2004; Pham et al., 2004a,b,c; Nguyen et al., 2011; Le et al., 2012).

From 1990 to 1994, thousands of independent miners moved to the Luc Yen district. Many new discoveries were made in both primary deposits and placers. These gems were sold in the Luc Yen mar-

## In Brief

- Since the discovery of corundum and spinel deposits in 1987, Luc Yen has become Vietnam's most important gemstone-trading center.
- After a brief period of state-controlled operation, mining is again being done by local farmers working primary and secondary deposits.
- Activities related to the Luc Yen market include sales of gem-quality stones and gem-related artwork.

ket. In 1995, the mines went under the management of the Vietnam National Gems and Gold Corporation (VIGEGO). A 2003 merger formed the Vietnam Minerals Corporation (VIMICO), and the Luc Yen mines are no longer controlled by the state. Local

Figure 3. Local miners take advantage of the low water level at Thac Ba Lake to dig for rubies during the spring of 2005. Photo by Vincent Pardieu, courtesy of AIGS/Gübelin Gem Lab.



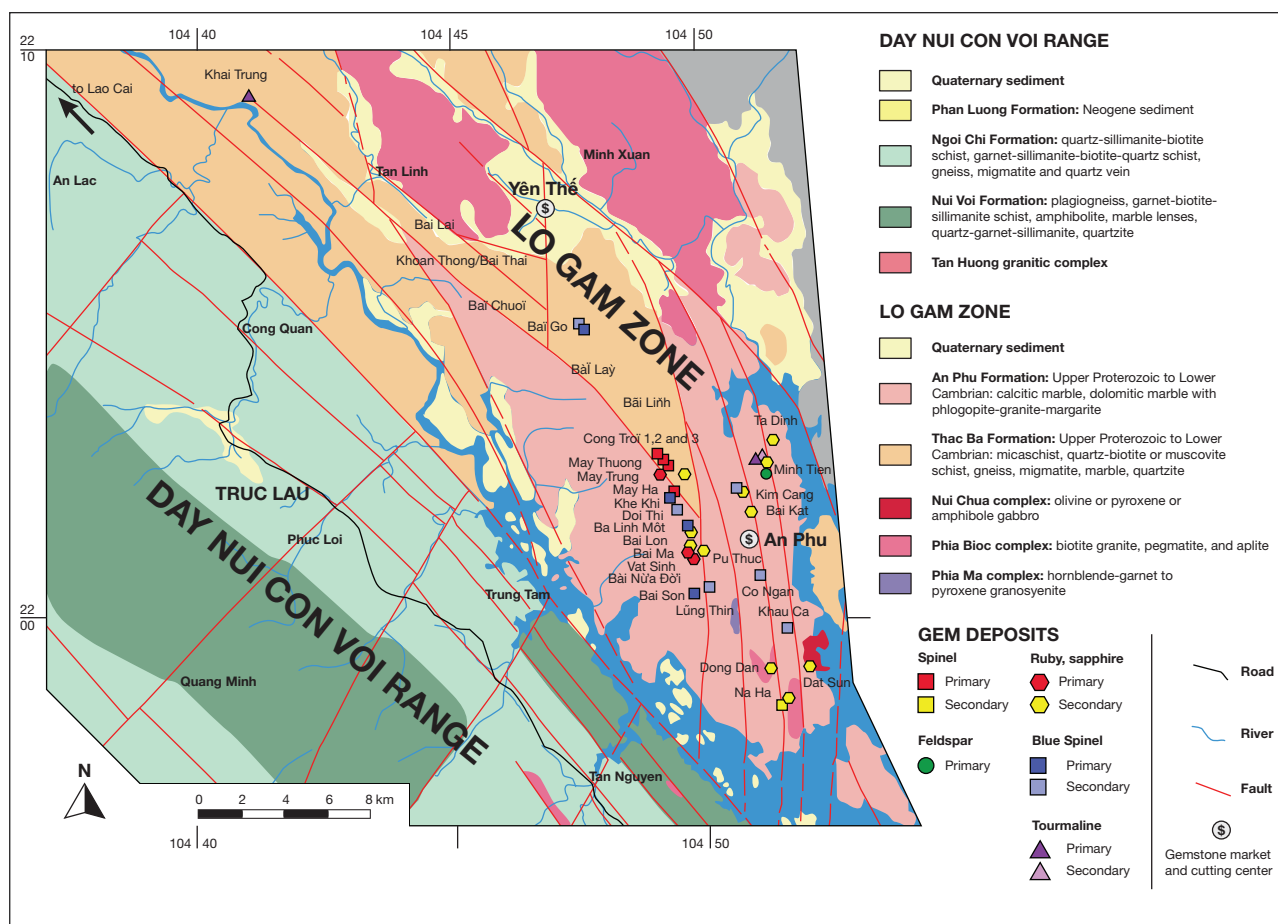


Figure 4. This geological map of the Yen The, modified from Pham and Al (2004), shows the primary and secondary deposits of ruby, sapphire, spinel, tourmaline, and feldspar visited by one of the authors during seven field expeditions between 2005 and 2012. Modified by Vincent Pardieu.

farmers, working in small-scale operations, do much of the mining throughout the region.

Mining activity in Khoan Thong and the surrounding mountains continues, though it is only a shadow of its past. Today, two large memorial stones located at the entrance of the valley serve as reminders of bygone ruby mining.

### THE LUC YEN MINING DISTRICT

The deposits of Yen Bai and Luc Yen are hosted by metamorphic belts associated with large-scale shear zones. The Red River shear zone (figure 4) comprises the Day Nui Con Voi metamorphic belt and, on its eastern flank, the Lo Gam tectonic zone (Garnier, 2003; Pham et al., 2004a,c). The Luc Yen ruby and spinel deposits occur in the Lo Gam zone, in a thick metasedimentary sequence of Cambrian age, composed of marble and overlying sillimanite-biotite-garnet schist. This zone is also known for fine tourmaline. These units, bounded by left-lateral faults,

are intruded by granitic rocks and related pegmatites of Triassic age. The primary and secondary (placer) deposits of ruby and spinel, as well as sapphire, tourmaline, amazonite, pargasite, and humite, are presented within a geological framework.

**Ruby and Sapphire Deposits.** Luc Yen's corundum deposits are set in moderate- to high-temperature recrystallized marble units of Upper Proterozoic to Lower Cambrian age, in the eastern side of the Red River shear zone, specifically the Lo Gam tectonic zone (Hoang et al., 1999; Garnier et al., 2002, 2008; Pham et al., 2004a; Nguyen et al., 2011). Two types of deposits are mined there (Giuliani et al., 2003):

- Primary ruby occurs as: (a) disseminated crystals within marble associated with phlogopite, dravite, margarite, pyrite, rutile, spinel, edenite, and graphite (An Phu, Minh Tien, Luc Yen, and Khoan Thong areas); (b) veinlets associated with calcite, dravite, pyrite, margarite, and



Figure 5. Rough ruby and sapphire crystals from An Phu (left) and small rounded rubies hosted in placers (right) are sold in the Luc Yen gem market. Photos by Vincent Pardieu, © GIA.

phlogopite (An Phu); and (c) fissures with graphite, pyrite, phlogopite, and margarite (Bai Da Lan mine and Minh Tien).

- Secondary deposits (i.e., placers) consist of gravel concentration in karst pockets and alluvial fans found all over the Luc Yen region (Kane et al., 1991; Garnier et al., 2004). The gem-bearing valleys are often narrow and correspond to small depressions typically ranging from 2 to 3 km<sup>2</sup>. Corundum crystals are pink, purple to red, and blue; colorless sapphire coexists with ruby, as well as gray to brown and bipyramidal sapphire and trapiche ruby. Gem corundum is associated with spinel (red, pink, and pale blue), multicolored tourmaline, and garnet. These placers furnish a variety of gem-quality material for the market, which has been open daily since 1987 (figure 5).

**Spinel Deposits.** Gem spinel, hosted in either marble or placers, was discovered in Luc Yen in 1987, together with ruby and sapphire. Local farmers mine gem-quality spinel from placers along the streams and from alluvial deposits. The specimens exhibit red, brownish red, pink, purple, sea-blue, and sky-blue colors (figure 6). Faceted spinels of up to several hundred carats are known, but most of the faceted gems weigh less than 10 carats. The red, brownish red, and pink spinels are found in An Phu, Minh Tien, Bai Gau, and Khoan Thong. Cong Troi is the source of pink and purple spinels, while dark sea-blue specimens are mined mostly in Co Ngan and Bai Gau. Fine “electric” blue spinel crystals (usually small and/or included and under three grams) come from Khe Khi, Ba Linh Mot, and Khau Ca. Sky-blue material is produced in the Bai Son and Lung Thin areas, as well as near Bai Gau (Senoble, 2010).

Figure 6. The rough sky-blue spinel on the left is from the Bai Son mine. The cut spinels from Luc Yen (right) weigh 2.3 to 11.9 ct. Photos by Vincent Pardieu, © GIA (left) and Pham Van Long (right).





Figure 7. The rubellite crystals are from Tan Lap (left) and Khai Trung (bottom right); the green tourmalines are from An Phu (top right). Photos by Pham Van Long.

In Luc Yen, rough spinel crystals occur in dolomitic marble with calcite, phlogopite, humite, and pargasite. Formation takes place in metasomatic zones resulting from the percolation of fluids in the marble. The crystals, which range in size from a few millimeters to five centimeters, are of octahedral habit and have a red to brownish red color. Spinel crystals in placers are more transparent and are used for gem cutting. Larger crystals in host rock are usually translucent to opaque, and suitable only as collection samples.

**Tourmaline Deposits.** Tourmaline-bearing pegmatites have been reported in Luc Yen (Nguyen, 1995), but gem tourmalines have not been found in these rocks thus far. They have been recovered instead from alluvial gravels associated with gem corundum; these gravels may be found in weathered crust. The crystals are striated prisms with rounded triangular cross-sections and various terminations. The color of Luc Yen tourmaline ranges from green to brown, black, yellow, and red (figure 7). Multicolored zoned crystals usually contain alternately pink, purple, and yellowish green colors. Color zoning is often observed from the center of the crystals to their periphery, with a combination of pink, purple, and dark green.

**Feldspar Deposits.** Gem-quality feldspar, found with tourmaline in weathered pegmatites in the Minh Tien area, was first discovered in 1999. Production has fallen in recent years, because the deposit's location

in paddy fields has restricted mining. This feldspar ranges from light to dark green, and from opaque to transparent. Most of the production has only been suitable for cabochon cutting. The stones are typically traded as amazonite, a variety of microcline feldspar, which is found in rare-element pegmatites (Nguyen, 2010). It is associated with smoky quartz, albite

Figure 8. These faceted gem-quality green feldspars, weighing between one and three carats, are from Luc Yen. Photo by Vincent Pardieu, © GIA.





Figure 9. Pargasite (left) and humite crystals (right) occur in marble at Luc Yen. Photos by Vincent Pardieu, © GIA.

(cleavelandite), tourmaline (elbaite), and Li-mica (lepidolite). Facet-grade transparent green feldspar (figure 8), which is very rare here, has been identified as green orthoclase (Laurs et al., 2005).

**Pargasite and Humite Occurrences.** Pargasite and humite are often associated with spinel in the marbles around An Phu, Phan Thanh, and Khoan Thong. They tend to be interspersed alongside spinel in alternating bands within the marbles. The pargasite appears as dense clusters or wide bands formed of long prismatic crystals, sometimes with a hexagonal cross-section. They can form as groups of crystals from 0.5 to 2 cm and sometimes up to 1.5 × 7 cm. The pargasite is usually dark to light green (Cong Troi) but can be yellowish green when associated with ruby (Khoan Thong). Its transparency is often very poor, and the material is sold in Yen The for “gem paintings” (described in the “Gemstone Trading Activities” section below).

Humite (clinohumite), distributed with spinel in white marble, forms in groups of crystals and usually has a honey to dark yellow color (figure 9). Their size

varies from 1 × 1.5 cm to 3 × 5 cm. Like the Luc Yen pargasite, the humite has poor transparency and is typically used for gem paintings<sup>1</sup>. Attractive samples of spinel, pargasite, and humite in white marble, ranging in height from 6 to 10 cm, are typically sold to collectors; sometimes they are carved into ornamental artworks.

## MINING ACTIVITIES IN LUC YEN

**Primary Deposits. Ruby.** At present, ruby is mined in white marble at the May Ha and May Thuong (translated as the Lower and Upper Cloud) mines. In May 2011, May Thuong was mined by a handful of men working every day, living in a canvas-covered shack halfway up the mountain. The mining tools consisted of a power generator, drilling machines, and crowbars to open the quarry.

In May Thuong, ruby crystals form bands in the marble along a single direction corresponding to the foliation plane of the metamorphic rocks. Upon detecting signs of ruby or phlogopite (a mineral commonly considered an indicator for rubies), the miners drill a hole to conduct blasting and then remove the white marble block (figure 10).

The ruby crystals often present a bipyramid hexagonal shape, with a dark red or dark purple-red color. They are generally opaque, but sometimes translucent and suitable for cabochon cuts. Their size usually ranges from 3 mm to 1.5 cm in diameter and from 2 to 10 cm in length. The ruby-bearing blocks range from 0.5 to 700 kg, with dimensions between 5 cm and 1.2 m. Each block may contain hundreds of different-sized crystals (figure 11).

<sup>1</sup> One of the authors has observed humite in other spinel deposits around the world, but with several differences. Pargasite crystals similar to those from Luc Yen are associated with spinel and corundum in marbles of the Hunza Valley in Pakistan. At Kul I Lal, Tajikistan, pink to purple and red spinel is hosted in marbles with gem-quality clinohumite. In Mahenge, Tanzania, spinel is also formed in marble with clinohumite and blue apatite. Near Kasigau Mountain in Kenya, red spinels are hosted in marbles with blue apatite, green amphibole, and graphite. Burmese spinels from Mogok are sometimes found with blue apatite and chondrodite, a member of the humite group. Besides Hunza, the author has never witnessed gem-quality spinel and corundum within 20 cm of one another.



Figure 10. A young miner stands with his jackhammer in front of a ruby mine at May Thuong. Photo by Vincent Pardieu © GIA.

In 2010, ruby was discovered in the marble at Bai Gau (Bear Site), near the Bai Chuoi (Banana Site) area. These ruby crystals, associated with pargasite, have a fine color.

To carry ruby-bearing blocks to the bottom of the hill, the miners employ locals (usually Man or Tay ethnic minorities), who carry the material on their shoulders for a fee of 2,000 to 3,000 Vietnamese dong (US\$0.10–\$0.15) per kilogram. Despite the incredibly difficult terrain, one man or woman can usually carry 50–80 kg. Until the middle of the last decade, An Phu and Luc Yen were home to several family-sized cutting factories. Most of the cutters were also traders, working at home with simple machines; only large or high-value stones were taken to professional cutters. Some of these cutting factories have begun specializ-

ing in carving and trimming ruby on marble specimens, as shown in figure 12. They may be carved into decorative shapes, such as trees or animals. Such carved gemstones in matrix are highly valued in Vietnam, where there is a market for items related to traditional beliefs associated with *phong thuy* (the Vietnamese version of Chinese feng shui).

**Spinel and Pargasite in White Marble.** Since the turn of the 21st century, spinel and pargasite mining activities have been focused in the Cong Troi (Sky Gate) area (Pardieu, 2010). In 2009–2010, mining li-

Figure 11. Crystals of ruby in marble matrix. Photo by Vincent Pardieu, © GIA.



Figure 12. In Luc Yen, spinel specimens are carved and trimmed for decorative and feng shui purposes. Photo by Vincent Pardieu, © GIA.







Figure 13. A view of the Cong Troi marble cliff, the largest pink spinel mining area in the Luc Yen region, with the mining camp in the foreground. Photo by Vincent Pardieu © GIA.

censes were allocated to some Indian companies for extracting white marble intended for export. When geological drilling operations began in the area, local miners had to stop mining. Once drilling was completed in late 2010, work resumed. In 2012, approximately 20 miners were at Cong Troi (figure 13), most of them between 17 and 35 years old.

Since spinel and pargasite are distributed in bands

parallel to the foliation of the marble, spinel mining often occurs over a large area, covering the entire mountain from the base to the top. Spinel from Cong Troi exhibits a variety of colors, typically brownish red, reddish brown, brown, purple, black, pink, and purplish pink. The size varies from 1 × 1 mm to 5 × 5 cm (figure 14). The crystals are usually octahedral, though many also exhibit spinel-law twinning.

Blue spinel is found in the white marble at Bai Son, but the crystals usually have a dull color and low transparency. Blue spinel is associated with phlogopite, humite, and sometimes pyrite. Other occurrences are at May Trung, Ba Linh Mot, and Khe Khi.

**Secondary Deposits (Placers).** *Ruby, Sapphire, and Spinel.* Corundum and spinel are mingled in alluvial placers. Mining is conducted on a small scale, from Bai Lai in the northeast of Luc Yen to the Na Ha area in the south, near the banks of Thac Ba Lake. The most active sites are along the streams of Cong Troi, in Nuoc Ngap (An Phu area). Material is also removed from old mines in areas such as Minh Tien, Khoan Thong, and Bai Chuoi (figure 15), where big companies mined the most accessible and profitable material, often missing areas between marble pinnacles that excavators could not easily reach. As a result, some gem-rich ground was left behind; this is now collected by locals with shovels and buckets. In



Figure 14. Left: A miner shows the association of spinel and pargasite in marble. Right: Red (top) and blue (bottom) spinel in marble. Photos by Vincent Pardieu, © GIA.

some places, locals mine in karsts or caves of white marble (see Cong Troi 2, Cong Troi 3, May Thuong, May Ha, and Dong Dan in the figure 4 map).

Most of the mining in each area is done by small groups of local farmers using mini-generators and water hoses. Activity fluctuates according to agricultural cycles. Excavators and high-pressure water hoses are used in some places, but most of the miners use basic tools, washing with rattan buckets and picking the gemstones by hand.

In the Bai Chuoi area, near the Khoan Thong mine, miners work within pits. They have a small water reservoir and a pump with a sluice for washing and sorting gems. The mine has produced ruby (including many trapiche rubies), tourmaline, rutile, and quartz, as well as some blue sapphire and light blue spinel. It has also yielded large, opaque, purplish red ruby crystals that are suitable for cabochons or carvings. After three or four workdays, the stones are gathered, classified, and brought to the Luc Yen market; some are sold directly to the dealers.

Spinel from An Phu and the surrounding area have typical features. Their color can be red, brownish red, reddish brown, purple, pink, purplish pink, blue, or sky blue. The pink to red spinel can be found throughout the area, but blue specimens are recovered mainly from Co Ngan, Khau Ca, and Kim Cang. The sky-blue spinels are mostly found in colluvial material from crevasses in the Bai Son and Lung Thin areas, where miners follow the caves underground to a 5–8 m depth (figure 16).

*Figure 15. Farmers dig for gems in the paddy fields near Minh Tien. Photo by Vincent Pardieu, © GIA.*



*Figure 16. A team of miners works a deep and wide crevasse in the karsts at Bai Son in search of beautiful light blue spinel. Photo by Vincent Pardieu, © GIA.*

**Tourmaline.** Compared to corundum and spinel, mining activities for tourmaline in Luc Yen are less intensive. Tourmaline is often extracted by locals along the streams in Minh Tien and Nuoc Ngap (An Phu municipality).

Tourmaline is mined in weathered pegmatites (Nguy, 1996). Peak mining activity occurred at An Phu between 1989 and 2000. The size of the crystals is highly variable, but some can reach 20 cm long and 10 cm across (3–4 kg). The colored tourmaline belongs to the elbaite and dravite series, at 57.6–97.4 mol.% and 56.9–87.7 mol.%, respectively (Nguy, 1996).

In 2008 and 2009, new tourmaline occurrences were found in Khai Trung (Yen The ward) and Tan Lap (Phan Thanh ward). In Khai Trung, heavy mining activity occurred between 2008 and 2010. Several blocks of rubellite weighing hundreds of kilograms were sold to collectors. Some of the blocks are also displayed as

**TABLE 1.** Summary of gem mining sites in the Luc Yen district.<sup>a</sup>

Name	Location	Main Production	Deposit Type	Mining Activity Witnessed
Yen The	22°06'46"N 104°46'17"E	Mix (ruby)	Secondary	None
Bai Lai	22°06'27"N 104°44'41"E	Mix (ruby)	Secondary	None
Khoan Thong/Bai Thai	22°05'37"N 104°45'23"E	Mix (ruby)	Mostly secondary	Three groups (20 people max.)
Bai Chuoi	22°05'26"N 104°46'05"E	Mix (ruby)	Mostly secondary	Two groups (10 people max.)
Bai Go	22°04'45"N 104°47'04"E	Ruby, spinel (blue, pink)	Mostly secondary	Several groups (100 people max.)
Bai Lay	22°04'05"N 104°47'50"E	Mix (ruby)	Mostly secondary	Two groups (10 people max.)
Bai Linh	22°03'44"N 104°48'02"E	Mix (ruby)	Mostly secondary	One group (5 people max.)
Cong Troi 1	22°02'02"N 104°48'46"E	Spinel (pink, red)	Mostly primary	Several groups (30 people max.)
Cong Troi 2	22°02'12"N 104°48'43"E	Spinel (pink, red)	Mostly primary	Several groups (15 people max.)
Cong Troi 3	22°02'21"N 104°48'34"E	Spinel (pink, red)	Mostly primary	Several groups (10 people max.)
May Thuong	22°02'04"N 104°48'31"E	Ruby	Primary	Two groups (10 people max.)
May Trung	22°01'48"N 104°48'43"E	Spinel (pink, blue)	Primary	One group (5 people max.)
May Ha	22°01'49"N 104°48'36"E	Ruby	Mostly secondary	One group (5 people max.)
Khe Khi	22°01'35"N 104°48'39"E	Spinel (blue)	Mostly secondary	None, or one group (2 people max.)
Doi Thi	22°01'32"N 104°48'46"E	Mix	Mostly secondary	None
Ba Linh Mot	22°01'18"N 104°48'49"E	Mix	Mostly secondary	One or two groups (4 people max.)
Bai Lon	22°01'12"N 104°48'59"E	Mix	Mostly secondary	None
Pu Thuc	22°01'42"N 104°49'18"E	Ruby	Mostly secondary	None
Bai Ma	22°00'43"N 104°49'03"E	Mix	Mostly secondary	One group (5 people max.)
Vat Sinh	22°00'39"N 104°49'00"E	Ruby	Mostly secondary	Two groups (10 people max.)
Bai Nua Doi	22°00'31"N 104°49'04"E	Ruby	Mostly primary	One group (5 people max.)
Bai Son	21°59'57"N 104°49'09"E	Spinel (blue)	Primary and secondary	Two groups (10 people max.)
Lung Thin	22°00'01"N 104°49'26"E	Spinel (blue, pink)	Mostly secondary	Three groups (12 people max.)
Ta Dinh	22°02'42"N 104°50'45"E	Mix	Mostly secondary	Three groups (12 people max.)
Minh Tien	22°02'14"N 104°50'23"E	Mix	Mostly secondary	Four groups (20 people max.)
Kim Cang	22°01'45"N 104°50'09"E	Mix (ruby, spinel)	Mostly secondary	Three groups (10 people max.)
Bai Kat	22°01'26"N 104°50'16"E	Mix (ruby, spinel)	Mostly secondary	One group (7 people max.)
Co Ngan	22°00'10"N 104°50'24"E	Mix (ruby, spinel)	Mostly secondary	Three groups (12 people max.)
Khau Ca	21°59'22"N 104°50'54"E	Mix (ruby, spinel)	Mostly secondary	Three groups (12 people max.)
Dong Dan	21°58'29"N 104°50'37"E	Mix	Mostly secondary	One group (7 people max.)
Dat Sun	21°58'30"N 104°51'24"E	Mix	Secondary	None
Na Ha	21°57'57"N 104°50'59"E	Mix	Secondary	Two groups (10 people max.)

<sup>a</sup>Based on GIA field expeditions in 2009, 2010, 2012, and 2013.

feng shui stones. The tourmaline often has light red to pink colors, but the crystals are broken. The transparency is poor, and the percentage of facet-grade gems is very low (usually less than 5%). These resemble the tourmalines found in Bac Kan province. The Khai Trung tourmalines are zoned, and their light green and yellowish green colors are mixed with pink, light red, and dark purple zones. The crystals have a needle-like habit and range from 0.4 to 0.6 mm in diameter and

from 2 to 6 cm in length. Associated minerals included quartz, feldspar, and mica.

The occurrence in Tan Lap, discovered at the end of 2010, covers approximately 300 km<sup>2</sup>. The tourmaline is hosted by weathered pegmatites formed by kaolinized feldspar, quartz, and black tourmaline (schorl). Reddish purple rubellite is often found in the middle of the weathered pegmatite bodies. As in the Khai Trung area, many crystals are broken and have



Figure 17. Though only a fraction of its size during the 1990s, the Luc Yen gemstone market is still held daily. Photos by Pham Van Long (left) and Vincent Pardieu, © GIA (right).

low transparency, making them suitable only for cabochon cutting or as collection samples. Local farmers are officially forbidden to mine there, but some still occasionally find pockets of rubellite weighing tens of kilograms.

### GEMSTONE TRADING ACTIVITIES

Before the 1990s, Luc Yen was a small, impoverished town that derived most of its income from agriculture and timber. But after the gem discoveries, the town grew rapidly. The first market opened in 1987, and today Luc Yen is the busiest gem-trading center in northern Vietnam.

During the 1990s, the exhibition area of the market extended over 1,000 square meters, with hundreds of local farmers selling gems from 5:30 to 7:30 every morning. When the market was closed, the farmers would return to the mountains to mine. The buyers at the market were Vietnamese tradespeople, mainly from Hanoi and Ho Chi Minh City (formerly Saigon), with some foreign traders from Thailand and other countries.

Today the market is only about a tenth of its former size. Although business is still conducted every morning, the miners and traders have mobile phones and no longer need to meet there. The traders often try to buy directly from local farmers at the foothills when they return from mining. The sellers at the market are mainly women who display parcels of both rough and faceted gemstones on small tables (figure 17).

Currently, about 30 stores are concentrated in the streets around the central lake and the surrounding area of the old market. Traders often pool their money to-

gether to purchase particularly high-value gemstones. Only professionals and well-known buyers have the opportunity to see the exceptional stones. Some of the gemstones sold in the market are not from the Luc Yen mines, including beryl, peridot, quartz, chalcedony, jade, and fluorite (figure 18).

In Luc Yen, most of the dealers are also skilled cutters, with one or two cutting machines at home. Nevertheless, some local family businesses have evolved into small factories equipped with a few machines, cutting gems directly for customers. A number of old cutting factories have switched to carving

Figure 18. Common misspellings in the Luc Yen gem market include “rubi,” “sapier” for sapphire, “sitilen” for spinel, “phelydot” for peridot, and “siclin” for citrine. Photo by Vincent Pardieu, © GIA.





Figure 19. Left: A man trimming a block of red spinel in marble at his home. Right: A small cutting factory in Luc Yen. Photos by Vincent Pardieu, © GIA (left) and Pham Van Long (right).

feng shui stones. The original gem-bearing marble blocks are carved to reveal the gems and to produce artworks and artifacts (figure 19).

At present, one of the most exciting activities in Luc Yen is gemstone painting. The small stones used to create these paintings come in a variety of colors: red ruby, garnet, and spinel; blue sapphire; green peridot, pargasite, or chalcedony; purple fluorite or amethyst; and pink rose quartz. The gems may be left intact or crushed into powder to produce the paintings, which are modeled after Vietnamese art-

Figure 20. Gemstone paintings are produced and sold in Luc Yen. Photo by Vincent Pardieu, © GIA.



works (figure 20). Gem grains may be polished for higher-quality paintings.

Using a sheet of white acrylic as a base, the artist paints a pattern for the picture. The sheet is covered with white powder made from calcite, and suitably colored stones are applied to the pattern. The stones and powder are held together by special glue. One worker can complete a 40 × 60 cm painting in a single day. There are about 10 manufacturers who distribute these products, which are sold in stores from Hanoi to Ho Chi Minh City.

Gem painting and carving are of particular interest to the Luc Yen miners, providing a steady local market for their daily production. These activities cover the miners' costs most of the time, even if they are not making profitable discoveries in the field. Having a steady market for their production enables them to occasionally find some exceptional gemstones.

## CONCLUSION

Since the discovery of gems in Luc Yen in 1987, the local industry has undergone many changes. The early finds were made by local farmers. Later discoveries occurred along Highway 70, between Yen Bai and Luc Yen, which became Vietnam's most important ruby, sapphire, and spinel producer, as well as its busiest processing and trading center. Unorganized mining operations by locals, along with illegal exportation, led the Vietnamese government to form a national corporation to manage the country's gemstone production. Yet industrial-scale mining in the Luc Yen area has not been effective, because the placer gemstones are

often distributed in karsts, caves in mountains, or narrow valleys, none of which permit large-scale operations. These difficulties caused VIGEGO to relinquish control of gemstone mining in Luc Yen in 2000. Since

then, the area has returned to small-scale artisanal mining. In the near future, officials from Yen Bai province plan to turn Luc Yen into a gemstone trade center and a geological reserve (Pham et al., 2011).

#### ABOUT THE AUTHORS

Dr. Pham (Ingphamvan@yahoo.com) is director of the Centre for Gems and Gold Research and Identification of Vietnam. Mr. Pardieu is senior manager of field gemology at GIA's Bangkok laboratory. Dr. Giuliani is senior researcher at the Institute of Research for Development in Toulouse, France.

#### ACKNOWLEDGMENTS

This article was completed with the financial support of the National Foundation for Science and Technology Development of Vietnam (NAFOSTED), codes 105.02-2010.11. Dr. Giuliani gives special thanks to the University of Lorraine for supporting his trip

to Vietnam. The authors would like to thank Nguy Tuyet Nhung from the Gemmological Laboratory of the Vietnam Gemstone Association; Pham Thi Thanh Hien from the Geology Department, Hanoi Mining College; Pham Duc Anh from the Center for Gem and Gold Research and Identification; Nguyen Ngoc Khoi from the Gemmological Laboratory of the DOJ Group. They would also like to thank Hoang Quang Vinh from the Geological Institute of the Vietnam Science and Technology Institute; Jean Baptiste Senoble and Lou Pierre Bryl from Senoble & Bryl; Philippe Ressigeac from Gemfields; Stephane Jacquat from Gem Precision Cutting in Geneva, Switzerland; and Boris Chauvire from the University of Nantes, France.

#### REFERENCES

- Garnier V., Giuliani G., Maluski H., Ohnenstetter D., Phan T.T., Hoang Q.V., Pham V.L., Vu Van T., Schwarz D. (2002) Ar-Ar ages in phlogopites from the marble-hosted ruby deposits in northern Vietnam: Evidence for Cenozoic ruby formation. *Chemical Geology*, Vol. 188, No. 1–2, pp. 33–49, [http://dx.doi.org/10.1016/S0009-2541\(02\)00063-3](http://dx.doi.org/10.1016/S0009-2541(02)00063-3).
- Garnier V. (2003) Deposits of ruby from marble in central Southeast Asia: Genesis and isotopic characterization [in French]. PhD Thesis INPL, Nancy, France, 390 pp.
- Garnier V., Maluski H., Giuliani G., Ohnenstetter D., Schwarz D. (2006) Ar-Ar and U-Pb ages of marble-hosted ruby deposits from central and southeast Asia. *Canadian Journal of Earth Sciences*, Vol. 43, pp. 509–532, <http://dx.doi.org/10.1139/e06-005>.
- Garnier V., Giuliani G., Ohnenstetter D., Fallick A.E., Dubessy J., Banks D., Hoàng Q.V., Lhomme T., Maluski H., Pêcher A., Bakhsh K.A., Pham V.L., Phan T.T., Schwarz D. (2008) Marble-hosted ruby deposits from central and Southeast Asia: Towards a new genetic model. *Ore Geology Reviews*, Vol. 34, No. 1–2, 169–191, <http://dx.doi.org/10.1016/j.oregeorev.2008.03.003>.
- Giuliani G., Dubessy J., Banks D., Hoàng Q.V., Lhomme T., Pironon J., Garnier V., Phan T.T., Pham V.L., Ohnenstetter D., Schwarz D. (2003) CO<sub>2</sub>-H<sub>2</sub>S-COS-S<sub>8</sub>-AlO(OH)-bearing fluid inclusions in ruby from marble-hosted deposits in Luc Yen area, North Vietnam. *Chemical Geology*, Vol. 194, No. 1–3, pp. 167–185, [http://dx.doi.org/10.1016/S0009-2541\(02\)00276-0](http://dx.doi.org/10.1016/S0009-2541(02)00276-0).
- Hoàng Q.V., Giuliani G., Phan T.T., Coget P., France-Lanord Ch., Pham V.L. (1999) Origin of ruby formation in Yên Bái Province. *Journal of Geology, Series B*, Vol. 13–14, pp. 118–123.
- Hughes R.W., Sersen W.J. (1991) Bangkok gem market review: Vietnamese ruby. *Gemmological Digest*, Vol. 3, No. 2, pp. 68–70.
- Kammerling R.C., Scarratt K., Bosshart G., Jobbins E.A., Kane R.E., Gübelin E.J., Levinson A.A. (1994) Myanmar and its gems—An update. *Journal of Gemmology*, Vol. 24, No. 1, pp. 3–40.
- Kane R.E., McClure S.F., Kammerling R.C., Khoa N.D., Mora C., Repetto S., Khai N.D., Koivula J.I. (1991) Rubies and fancy sapphires from Vietnam. *G&G*, Vol. 27, No. 3, pp. 136–155, <http://dx.doi.org/10.5741/GEMS.27.3.136>.
- Laurs B.M., Rossman G.R., Shigley J.E. (2005) Gem News International: Green orthoclase feldspar from Vietnam. *G&G*, Vol. 41, No. 4, pp. 354–355.
- Le T.-T.H., Häger T., Hofmeister W., Hauzenberger C., Schwarz D., Pham V.L., Wehmeister U., Nguyen N.K., Nguy T.N. (2012) Gemstones from Vietnam: An update. *G&G*, Vol. 48, No. 3, pp. 158–177, <http://dx.doi.org/10.5741/GEMS.48.3.158>.
- Nguy T.N., Vu T.H. (1996) Gemological characteristics of tourmaline from Luc Yen [in Vietnamese]. *Journal of Geology (Hanoi, Vietnam)*, A/237, pp. 48–51.
- Nguy T.N., Nguyen T.M.T., Nguyen N.T., Vu N.A. (2005) Mineralogical characters of tourmaline-bearing pegmatite from the Luc Yen area. *Proceedings of the 60th Anniversary of Vietnamese Geology*, pp. 713–722.
- Nguyen T.M.T., Nguy T.N., Hofmeister W., Häger T. (2010) Amazonite from the Luc Yen mining area, Yen Bai, Vietnam. *The Fifth International Workshop on Provenance and Properties of Gem and Geo-Materials*, 17–24 October, 2010, pp. 40–52.
- Nguyen N.K., Sutthirat C., Duong A., Nguyen V.N., Nguyen T.M.T., Nguy T.N. (2011) Ruby and sapphire from the Tan Huong-Truc Lau area, Yen Bai province, northern Vietnam. *G&G*, Vol. 47, No. 3, pp. 182–195, <http://dx.doi.org/10.5741/GEMS.47.3.182>.
- Pardieu V., Pham V.L. (2010) Gem News International: Ruby, sapphire, and spinel mining in Vietnam: An update. *G&G*, Vol. 46, No. 2, pp. 151–153.
- Pham V.L., Giuliani G., Garnier V., Ohnenstetter D., Pardieu V., Pham D.A., Pham T.T.H. (2011) Gemstones in Vietnam: a review. *Abstract of the Proceeding of the Second Asia-Pacific Geoparks Network Symposium on Geopark and Geotourism for Regional Sustainable Development*, Hanoi, Vietnam, p. 57.
- Pham V.L., Garnier V., Giuliani G., Ohnenstetter D., Hoàng Q.V., Phan T.T., Schwarz D. (2004a) Gem corundum deposits in Vietnam. *Journal of Gemmology*, Vol. 29, No. 3, pp. 129–147.
- Pham V.L., Hoàng Q.V., Garnier V., Giuliani G., Ohnenstetter D. (2004b) Gemstones in Vietnam: A review. *Australian Gemmologist*, Vol. 22, No. 4, pp. 162–168.
- (2004c) Marble-hosted ruby from Vietnam. *Canadian Gemmologist*, Vol. 25, No. 3, pp. 83–94.
- Pham V.L., Garnier V., Giuliani G., Ohnenstetter D. (2008) Mechanics to form ruby in marble from the Luc Yen area [in Vietnamese]. *Proceedings of the 4th International Workshop on Geo- and Material- Science on Mineral Resources of Vietnam*, September 14–October 2, pp. 114–127.
- Senoble J.B. (2010) Beauty and rarity—A quest for Vietnamese blue spinel. *InColor*, No. 14, pp. 18–23.

# CHARACTERISTICS OF COATED JADEITE JADE

Jian Zhang, Taijin Lu, and Hua Chen

Ten coated jadeite jade samples were investigated by standard gemological testing, DiamondView imaging, confocal laser scanning microscopy, and spectrophotometry, including visible-range, FTIR, and Raman. The light green coating's Mohs hardness and refractive index were much lower than that of uncoated jadeite. Portions of the coating had peeled off in some cases, exposing the true color of the jadeite below. Measurements using a confocal scanning microscope indicated an average coating thickness of about 16  $\mu\text{m}$ . DiamondView observations revealed a difference in fluorescence reaction between the surface coating and the jadeite beneath it. Visible-range spectroscopy showed a weaker broad band at approximately 630 nm and a moderate peak at 437 nm, without the approximately 691 nm band found in untreated jadeite containing chromium. The coated samples' FTIR spectra contained four characteristic bands at about 2856, 2873, 2928, and 2958  $\text{cm}^{-1}$ , while the Raman spectra showed a broad band near 2000  $\text{cm}^{-1}$ . These results indicated the presence of an organic polymer in the coating material.

Jadeite jade can be coated with a thin organic layer to improve color and transparency, and to conceal internal or external features (Koivula et al., 1994; Zhang, 2006). The attractive luster of coated jadeite can be quite deceptive, as shown in figure 1. After emerging in the early 1980s, the material enjoyed great popularity in the mid-1980s, before gradually diminishing (Ouyang, 2000; Zhang, 2006). Since 2011, with the industry facing a serious shortage of rough jadeite due to the political and economic instability in Myanmar, the coating of low-quality

jadeite has reemerged in the Chinese markets, especially in Guangdong and Yunnan provinces (Liang, 2012), where the important jadeite dealers and manufacturers are located.

The early form of the coating was applied mostly to jadeite bangles and cabochons. Because of surface tension, epoxy resin often cools to form a natural curved shape, which would not significantly alter the appearance of these items. With developments in coating technology, dry-color (low luster and transparency) jadeite carvings such as kosmochlor and *hte long sein* have also been coated to add luster. Both have an attractive green color but poor transparency (Cui et al., 1999; Ouyang and Qi, 2001). The new coating is better at removing air bubbles between the coating and the jade, and it adheres more firmly to the gem material. It also enhances color and transparency and is more difficult to detect. With advances in coating technology, the treatment has been applied not only to jadeite, but also to other gems such as amber and pearl (Li et al., 2011; Hyatt, 2012).

Although Koivula et al. (1994) reported on the major identifying characteristics of coated jadeite, such as microscopic features and the difference in RI between the coated layer and the material beneath it, a detailed study is warranted. This paper presents an investigation of the coating material using advanced analytical techniques.

## MATERIALS AND METHODS

Ten coated green jadeite cabochons ranging from 1.43 to 2.71 ct (figure 1) were obtained from the Guangzhou gem market in China's Guangdong province. In three of the samples, part of the coating had peeled off, exposing a light green transparent coating and light green jadeite underneath. In one sample, we intentionally removed the coating for this study. Figure 2 shows this sample before and after the coating was removed. For comparison, we also examined five uncoated green jadeite cabochons between 4.17 and 6.07 ct (figure 3) from the National Gemstone Testing Center in Beijing. Hardness of both the coating and the jadeite was tested.

See end of article for About the Authors and Acknowledgments.

GEMS & GEMOLOGY, Vol. 49, No. 4, pp. 246–251,  
<http://dx.doi.org/10.5741/GEMS.49.4.246>.

© 2013 Gemological Institute of America



Figure 1. In recent years, the coating of low-quality jadeite has reemerged in the Chinese markets. These coated jadeites (1.43–2.71 ct) were examined in the study. Photo by Jian Zhang.

The samples were observed with a standard binocular microscope using various lighting techniques (reflected light, fiber-optic, and darkfield illumination) and magnification up to 20×. UV fluorescence reaction was observed in a dark room with a conventional 4-watt combination long-wave (365 nm) and short-wave (254 nm) UV lamp. The coated samples were also examined with a De Beers DTC DiamondView deep-UV (<230 nm) luminescence imaging system (Zhang et al., 2012). All samples were observed under a Chelsea color filter. Refractive indices were measured with a standard refractometer, and specific gravity was determined hydrostatically.

The thickness of the coating was measured with a confocal laser scanning microscope (Olympus LEXT OLS4000 3D) using brightfield illumination. The microscope has five key laser technologies, three observation modes, and seven measurement modes, so it can offer high resolution, accurate depth posi-

tioning, dynamic observation, and longitudinal scanning (Knebel and Ulrich, 2002), making it suitable for measurement of the coating. We used the step measurement mode, which allows measurement between any two arbitrary points on a surface profile with a scale resolution up to 10 nm. The accuracy of the thickness measurement depends on the magnification and software used. Normally, the accuracy is about ±2%. When measuring the thickness of the coating in the measurement window of the LEXT OLS4000 software, we followed these steps: First, we adjusted the focal point of the microscope onto the surface of the coating and selected the desired measurement position. Next, we selected the vertical measurement mode and dragged a line from the position to the uncoated area, which allowed the machine to focus on two different surfaces and determine the depth in between.

A variety of spectroscopic techniques were used to analyze the samples. For 10 coated and four un-

Figure 2. This jadeite sample is shown with its coating (left) and after the coating was removed (right). Photo by Jian Zhang.

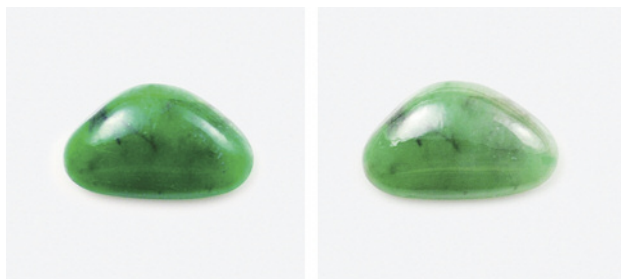


Figure 3. These uncoated samples weighing 4.17–6.07 ct were also examined. Photo by Jian Zhang.





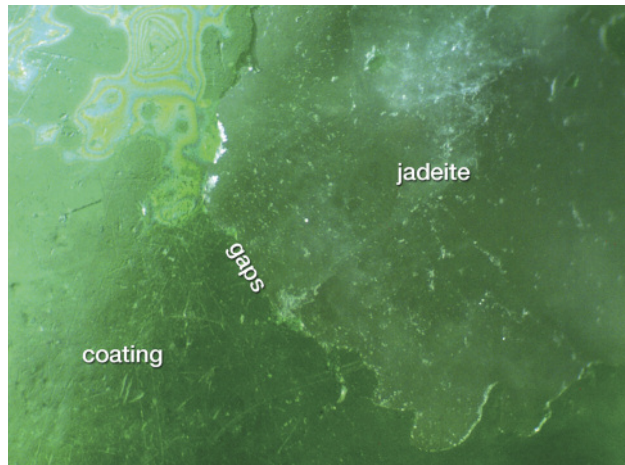


Figure 4. In this specimen, part of the coating has chipped away. Photomicrograph by Jian Zhang; magnified 20 $\times$ .

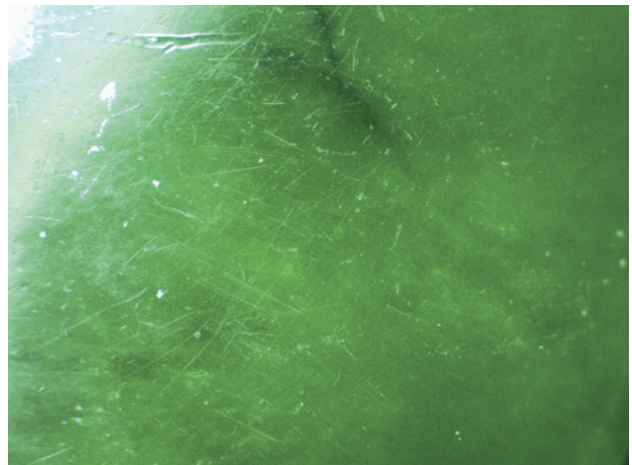
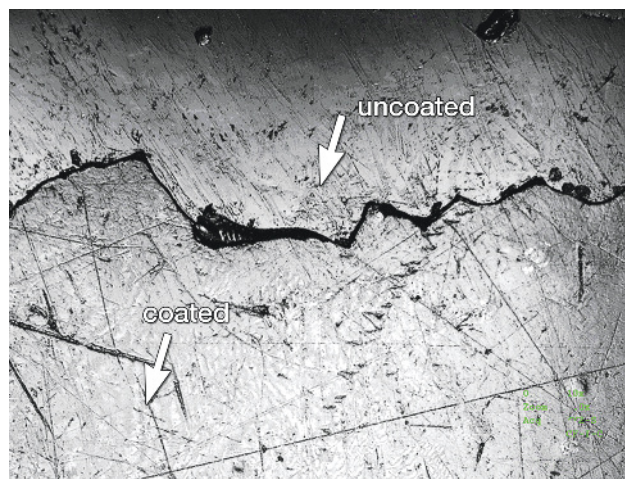


Figure 5. Surface scratches are visible on this coated jadeite. Photomicrograph by Jian Zhang; magnified 20 $\times$ .

coated green jadeites, we collected absorption spectra in the visible-range (400–700 nm) at room temperature using a Hitachi UV-3300 spectrophotometer with a sampling interval of 0.1 nm and a spectral bandwidth of 1 nm. Absorption spectra in the mid-IR region (4000–400  $\text{cm}^{-1}$ ; 1  $\text{cm}^{-1}$  resolution) were recorded for 10 coated and five uncoated samples at room temperature with a Thermo-Nicolet Nexus 670 Fourier-transform infrared (FTIR) spectrometer. A total of 128 scans per spectrum were collected to improve the signal-to-noise ratio. Raman spectra were recorded on four of the coated samples using a

Figure 6. Laser scanning confocal microscopy showed that the loosely adhered coating had a thickness of nearly 16  $\mu\text{m}$  thick. Photomicrograph by Jian Zhang; magnified 240 $\times$ .



Renishaw Raman-1000 microspectrometer with an Ar-ion laser operating at 514.5 nm excitation between 100 and 4000  $\text{cm}^{-1}$ . Raman spectra were collected at room temperature, and up to three scans were accumulated to achieve a better signal-to-noise ratio.

## RESULTS AND DISCUSSION

**Gemological Features.** Coated jadeite feels dry and rough to the touch. Due to the coating's poor thermal conductivity, the material also feels warm, unlike the smooth, cold surface of uncoated jadeite. The Mohs hardness of the coating was approximately 3, much lower than that of uncoated jadeite (about 7). Observed under magnification, the coated jadeite often displayed small traces of scratching. These irregular scratches were different from the polishing lines on uncoated jadeite. The green color was concentrated in the surface layer, while the material below had a less attractive color. In addition, gaps could be found between the coating and the jadeite, as shown in figure 4.

Using a laser scanning confocal microscope, the observer can clearly distinguish between the coated and uncoated areas, while also measuring the thickness of the coating. Figure 6, magnified 240 $\times$ , clearly demonstrates these irregular surface scratches. The measured thickness of the coating was 15.982  $\mu\text{m}$ .

The coated samples showed consistent fluorescence reactions to short- and long-wave UV radiation. When exposed to long-wave UV radiation, the coating exhibited a weak slightly blue reaction while the

jadeite below gave a slightly yellowish green reaction of weak to moderate intensity. Exposure to short-wave UV produced weaker reactions of the same color.

The samples displayed a variety of DiamondView reactions. The coating typically fluoresced slightly blue with alternating brighter spots, while the uncoated areas exhibited a weak to strong yellowish green fluorescence (figure 7).

Testing of the 10 coated samples showed that the coated areas had an average RI of about 1.53, measured by the distant vision method, while the un-

## In Brief

- A variety of analytical techniques were used to characterize coated jadeite.
- The coating typically fluoresced slightly blue in the DiamondView, while the uncoated areas exhibited a yellowish green fluorescence.
- Laser scanning confocal microscopy clearly distinguished the coated areas and measured the thickness of the coating.
- The jadeites' peaks in the mid-infrared region suggested an epoxy resin coating.

coated areas averaged 1.66. The color did not change under the Chelsea color filter. The average SG of the coated samples was 3.29, essentially indistinguishable from that of uncoated jadeite.

Figure 7. DiamondView imaging shows the UV fluorescence characteristics of a coated jadeite sample. Photo by Jian Zhang.

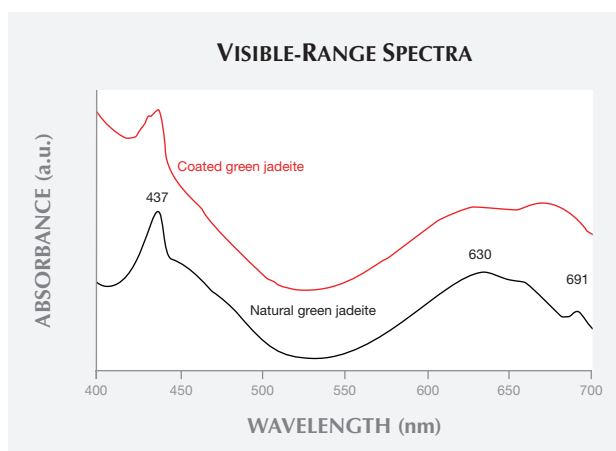
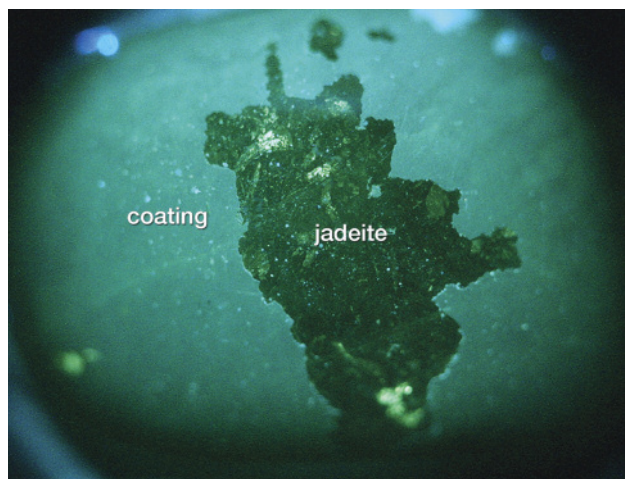


Figure 8. The visible-range spectrum of the coated green jadeite show a 437 nm band and a weaker broad band centered at 630 nm, without the 691 nm peak found in uncoated jadeite.

**Spectroscopic Features.** Viewing the coated samples with a standard desk-model spectroscope, we typically observed a weak to moderate band at 437 nm and a weaker broad band at approximately 630 nm, without the 691 nm peak found in uncoated jadeite containing chromium. The 437 nm absorption band caused by a trivalent (ferric) ion is common in jadeite of various colors (Koivula et al., 1994; Yuan et al., 2003). The broad band centered at 630 nm and the 691 nm band are induced by trivalent chromium, the most important color-causing element in untreated green jadeite (Yuan et al., 2003). Yet the absorption of the weaker broad band at approximately 630 nm in the coated samples may have been caused by the chromium in the coating (Ouyang, 2000). The visible-range spectra of the coated and uncoated green jadeite can be seen in figure 8.

The FTIR spectra of the coated jadeites revealed two distinct bands at 2343 and 2385  $\text{cm}^{-1}$ , as well as four characteristic peaks at 2856, 2873, 2928, and 2958  $\text{cm}^{-1}$ . The two distinct bands at 2343 and 2385  $\text{cm}^{-1}$ , which are not found in the absorption spectra of uncoated jadeite, may be related to carbon dioxide at room temperature (Ning, 2010). The four bands, absent from the spectra of uncoated jadeite, are related to the composition of the coating. The 2873 and 2928  $\text{cm}^{-1}$  bands are caused by the symmetric and asymmetric stretching vibrations of  $\text{CH}_2$  in epoxy resin, while the 2958  $\text{cm}^{-1}$  infrared absorption band caused by the asymmetric stretching vibration of  $\text{CH}_3$  in epoxy resin is relatively weak (Fritsch et al., 1992; Qi et al., 2005). The results indicate the existence of an epoxy resin. The IR spectra of the coated and uncoated jadeite can be seen in figure 9.

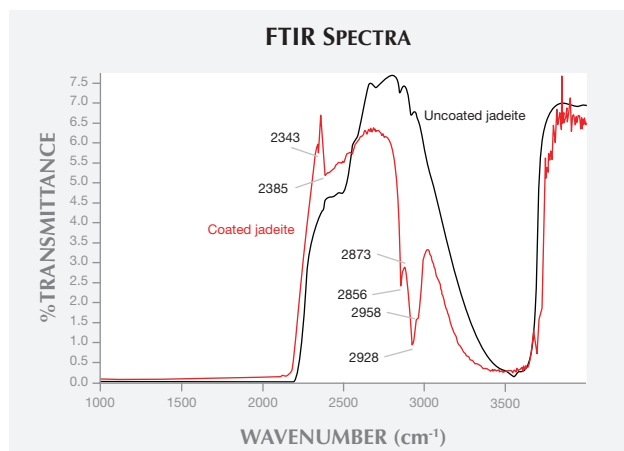


Figure 9. FTIR spectra of the coated jadeite exhibit four characteristic peaks at 2856, 2873, 2928, and 2958  $\text{cm}^{-1}$ .

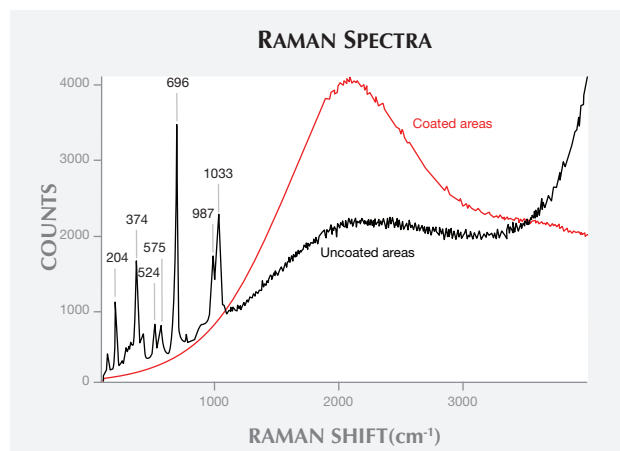


Figure 10. The Raman spectrum of the coated jadeite contains only a strong band near 2000  $\text{cm}^{-1}$ , without the peaks normally found in uncoated jadeite.

In figure 10, Raman spectroscopy of the samples' coated and uncoated areas reveals fingerprint spectral bands in areas where the coating has chipped away. The most prominent Raman feature of uncoated jadeite is the very strong sharp band near 700  $\text{cm}^{-1}$ , attributed to symmetric Si-O-Si stretching (Shurvell et al., 2001; Prencipe, 2012). Other characteristic features are a doublet, consisting of a strong band near 1040  $\text{cm}^{-1}$  plus a band of lower intensity near 990  $\text{cm}^{-1}$ , and a strong band near 375  $\text{cm}^{-1}$  related to Al-O stretching or O-Si-O deformation. This band usually has a shoulder on the high-wavenumber side. The strong peak at 1033  $\text{cm}^{-1}$  is due to asymmetric stretching, while the lower-intensity peak at 987  $\text{cm}^{-1}$  is attributed to Si-O<sub>nb,br</sub> (representing *non-bridged* and *bridged*) stretching (Shurvell et al., 2001; Prencipe, 2012). In addition, absorption peaks at 204, 524, and 575  $\text{cm}^{-1}$  were observed in the Raman spectra. These bands were absent in the areas covered by the coating. The coated area showed only a strong broad band near 2000  $\text{cm}^{-1}$ , which may be caused by the coating's strong fluorescence background in the Raman spectra.

## CONCLUSION

Classic gemological methods are useful in identifying jadeite that has undergone a coating process. Samples treated in this fashion are likely to have a warm feel, a relatively low hardness, and a low RI. But the definitive tests are microscopy, DiamondView imaging, and infrared spectroscopy. Observed under magnification, coated jadeite often displays traces of scratching, and the attractive green color is concentrated only in the surface layer. When examined with the DiamondView, the coating fluoresces slightly blue with alternating brighter spots. The presence of a very intense group of peaks at 2856, 2873, 2928, and 2958  $\text{cm}^{-1}$  in the mid-infrared region may be characteristic of a coating that contains epoxy resin.

The coated and uncoated areas were clearly distinguished by laser scanning confocal microscopy, which can also measure the thickness of the coating. This technique has also been used to identify and measure the coating thickness of diamond, tanzanite, and cubic zirconia (Shen et al., 2007; McClure and Shen, 2008; Shigley et al., 2012). In addition, the visible-range and Raman spectra showed distinct bands for the coating and the material below.

### ABOUT THE AUTHORS

Mr. Jian Zhang (zj7975@sina.com) is an engineer, Dr. Taijin Lu is chief researcher, and Ms. Hua Chen is director of the research department at the National Gems & Jewellery Technology Administrative Center (NGTC) in Beijing.

### ACKNOWLEDGMENTS

The authors thank Ms. Meidong Shen (NGTC) for supplying the coated jadeite jade samples, and Ms. Manjun Wang (NGTC) for supplying the uncoated jadeite samples. We are also grateful to Ms. Manjun Wang for constructive discussions about this paper.

## REFERENCES

- Cui W.Y., Shi G.H., Lin Y. (1999) Study on kosmochlor-jade and related amphibole-jade. *Journal of Gem and Gemmology*, Vol. 1, No. 4, p. 16–22 (in Chinese).
- Fritsch E., Wu S.T., Moses T., McClure S.F., Moon M. (1992) Identification of bleached and polymer-impregnated jadeite. *G&G*, Vol. 28, No. 3, pp. 176–187, <http://dx.doi.org/10.5741/GEMS.28.3.176>.
- Hyatt A. (2011) Lab Notes: Coated bead-cultured freshwater pearls. *G&G*, Vol. 47, No. 4, pp. 313–314.
- Knebel W., Ulrich H. (2002) *Confocal laser scanning microscope*. U.S. patent 6388807, issued May 14.
- Koivula J.I., Kammerling R.C., Fritsch E., Eds. (1994) Gem News: Coated jadeite. *G&G*, Vol. 30, No. 3, p. 199.
- Li H.B., Lu T.J., Shen M.D., Zhou J. (2011) Identification and nomenclature of coated amber. In *Proceedings of 2011 China Gems & Jewelry Academic Conference*, November 22, 2011, Beijing. Geological Press, Beijing, 2011, pp. 134–137 (in Chinese).
- Liang H.L. (2012) Present situation and countermeasures of jadeite industry. In *GAC and NGTC, 2012 Chinese Jewellery Industry Yearbook*. Geological Press, Beijing, pp. 84–91 (in Chinese).
- McClure S.F., Shen A.H. (2008) Coated tanzanite. *G&G*, Vol. 44, No. 2, pp. 142–147, <http://dx.doi.org/10.5741/GEMS.44.2.142>.
- Ning Y.C. (2010) *Interpretation of Organic Spectra*. Science Press (in Chinese), Beijing.
- Ouyang Q.M. (2000) *Jadeite Jade*. Cosmos Books Ltd., Hong Kong.
- Ouyang Q.M., Qi L.J. (2001) Hte long sein—a new variety of chrome jadeite jade. *Journal of Gemmology*, Vol. 27, No. 6, p. 321–327.
- Prencipe M. (2012) Simulation of vibrational spectra of crystals by ab initio calculations: an invaluable aid in the assignment and interpretation of the Raman signals. The case of jadeite (NaAlSi<sub>3</sub>O<sub>6</sub>). *Journal of Raman Spectroscopy*, Vol. 43, No. 11, pp. 1567–1569, <http://dx.doi.org/10.1002/jrs.4040>.
- Qi L.J., Yuan X.Q., Peng G.Z., Yang G.H. (2005) Scale determination of wax and macromolecule polymer-filled jadeite jade. *Journal of Gems & Gemmology*, Vol. 7, No. 3, pp. 1–7 (in Chinese).
- Shen A.H., Wang W., Hall M.S., Novak S., McClure S.F., Shigley J.E., Moses T.M. (2007) Serenity coated colored diamonds: detection and durability. *G&G*, Vol. 43, No. 1, pp. 16–34, <http://dx.doi.org/10.5741/GEMS.43.1.16>.
- Shigley J.E., Gilbertson A., Eaton-Magaña S. (2012) Characterization of colorless coated cubic zirconia (Diamantine). *G&G*, Vol. 48, No. 1, pp. 18–30, <http://dx.doi.org/10.5741/GEMS.48.1.18>.
- Shurvell H.F., Rintoul L., Fredericks P.M. (2001) Infrared and Raman spectra of jade and jade minerals. *Internet Journal of Vibrational Spectroscopy*, [www.ijvs.com](http://www.ijvs.com), Vol. 5, Ed. 5, No. 4 [date accessed: Feb. 13, 2013].
- Yuan X.Q., Qi L.J., Du G.P., Chen X.Y. (2003) UV-Vis-NIR spectrum of jadeite jade from Burma. *Journal of Gems and Gemmology*, Vol. 5, No. 4, p. 11–16 (in Chinese).
- Zhang J., Chen H., Lu T.J., Qiu Z.L., Wei R., Ke J. (2012) Microanalysis of the carbon isotopic composition in diamonds from Shandong of China by secondary ion mass spectrometry. *Rock and Mineral Analysis*, Vol. 31, No. 4, pp. 591–596 (in Chinese).
- Zhang P.L. (2006) *Systematic Gemmology*. 2nd ed. Geological Press, Beijing (in Chinese).

## Editors

Thomas M. Moses | Shane F. McClure



## DIAMOND

**Black, with Unusual Color Origin**

A 1.75 ct Fancy black round brilliant diamond (figure 1) was submitted to the Carlsbad laboratory for color origin determination. Natural black diamonds are usually colored by inclusions of sulfides, graphite or other mineral inclusions or, in rare cases, hydrogen-related clouds that extend throughout the stone. Treated black diamonds are generally heavily fractured stones that are subjected to high-temperature, low-pressure treatment, which graphitizes the fractures, turning them black. Artificial irradiation can also produce a dark enough color so as to appear black, but this is less common (H. Kitawaki, "Gem diamonds: Causes and colors," *New Diamond and Frontier Carbon Technology*, Vol. 17, No. 3, 2007, pp. 119–126).

Upon initial examination, the stone was noted to be covered in large, deeply penetrating fractures; therefore, high-pressure, low-temperature treatment was suspected. Yet closer examination revealed that the fractures were surrounded by dark brown radiation stains. Patches of non-fractured surface on the pavilion showed the normal transparency of diamond, causing the radiation staining to stand out in relief. Because radiation stains in diamond are

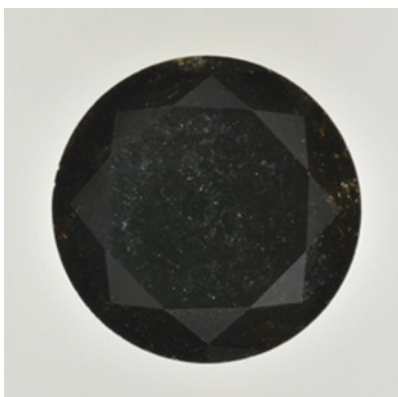
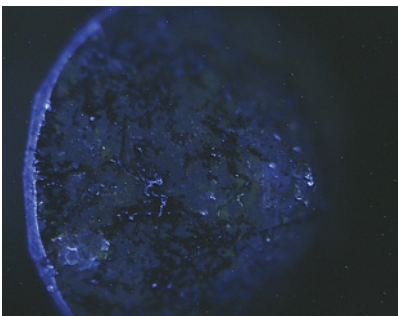


Figure 1. A face-up view of the 1.75 ct black diamond.

inert to short-wave ultraviolet light, we placed the stone in a DTC DiamondView to confirm their identity. Figure 2 shows numerous fractures surrounded by dark bands, which are the radiation stains.

Natural radiation stains provide an important clue to the color origin of a

Figure 2. A DiamondView image showing the pattern of inert radiation stains following the fractures in the stone.



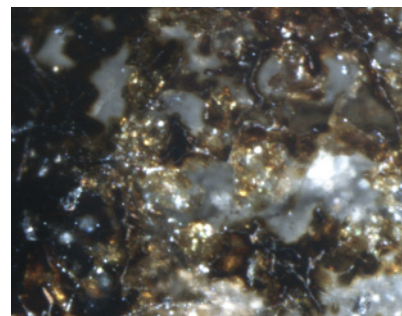
diamond. Diamonds that have been naturally colored by radiation can have stains associated with that color, though this is not a definitive criterion. In this case, the stains are so numerous and thick that they cause the diamond color. A close-up view of the pavilion (figure 3) shows the relative transparency of the diamond contrasted with the highly saturated color of the radiation staining of the fractures. The coverage of the stains is so complete that only a few transparent areas can be seen in the face-up view. Some of the color was due to the presence of small black inclusions, but most was due solely to the natural radiation stains, an unusual cause of color.

Troy Ardon

**Silicon in Natural Type IIa and Type IaB**

The presence of Si in diamond is typically revealed by detection of the

Figure 3. This image of the pavilion shows the patchwork nature of the radiation staining. Magnified 55x.



Editors' note: All items were written by staff members of GIA laboratories.

GEMS & GEMOLOGY, Vol. 49, No. 4, pp. 252–256, <http://dx.doi.org/10.5741/GEMS.49.4.252>.

© 2013 Gemological Institute of America

736.6/736.9 nm ("737 nm") doublet zero-phonon line (ZPL), observed by either absorption or photoluminescence (PL) spectroscopy. This feature has been assigned to the negatively charged state of the silicon split-vacancy defect,  $\text{SiV}^-$ , which is frequently incorporated into CVD synthetic diamonds due to the etching of silicon-containing growth chamber components. Conversely, reports of the 737 nm peak in natural or HPHT synthetic diamonds are notably rare (see C.M. Breeding and W. Wang, "Occurrence of the Si-V defect center in natural colorless gem diamonds," *Diamond and Related Materials*, Vol. 17, 2008, pp. 1335–1344; Winter 2010 Lab Notes, p. 302; Winter 2012 Lab Notes, pp. 304–305). Consequently, this feature is considered an important tool for identifying CVD synthetic diamonds.

Recently,  $\text{SiV}^-$  was detected in the PL spectra (liquid-nitrogen temperature with 633 nm laser excitation) of five diamonds submitted to GIA's Mumbai laboratory. These 0.31–0.90 ct round brilliants were issued colorless grades of either D or E. Their clarity grades ranged from  $\text{VVS}_1$  to  $\text{SI}_2$ , where the lower grades arose from the presence of trapped crystalline inclusions.

FTIR spectroscopy revealed that four of the samples were type Ia, with hydrogen-related peaks at 3107 and 1405  $\text{cm}^{-1}$ . The remaining sample was type IIa, with no discernible impurity-related IR features. Multi-laser, liquid-nitrogen-cooled PL spectra acquired for the fifth sample were similar to those reported in Breeding and Wang's 2008 investigation of  $\text{SiV}^-$  in natural diamonds. The latter also showed luminescence at 737, 714.6, 589.8, 557.8/558.2, 554.2, and 550.3 nm, in addition to  $\text{NV}^{0-}$  (575 and 637 nm, respectively) and 3H (503.4 nm). This  $\text{SI}_2$  sample contained several inclusions with intact crystalline faces, identified by Raman spectroscopy as olivine, consistent with the former investigation (figure 4, top). Through gemological and spectroscopic observations, it was possible to distinguish this natural type IIa diamond from Si-containing type IIa CVD synthetics.

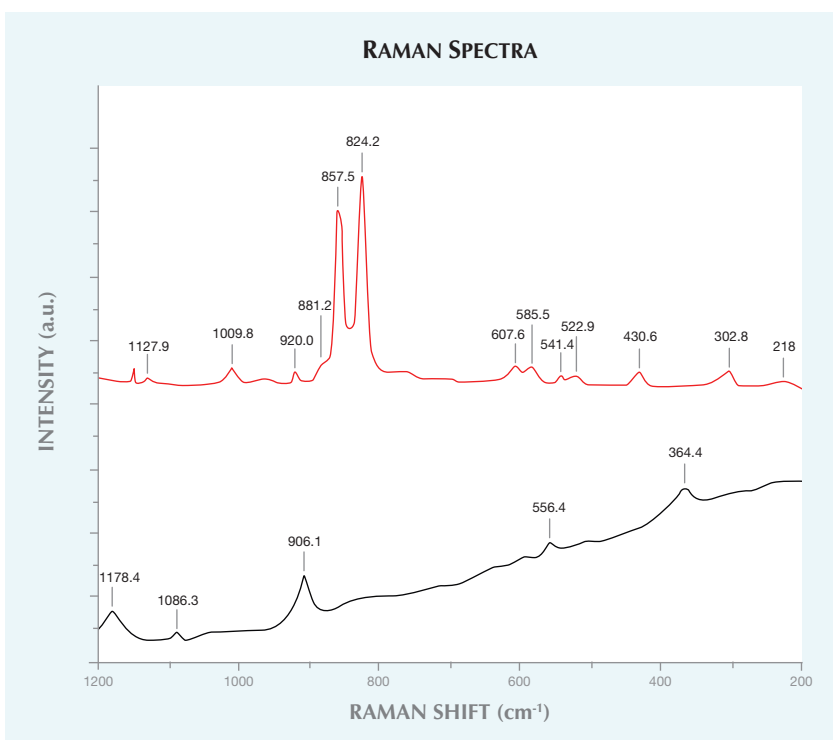


Figure 4. Room-temperature Raman spectroscopy (830 nm laser excitation) identified the different inclusions in the type IIa,  $\text{SI}_2$  (top) and type IaB,  $\text{SI}_1$  (bottom) natural diamonds containing silicon. The former spectrum is consistent with olivine, while the latter is attributed to spessartine garnet.

The type Ia diamonds studied by Breeding and Wang all contained A-aggregates and varying concentrations of B-aggregates (type IaA+B). In the present group of type Ia diamonds, only B-aggregates were detected (pure type IaB). With the exception of the 737 nm feature, the type IaB diamonds' PL spectra did not include any of the spectroscopic features characteristic of Si-containing type IaA+B diamonds. An emission line at 664.3 nm was detected in all the type IaB specimens, however. These samples also showed emissions from  $\text{NV}^{0-}$  (575 and 637 nm, respectively), H3 (503.2 nm), and H4 (495.9 nm), where H4 was remarkably strong for three of the diamonds. Interestingly, the diamond with the lowest H4 concentration was also distinctly included ( $\text{SI}_1$  clarity). Raman spectroscopy identified the inclusions as spessartine garnet (figure 4, bottom). Breeding and Wang also reported the presence of garnet in Si-containing diamonds. The presence of olivine and garnet inclusions in natural diamonds

containing  $\text{SiV}^-$  has been suggested to indicate that they crystallized in an area of mixed-composition peridotite in the upper mantle.

These results emphasize that the detection of  $\text{SiV}^-$  in diamonds does not unequivocally signify CVD synthetic origin. Nevertheless, careful analysis of spectroscopic features and crystalline inclusions can be used to separate these natural diamonds and their synthetic counterparts.

Ulrika F. S. D'Haenens-Johansson,  
Manisha Bhoir, and Kyaw Soe Moe

### Stellate Zircon Inclusions in Vivid Purple-Pink MORGANITE

The Carlsbad laboratory recently examined a 4.95 ct vivid purple-pink morganite. In addition to its saturated color, the stone was particularly noteworthy because of the inclusions it contained. Microscopic examination revealed numerous stellate inclusions, each with many delicate tapered legs (figure 5).

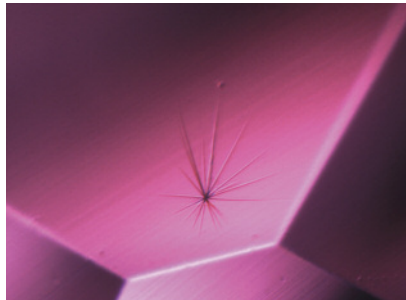


Figure 5. Stellate clusters of zircon needles were observed in this purple-pink morganite. Vertical field of view 0.58 mm.

Gemological properties revealed an RI of 1.577–1.583 and a hydrostatic SG of 2.73. It did not show fluorescence under either long- or short-wave UV. All of these properties were consistent with beryl, which was further confirmed by FTIR and Raman spectroscopy.

Figure 6. The needle-like zircons showed a sub-adamantine luster when examined using reflected light. The largest surface-breaking needle measures approximately 10 microns in the longest cross-sectional direction.



Inclusions in the stone showed an interesting starburst pattern, with thin needles radiating from a central point of nucleation. Viewed with polarized light, the needles exhibited birefringence. A sub-adamantine luster was observed where some of the needles broke the surface (figure 6). Raman spectroscopy identified the inclusions as zircon, consistent with our initial observations. Zircon inclusions are occasionally found in pegmatitic beryl, but they usually occur as prismatic or rounded crystals that cause damage to their host due to zircon's relative instability (E.J. Gübelin and J.I. Koivula, *Photoatlas of Inclusions in Gemstones*, ABC Edition, Zurich, 1986, p. 197).

In addition to the zircon clusters, the stone also contained fluid inclusions, transparent crystals, particulate clouds, and singular needles. The distinctive morphology of the zircon inclusions, coupled with the vivid purple-pink color, create a rather unique gemstone.

Tara Allen and Nathan Renfro

### SPINEL Submitted as Diamond

Diamond simulants remain in wide circulation and are a common sight in the GIA laboratory. Even so, it is rare that we encounter a natural gemstone masquerading as a colored diamond. The New York laboratory recently received a 0.50 ct rough sample with a remarkably saturated Fancy Intense

Figure 7. This rough spinel, submitted as a diamond, displayed trigons oriented in the direction opposite that of the crystal face.



Figure 8. In addition to trigons, the spinel displayed a conchoidal fracture (see arrow), a feature not found in diamond. Magnified 40x.

to Vivid pink color (figure 7) for a Colored Diamond Identification and Origin Report. The stone displayed octahedral crystal form with numerous trigons on its crystal faces. These triangular etch pits, caused by chemical dissolution, are common characteristics of both natural diamond and spinel but have also been observed in flux synthetic spinels (M.S. Krzemnicki, "Trade Alert: Flux grown synthetic red spinels again on the market," *SSEF Newsletter*, October 14, 2008, p. 3). When found on octahedrons, trigons point in the direction opposite that of the crystal face, as in figure 7. Figure 8 shows a distinctive conchoidal fracture amid the trigons, a feature alien to diamond. This feature, along with the sample's striking color, indicated something other than diamond.

The high-resolution UV-Vis spectrum displayed emission bands and absorption peaks not seen in natural diamond. Closer examination of the photoluminescence spectrum affirmed chromium peaks at 685, 687, 689, and 700 nm. Chromium causes the red/pink color in spinel but is not present in diamond. The narrow bandwidth of the 685 nm peak, along with the presence of the ~533 nm band in the UV-Vis spectrum, proved this was an untreated stone (S. Saeseaw et al., "Distinguishing heated spinels from unheated natural spinels and from synthetic spinels: A short review of ongoing research," [www.giathai.net/pdf/Heated\\_spinel\\_Identification\\_at\\_May\\_](http://www.giathai.net/pdf/Heated_spinel_Identification_at_May_)

25\_2009.pdf]. Other observations included a specific gravity of 3.45–3.48, consistent with spinel, as well as medium to strong red long-wave and short-wave UV. Though submitted for a diamond report, this stone was actually a natural pink spinel.

This finding serves as a reminder of the importance of both standard gemological techniques and advanced spectroscopy in identifying gem materials.

*Martha Altobelli, Paul Johnson, and Kyaw Soe Moe*

### Large SYNTHETIC MOISSANITE with Silicon Carbide Polytypes

Silicon carbide (SiC) is composed of a carbon atom surrounded by four silicon atoms in a tetrahedral form. Colorless synthetic moissanite is pure silicon carbide; the incorporation of impurities produces colors, including black. Its high hardness (second only to diamond) and thermal conductivity make it a convincing diamond simulant. Both transparent and opaque synthetic moissanites have been submitted to GIA's laboratory over the past two decades. In this report, we examine a 29.73 ct synthetic moissanite submitted as a black diamond (figure 9, left).

An uneven surface and surface-breaking black inclusions were visible with the unaided eye. Mosaic patterns of light and dark gray regions were observed under a microscope and became distinct in the Raman image (figure 9, right). Small cavities and polish lines in different directions

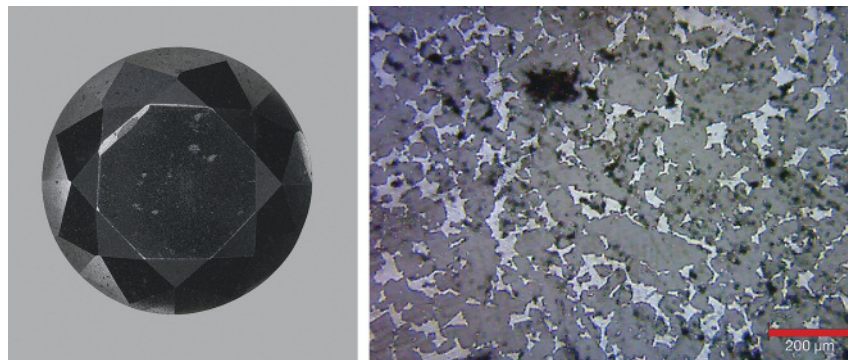


Figure 9. This 29.73 ct synthetic moissanite (left) was submitted as a black diamond. Surface-breaking graphite inclusions were easily observed, including the largest one at the upper left table edge. The mosaic patterns on the table surface became distinct when viewed under a Raman microscope (right).

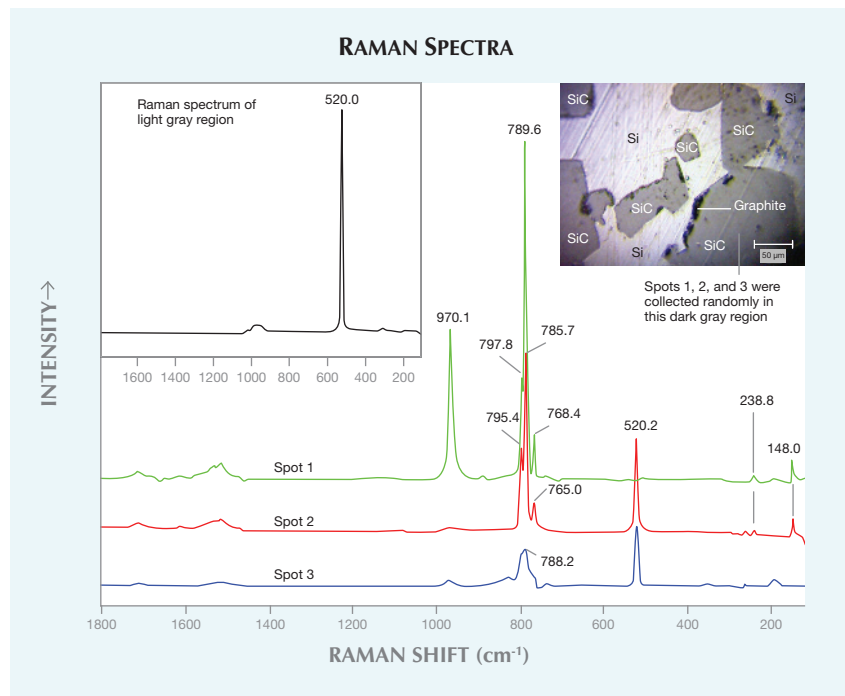


Figure 10. Each random spot showed mixed Raman bands of silicon carbide polytypes: 6H-SiC at 789.6, 765.0, and 148.0  $\text{cm}^{-1}$ ; 3C-SiC at 970.1, 968.4, 797.8, 795.4, and 788.2  $\text{cm}^{-1}$ ; 4H-SiC at 785.7  $\text{cm}^{-1}$ ; and 15R-SiC at 768.4  $\text{cm}^{-1}$ . Silicon was also found at 520.2  $\text{cm}^{-1}$  in spots 2 and 3. Bands at 238.8  $\text{cm}^{-1}$  (possibly related to 6H-SiC) and 148.0  $\text{cm}^{-1}$  (6H-SiC) were missing at spot 3. Light gray regions with a band at 520.0  $\text{cm}^{-1}$  (left inset) were identified as silicon; the black regions were identified as graphite. The spectra have been shifted vertically for clarity.

were present on the table surface, and a granular texture was observed in a large cavity on the girdle. Raman spectroscopy identified the dark gray regions as silicon carbide.

Interestingly, each random testing spot showed mixed bands of silicon carbide polytypes (i.e., identical chemical composition but a slightly different crystal structure). The polytype 6H-SiC (6 = the number of stacking se-

quences, H = hexagonal, and SiC = silicon carbide) was detected by Raman bands at 789.6, 765.0, and 148.0  $\text{cm}^{-1}$ . Other polytypes were also distinguished by Raman bands: 3C-SiC (C = cubic) at 970.1, 968.4, 797.8, 795.4, and 788.2,  $\text{cm}^{-1}$ ; 4H-SiC at 785.7  $\text{cm}^{-1}$ ; and 15R-SiC (R = rhombohedral) at 768.4  $\text{cm}^{-1}$  (figure 10; see also P. Colomban, "SiC, from amorphous to nanosized materials, the example of



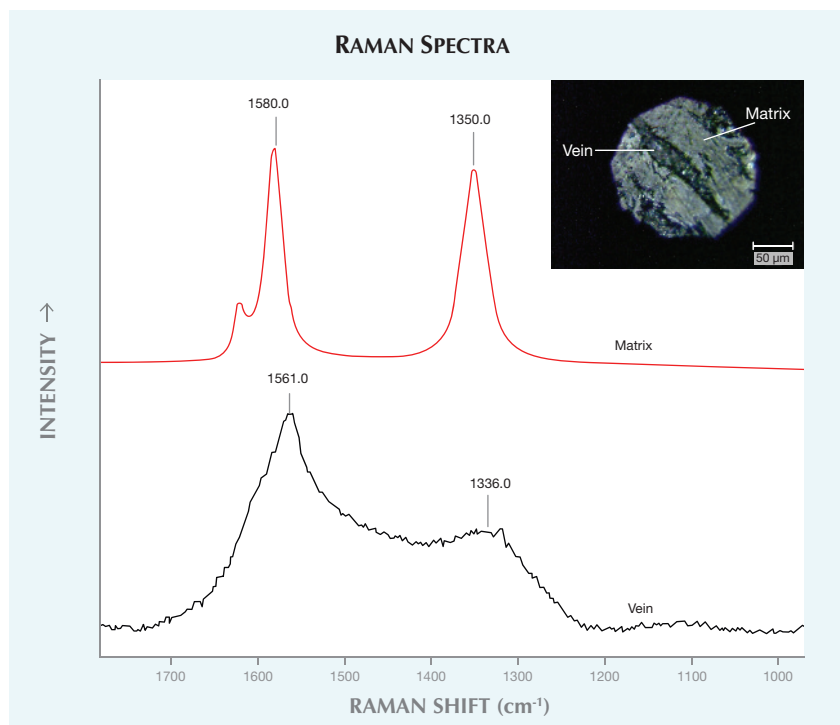


Figure 11. Micro-imaging of a graphite inclusion (inset) showed a vein in matrix. The matrix was composed of crystalline graphite, as suggested by sharp Raman bands at 1580.0 and 1350.0  $\text{cm}^{-1}$ . The vein was identified as amorphous graphite by broad bands at approximately 1561.0 and 1336.0  $\text{cm}^{-1}$ .

SiC fibers issued of polymer precursors," in M. Mukherjee, Ed., *Silicon Carbide—Materials, Processing and Applications in Electronic Devices*, InTech, 2011, pp. 161–186). In addition to these bands, a sharp Raman band assigned to silicon was detected at 520.2  $\text{cm}^{-1}$  at a few spots. Bands corresponding to 6H-SiC at 238.8 and 148.0  $\text{cm}^{-1}$  could not be detected at all measurement locations. Light gray regions were identified as silicon at 520.0  $\text{cm}^{-1}$  (figure 10, left inset). Black inclusions, both eye-visible and microscopic, were confirmed as graphite. As figure 11 illustrates, the micro-image of a graphite inclusion showed an amorphous graphite vein (broad Raman bands at approximately 1561.0 and 1339.0  $\text{cm}^{-1}$ ) inside a crystalline

graphite matrix (sharp bands at 1580.0 and 1350.0  $\text{cm}^{-1}$ ).

During SiC growth, rotation along the covalent bond generated alternate stacking layers of Si and C atoms along the c-axis with different structural sequence, which is noticeable in the (11 $\bar{2}$ 0) plane but not along the basal plane. This rotation can occur at very low energy. Since constant growth energy is difficult to control, two or more silicon carbide polytypes can form simultaneously during the growth process; this phenomenon is called *polytypism*. Raman spectroscopy has been used to detect these polytypes. Although there are more than 250 known polytypes, SiC can be classified as either beta ( $\beta$ ) or alpha ( $\alpha$ ) type. The beta type crystallizes in

cubic lattice symmetry (e.g., 3C-SiC), the alpha type in hexagonal symmetry (e.g., 6H-SiC).

Traditional growth methods for silicon carbide involve sintering and hot pressing, and there are also newer techniques. Reaction-bonded silicon carbide can form when liquid silicon reacts with porous graphite. This silicon carbide contains both pure silicon (as a bonding component), and graphite. Earlier studies have suggested that black synthetic moissanite containing silicon inclusions could be grown by the physical vapor transport (PVT) method (see Winter 2009 GNI, p. 308; Spring 2011 Lab Notes, pp. 54–55). Using PVT, researchers have grown large silicon carbide bulk crystals up to 50 × 25 mm at a rate of 1.2 mm per hour at 10 kPa pressure (Q.-S. Chen et al., "Growth of silicon carbide bulk crystals by physical vapor transport method and modeling efforts in the process optimization," *Journal of Crystal Growth*, Vol. 292, 2006, pp. 197–200). Nevertheless, Raman analysis at several testing points confirmed only the 6H-SiC polytype.

This sample was submitted for a Colored Diamond Identification and Origin Report, but one should always pay close attention to surface features, such as the mosaic pattern of light and dark gray regions in reflected light, together with surface-breaking black inclusions not observable in black diamond.

Kyaw Soe Moe, Paul Johnson,  
and Ren Lu

PHOTO CREDITS:

Robison McMurtry—1; Troy Ardon—2 and 3; Nathan Renfro—5 and 6; Joshua Balduf—7; Martha Altobelli—8; Sood Oil (Judy) Chia—9 (left); Kyaw Soe Moe—9 (right), 10 (right inset), and 11 (inset).

**Contributing Editors**

Emmanuel Fritsch, CNRS, Team 6502, Institut des Matériaux Jean Rouxel (IMN), University of Nantes, France (fritsch@cnsr-immn.fr)

Franck Notari, GCTL Laboratories, Geneva and Balzers, Liechtenstein (franck.notari@ggtl-lab.org)

Kenneth Scarratt, GIA, Bangkok (ken.scarratt@gia.edu)

**COLORED STONES AND ORGANIC MATERIALS**

**Demantoid garnet fossil pseudomorphs.** In 2010, two extremely rare fossil pseudomorphs in demantoid garnet were acquired from the classic demantoid deposit in Ambanja, Madagascar. One resembled a gastropod, the other a coral (figure 1). The brilliance, lozenge-shaped crystal faces, and green color of these samples were all consistent with the demantoid variety of andradite; this was confirmed by Raman spectroscopy. Both samples clearly showed typical andradite bands at 371 and 516  $\text{cm}^{-1}$ , with peaks at 817, 844, and 873  $\text{cm}^{-1}$  forming a triplet. Additionally, an intense quartz signal at 464  $\text{cm}^{-1}$  was observed. The general appearance was that of many small crystals (up to 1 mm in size) grown together, preserving the overall shape and some details of the fossils. Careful observation of neighboring microfacets in reflected light indicated that both pieces were actually single crystals of andradite (figure 2).

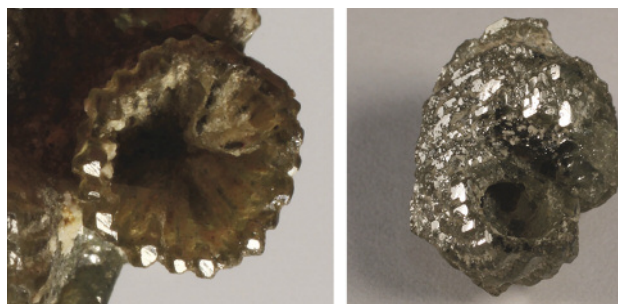
It is surprising to observe demantoid replacing a fossil, but some pseudomorphs in gem minerals have been documented, such as pseudomorphs of snail-like gastropods in emerald (P. Vuillet et al., "Les émeraudes de Gachalá, Colombie; historique, genèse et découvertes paléontologiques," *Le Règne Minéral*, Vol. 46, 2002, pp. 5–18). Most surprising is that these pseudomorphs were monocrystals. To investigate how the fossils were replaced by demantoid, we submitted the pieces for X-ray tomography analysis to the Laboratoire Français de Gemmologie (LFG) in Paris. They used an RX-Solutions DeskTom 130 system; results are given in figure 3. There are no remains of the original fossil. The objects were formed entirely out of andradite, which apparently grew from the solid parts of the animal towards the outside of the



Figure 1. These coral (left) and gastropod (right) fossils are pseudomorphs in demantoid garnet from Ambanja, Madagascar. The coral measures 1.5 × 1 cm. Photo by Pierre-Yves Chatagnier.

shell, and inward toward the hollow parts. Hence, some of the hollow parts were not yet completely filled. Lighter shades of gray were due to less-dense material.

Figure 2. Both the coral (left) and the gastropod (right) appear to be single crystals, as revealed by concomitant light reflection (in white) on multiple, parallel rhomboidal crystal faces. Photos by Benjamin Rondeau (left) and Pierre-Yves Chatagnier (right).



*Editors' note: Interested contributors should send information and illustrations to Justin Hunter at [justin.hunter@gia.edu](mailto:justin.hunter@gia.edu) or GIA, The Robert Mouawad Campus, 5345 Armada Drive, Carlsbad, CA 92008.*

GEMS & GEMOLOGY, VOL. 49, NO. 4, pp. 257–264,  
<http://dx.doi.org/10.5741/GEMS.49.4.257>.

© 2013 Gemological Institute of America

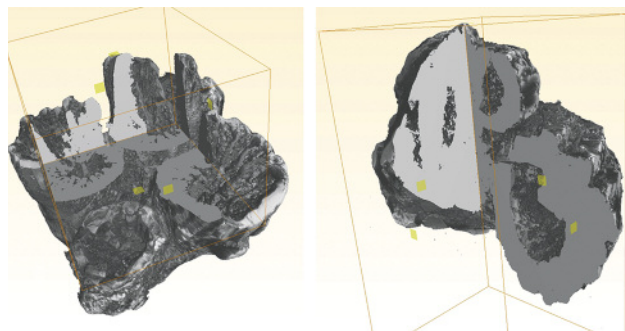


Figure 3. X-ray tomography revealed that both fossils are made entirely of demantoid, and that some internal cavities of the organism remained partially empty.

The fact that the present pieces appear polycrystalline but display evidence of being single crystals suggests that the original fossil was replaced by the growth of many small garnet crystals of random orientation. By that theory, they later coalesced and evolved into a single crystal through the process known as Ostwald ripening (I. Sunagawa, *Crystals*, Cambridge University Press, 2005, p. 258). These pieces are therefore not a pseudomorph *stricto sensu*, as details of the hard parts are lost, but more exactly, recrystallized pseudomorphs with relatively well-developed crystal faces.

Emmanuel Fritsch

Julien Raoul

Elancourt, France, and Antananarivo, Madagascar

Benjamin Rondeau

University of Nantes, France

Olivier Segura

LFG, Paris

**“Gran Dama” brooch featuring large Melo pearl.** After a surge in popularity during the 19th century, Melo pearls reemerged on the gem market in the 1990s. These exceedingly rare pearls are produced by the Indian volute, a sea snail indigenous to Southeast Asia. The pearls themselves are non-nacreous and found in shades of orange, yellow, gray, and brown. Upon acquiring a 98.67 ct Melo pearl, thought to be one of the largest in the world, acclaimed jewelry designer Gianmaria Buccellati created the “Gran Dama” brooch to showcase this exceptional gem (figure 4).

Created to honor the power of pregnancy, the brooch epitomizes, in Buccellati’s own words, “the highest and purest, I dare say divine, human state.” While many years were invested in the concept design and inspiration, the brooch itself required three years to complete, from original design to finished piece. The Melo pearl, representing the womb of the expectant mother, is accentuated by its setting in yellow, pink, and white gold, surrounded by 410 round brilliant diamonds and 139 fancy-color diamonds.

The pear-shaped, 18.21 ct South Sea cultured pearl used for the brooch’s head provides a striking visual contrast with the orange, spherical pearl at the centerpiece of this work of art.

Jennifer-Lynn Archuleta  
GIA, Carlsbad

**Greenish blue spodumene.** Green and yellow colors of spodumene, in addition to the widely known violet-pink variety kunzite, are now familiar to the trade and often submitted to gem labs. Recently, this contributor examined a greenish blue stone (figure 5) that unexpectedly turned out to be spodumene.

The 40.50 ct oval mixed-cut specimen measured 24.50 × 10.60 × 10.42 mm. It appeared quite dull, with areas of extinction caused by gray overtones and improper fashioning. The face-up color was heavily influenced by the two pleochroic colors, green and blue. The specimen’s overall appearance was similar to tourmaline, though gemological examination ruled out that possibility. The following gemological properties were recorded: optic figure—biaxial; RI—1.660–1.675; birefringence—0.015; hydrostatic SG—3.19; fluorescence—inert; and weak absorption bands in

Figure 4. Designed by Gianmaria Buccellati, the “Gran Dama” brooch celebrates pregnancy through its centerpiece 98.67 ct Melo pearl. Photo by Orasa Weldon.





Figure 5. This 40.50 ct greenish blue specimen was identified as irradiated spodumene. Photo by Gagan Choudhary.

the blue, green, and yellow-orange regions at around 440, 545, and 600–650 nm in the desk-model spectroscope. The RI and SG values are consistent with those reported for spodumene in the gemological literature. Magnification revealed a few long, conical growth tubes below the table facet and cleavage planes along the girdle edge—inclusions typical for spodumene. The most striking feature of the specimen was its strong pleochroism (figure 6), which displayed three colors: green, blue, and violet. Infrared and Raman spectroscopy further confirmed the sample as spodumene. EDXRF analysis revealed the presence of Al, Si, Fe, and Mn, with a higher amount of Fe than Mn. Polarized UV-visible-NIR spectroscopy in the 200–800 nm region (figure 7) revealed a difference in absorption patterns. The violet and green directions displayed small peaks at ~430 and 437 nm, and absorption bands in the region 500–700 nm. The violet direction showed broad features at ~545 and 630 nm, the green direction at ~545, 605, and 655 nm. The feature at ~437 nm has been assigned to  $\text{Fe}^{3+}$  (R. Lu, “Color origin of lavender jadeite: An alternative approach,” Winter 2012 *G&G*, pp. 273–278). The feature at ~430 nm has been assigned to  $\text{Mn}^{2+}$  and those in the 500–700 nm region to various states of Mn ( $\text{Mn}^{3+}/\text{Mn}^{4+}$ ) and its sites in the structure

Figure 6. The artificially irradiated greenish blue spodumene displayed strong pleochroism, exhibiting three colors: blue (left), violet (center), and green (right). Photos by Gagan Choudhary.

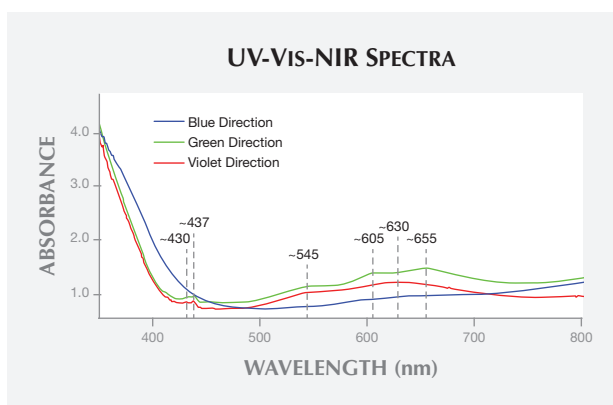


Figure 7. Polarized UV-Vis-NIR spectra of the greenish blue spodumene display bands related to  $\text{Fe}^{3+}$ ,  $\text{Mn}^{2+}$ ,  $\text{Mn}^{3+}$ , and  $\text{Mn}^{4+}$ . The band at ~630 nm is related to an irradiation-produced defect.

(see I. Petrov, “Role of natural radiation in tourmaline coloration: Discussion,” *American Mineralogist*, Vol. 75, 1990, pp. 237–239). The peak at ~630 nm indicates a defect usually produced by irradiation (E.W. Claffy, “Composition, tenebrescence and luminescence of spodumene minerals,” [www.minsocam.org/ammin/AM38/AM38\\_919.pdf](http://www.minsocam.org/ammin/AM38/AM38_919.pdf)). These samples were irradiated via X-ray.

It is widely known that green spodumene without chromium as the chromophore often results from irradiation, but this contributor had never observed a greenish blue color in spodumene. Irradiated green spodumene typically displays a strong blue pleochroic color along the c-axis. In this case, the c-axis was not determined, but one direction displayed a strong blue color, which was further supported by the peak at ~630 nm.

Gagan Choudhary ([gagan@gjepcindia.com](mailto:gagan@gjepcindia.com))  
Gem Testing Laboratory, Jaipur, India

## DIAMOND

**Bright yellow diamonds from Sierra Leone.** Diamonds referred to in the trade as “Canary yellow” are highly valued for their saturated yellow color, caused by isolated nitrogen



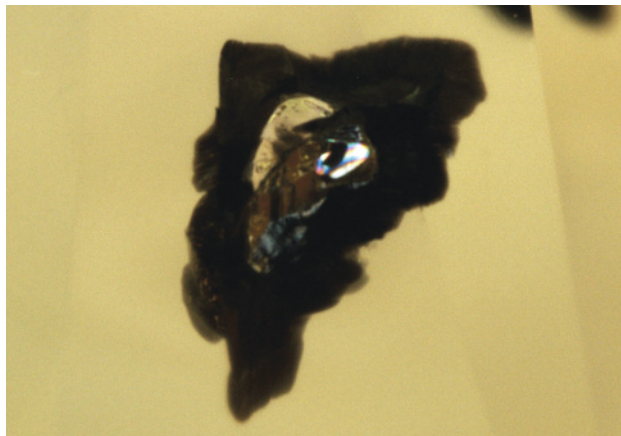
Figure 8. These two bright yellow diamonds (1.03 and 1.02 ct) are from alluvial deposits in the Zimmi mining area in southern Sierra Leone. In the rectangular stone, several black graphitized feather inclusions are visible. Photo by Robert Weldon.

impurities. When faceted, they can exhibit colors ranging from Fancy Intense to Fancy Vivid yellow in GIA's colored diamond grading system. It is unusual to see a group of these rare colored diamonds from a known mining locality (figure 8).

Recently, GIA's Carlsbad laboratory had the opportunity to examine eight faceted and five rough diamonds reportedly found in alluvial deposits in the Zimmi mining area in the Pujehun district of southern Sierra Leone. They were loaned to us for study by Israel Eliezri (Coldiam Ltd., Ramat Gan, Israel). According to Mr. Eliezri, bright yellow rough diamonds are recovered on a recurring basis from the Zimmi region.

The diamonds we examined showed highly saturated yellow colors and weighed between ~0.10 ct and just over 1.00 ct. Rough diamonds recovered from this locality are reported to occur in sizes up to about 4 ct. Under magnification, they often contain what appear to be crystalline sulfide mineral inclusions, with graphitized feathers extending outward (figure 9). Infrared spectroscopy analysis indicated

Figure 9. This diamond contains what is believed to be a metallic sulfide mineral inclusion, surrounded by a black, graphitized feather. Photomicrograph by Nathan Renfro; horizontal field of view is 1.08 mm.



that the samples ranged from pure type Ib to variable proportions of type Ib and IaA. Total nitrogen impurity concentrations varied from 8 ppm (all as type Ib) to ~340 ppm (~35 ppm type Ib, ~305 ppm type IaA). Hydrogen impurities were also detected in the samples with high total nitrogen content. Visible spectroscopy showed only gradually increasing absorption toward the violet end of the spectrum due to the isolated nitrogen.

Many yellow natural diamonds with isolated nitrogen occur as irregularly shaped rough crystals, often with inward faces in the form of re-entrant cubes. The rough diamonds from the Zimmi mine, however, showed smooth and rounded dodecahedral shapes. This rounded shape makes them much more suitable for cutting with minimal weight loss.

Type Ib diamonds are uncommon because with time and heat, isolated nitrogen impurities in the lattice tend to aggregate, forming more-complex defects that are characteristic of type IaA and IaB diamonds. The youngest dated diamonds are about a billion years old, and the youngest emplacement ages of diamondiferous kimberlites are less than 80 million years old. This suggests that nearly all diamonds spend most of their existence at great depths in the lower crust and upper mantle. It is unclear exactly how the isolated nitrogen impurities in type Ib diamonds avoided the aggregation process. This mystery makes the discovery of many "Canary yellow" diamonds from a single mine in Sierra Leone even more interesting, offering a potential tool for research into the formation and survival of type Ib diamonds in nature.

James Shigley and Christopher M. Breeding  
GIA, Carlsbad

## INCLUSIONS IN GEMS

### Scheelite and hübnerite inclusions in quartz from China.

Scheelite, a very popular mineral among collectors, is very rarely found as an inclusion in quartz (J. Hyršl and G. Niedermaier, *Magic World: Inclusions in Quartz*, Bode Verlag, Haltern, Germany, 2003, p. 147). One such quartz specimen, measuring 4.5 cm high and with very high luster (figure 10,

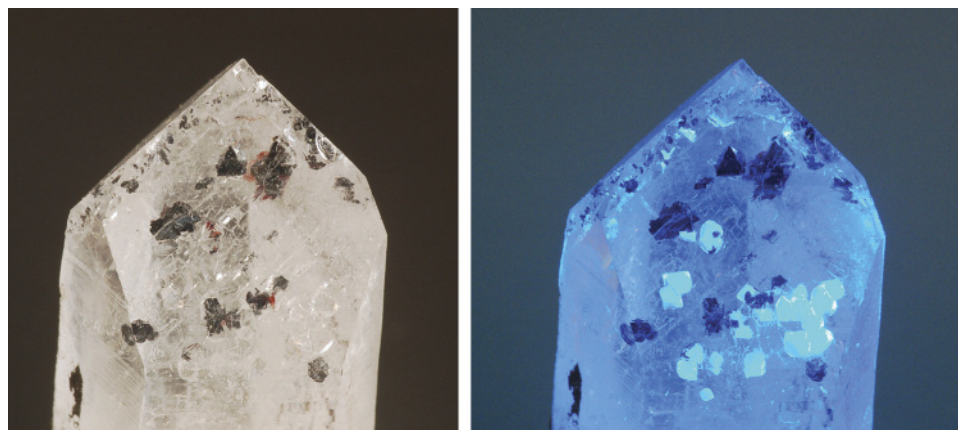


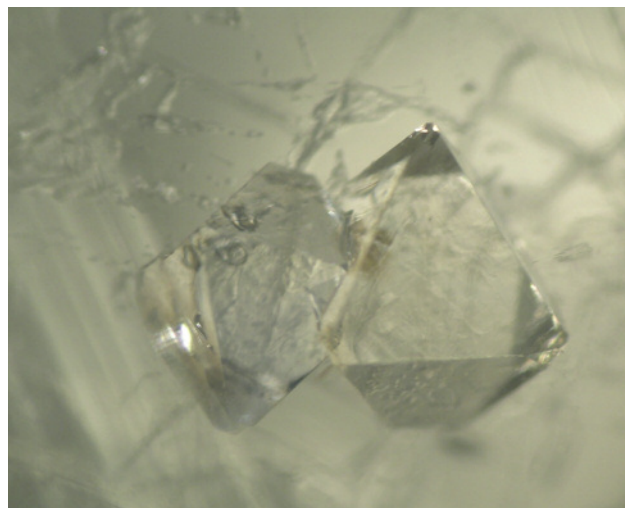
Figure 10. Quartz with scheelite and hübnerite inclusions from China, 2.3 cm wide, in daylight (left) and under short-wave UV light (right). Photos by Jaroslav Hyršl.

left), was collected in 2010 from the famous tungsten deposit at Yaogangxian in Hunan Province, China.

The specimen contained about 25 small pseudo-octahedral crystals up to 2 mm with an adamantine luster. Most of the crystals were black, but some were colorless. Under long-wave UV light, both crystal types are inert; under short-wave UV light, the colorless crystals showed a strong bluish fluorescence, indicating scheelite (figure 10, right). Nevertheless, the black crystals were not fluorescent and their edges were red-brown, a typical color for Mn-rich members of the wolframite group,  $(\text{Fe}, \text{Mn})\text{WO}_4$ . Raman testing (by Prof. Albert Gilg, Technical University of Munich) identified colorless crystals as scheelite (figure 11) and black crystals as the mineral hübnerite (figure 12), with the strongest peak at  $877 \text{ cm}^{-1}$ . Their pseudo-octahedral form confirmed their origin as a pseudomorph after scheelite.

Jaroslav Hyršl (hyrsj@hotmail.com)  
Prague, Czech Republic

Figure 11. Two scheelite crystals in quartz, image width 2 mm. Photomicrograph by Jaroslav Hyršl.



## LOCALITIES

**Faceted wurtzite from Tanzania.** Wurtzite is the hexagonal polymorph of  $\text{ZnS}$ . It is far less common than sphalerite, the cubic polymorph of  $\text{ZnS}$ . All previously identified wurtzite has been opaque to translucent, and therefore not facetable. Layers of wurtzite and sphalerite can alternate in so-called Schalenblende, a colloidal sphalerite variety used only rarely for cabochons. The first transparent wurtzite crystals were found in 2012, at the tanzanite deposit at Merelani Hills, south of Arusha, Tanzania (for identification, see [www.ruff.info](http://www.ruff.info)). The crystals, which measure up to 2 cm in diameter, are very rare. They have a tabular shape, with pyramidal faces. Some crystals from Merelani have clean parts, and several gemstones were faceted from them (figure 13).

Eight cut stones weighing 0.30–1.74 ct were studied. They were orange-brown, with a submetallic luster and very weak, almost invisible, pleochroism. Refractive indices of these stones were well over the refractometer limit, listed as 2.36 and 2.38 in the literature (J. Bernard and J. Hyršl, *Minerals and their Localities*, Granit, Czech Republic, 2004, p. 666). They had very low birefringence, confirmed by a lack of doubling of facet edges. The determined specific gravity values of two of the crystals were 3.78 and 3.85; their measured hardness was 3.5. The stones were uniaxial positive and inert under both long- and short-wave UV. Their UV-Vis-NIR (figure 14) exhibited a high cut-off at 545 nm. The stones showed anisotropic crystals and hexagonal growth structures when viewed under a microscope. Because of the rarity and high value of the Tanzanian crystals, the faceted wurtzites are sure to catch the attention of gemstone collectors.

Jaroslav Hyršl

## SYNTHETICS AND SIMULANTS

**Composite amber with an unusual structure.** With amber emerging as one of the most popular gems in the Chinese jewelry market, the quality of imitations also appears to be on the rise. Many of these simulants are composites

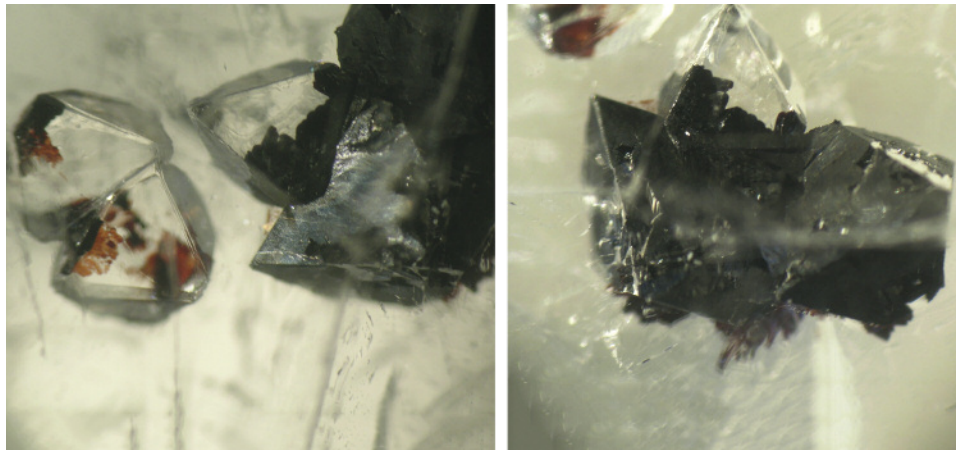


Figure 12. This group of scheelite crystals in quartz was partially replaced by hübnerite. Photomicrographs by Jaroslav Hyršl; image width 3 mm.

consisting of two or more substances, such as amber, copal, artificial resin, and plastic, joined together as a finished piece. Some composites incorporate small amber fragments. Manufacturers may also embed insect or lizard inclusions (Winter 2005 GNI, pp. 361–362). One notable composite amber specimen, a polished pebble-shaped pendant (figure 15), was recently identified at the National Gemstone Training Center (NGTC) lab in Beijing.

This specimen displayed no clear plane separating the two materials; instead there appeared to be an intersecting mixture of amber and polymer resin. The natural amber core had been covered by an outer shell of polymer resin, and about one-third of the natural amber was still exposed. Some of the small exposed portions were large enough for examination and identification. The most interesting aspect of the specimen was its pair of insect inclusions, one occurring naturally and the other artificially (figure 16).

The specimen had a waxy luster. Reflected light displayed scratches on the surface, suggesting a low hardness.

Figure 13. These wurtzites are from Merelani, Tanzania. The crystal measures 17 mm across, and the cut stones weigh 1.74 and 1.59 ct. Photo by Jaroslav Hyršl.



It was relatively easy to observe the boundary between the natural and artificial resin sections using reflected light. Unlike most intersections found in such pieces, there were no air bubbles or other features, only clear lines. We also saw some small circular areas using transmitted and reflected light. These proved to be natural amber sections, both on the surface and within the sample, that had been polished and exposed during fashioning. The entire structure of this specimen was an intersection of two substances, identified as natural amber and polymer resin.

Observed under the microscope with transmitted light, part of the sample showed reddish brown curved lines; these were flow lines from natural amber. The two parts of the composite were clearly visible. The top part consisted of natural amber with a naturally deposited insect inclusion. The insect was translucent and partially broken. The larger insect inclusion in the bottom part was in much better condition, with an opaque transparency and clearer outline. The air bubbles around the larger insect were more spherical and

Figure 14. UV-Vis-NIR spectrum of a 1.74 ct cut wurtzite from Tanzania.

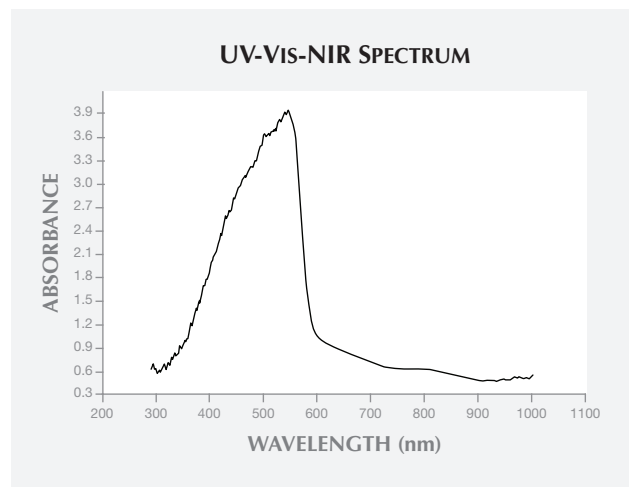




Figure 15. This pebble-shaped amber composite had a total weight of 9.12 g. Photo by Haibo Li.

concentrated, which is not typically seen in natural amber.

Under UV light, the composite gave an uneven fluorescence to long- and short-wave UV. The amber part showed a blue-white fluorescence, while the artificial resin fluoresced yellowish green.

To confirm the identity of the two different materials, we analyzed their infrared spectra (figure 17). Spectrum A displays main peaks at 1734.90 and 1160.99  $\text{cm}^{-1}$ , typical of Baltic region amber. Spectrum B shows a series of peaks; after comparison with spectra of amber, copal and some other synthetic materials, we used spectrum B to identify this sample as polymer resin. With its combination of natural and imitation amber, accompanied by natural and artificial insect inclusions, the piece presented an interesting identification study.

Jie Liang, Haibo Li, Taijin Lu,  
Meidong Shen, and Jun Zhang  
NGTC, Beijing



Figure 16. The smaller insect, circled in green, appeared in the natural amber part of the composite, while the larger one was artificially embedded in the surrounding resin. Photo by Haibo Li.

## CONFERENCE REPORTS

**2013 Gem-A Conference.** The Gemmological Association of Great Britain Conference took place November 1–5, 2013, in London. Seminars and workshops were held November 1 at Gem-A headquarters, and presentations were delivered November 2–3 at the historic Goldsmiths' Hall. Field trips to the Victoria and Albert and Natural History Museums, as well as the Museum of London, were held on November 4–5. The conference also celebrated the cente-

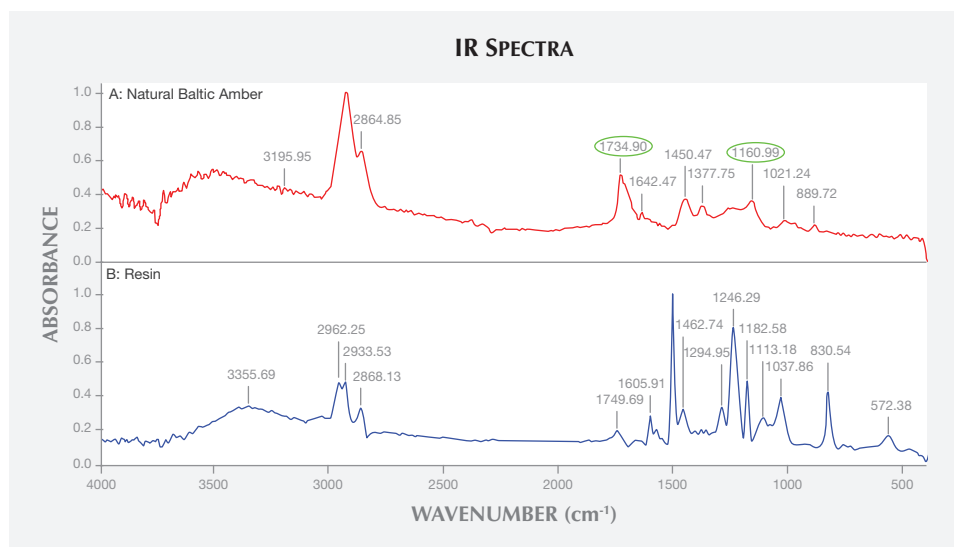


Figure 17. Reflected infrared spectra of the two parts of the specimen, with Kramers-Kronig (K-K) transformation method applied. Spectrum A represents natural amber, with typical peaks circled in green; spectrum B reveals many peaks, indicating the presence of polymer resin.



nary of the first Gemmology Diploma, as well as the 50th anniversary of the first Diamond Diploma.

**Chris Sellors** from C.W. Sellors Fine Jewellery (Derby, United Kingdom) reviewed the history of Blue John fluorite, noting that British Blue John got its name from *bleu-jaune* (French for “blue-yellow”), during its reported exportation to France in the late 18th century. Sellors was joined by **Rebecca Tucker** of W. Hamond (York, United Kingdom), who recounted the history of Whitby jet.

**Sonny Rope** of Suncrest Diamonds (Orem, Utah) discussed the effect of HPHT and irradiation treatments on colored diamonds, and explained how Suncrest uses these processes to treat different diamond types. **Gary Roskin** of the Roskin Gem News Report outlined the factors and challenges affecting diamond clarity grading.

**Dr. Jack Ogden**, a London-based jewelry historian, explained the history, origins, and cuts of the Cheapside Hoard gems. **David Callaghan** of the Institute of Registered Valuers described how renowned gemologist Basil Anderson founded London’s Gem Testing Laboratory during the 1920s, in response to the highly profitable natural pearl trade. Washington State-based consultant **Dr. John Emmett** presented an in-depth study of the issues of testing gemstones to understand their color by the way they absorb light. Through the use of advanced equipment such as spectrometers and spectrophotometers, Emmett showed that absorption, combined with the relative concentrations of coloring elements, could be used to predict the shade and saturation of corundum.

**Brian Jackson**, chairman of the Scottish Gemmological Association, reviewed Scottish gemstones, including arti-

facts set with gems. CairnGorm Mountain has long been a source of beryl and topaz. He noted that while it is illegal to fish for them, Scotland’s rivers do contain pearls. **Dr. Emmanuel Fritsch** (University of Nantes, France) discussed the use and effects of luminescence in gemology, and how it can be used to detect treatments in emeralds and glass-filled rubies.

**Dr. James Shigley** (GIA, Carlsbad) discussed gem identification challenges of the past 30 years. While fewer synthetic materials are on the market as compared to the 1960s and 1970s, an increase in the treatment of diamonds and colored stones makes it important to use scientific instruments in gem laboratories. **Martin Rapaport**, chairman of the Rapaport Group (Las Vegas, Nevada), compared prices of rough and polished diamonds, reviewed the causes of market fluctuations, and explored the current issues of the industry with regard to synthetic diamonds and retailer responsibility. **Shelly Sergent** of Somewhere In The Rainbow (Phoenix, Arizona) described the purpose and educational mission of the collection, pieces of which were showcased and available to the attendees.

**Arthur Groom** of Arthur Groom & Co. (Ridgewood, New Jersey) detailed major issues of emerald clarity enhancement, including materials historically used and the challenges of using different media. **John J. Bradshaw** of Coast-to-Coast Rarestones Intl. (Nashua, New Hampshire) explained the collector’s market for non-traditional gemstones, and provided in-depth information on localities and cutting consideration of six different rare gem species.

*Mehdi Saadian (msaadian@gia.edu)*  
GIA, London

## THANK YOU, REVIEWERS



GEMS & GEMOLOGY requires each manuscript submitted for publication to undergo a rigorous peer review process, in which each paper is evaluated by at least three experts in the field prior to acceptance. This is an essential process that contributes to the accuracy, integrity and readability of *G&G* content. In addition to our dedicated Editorial Review Board, we extend many thanks to the following individuals, who devoted their valuable time to reviewing manuscripts in 2013.

K.C. Bell • Roger Dery • Al Gilbertson • Bruce Harding • George Harlow • Jeff Harris • Stefanos Karampelas • Stephen Kotlowski • Michael Krzemnicki • Bill Larson • Ren Lu • Zhili Qiu • Ilene Reinitz • Nicholas Sturman • Fanus Viljoen • J.C. “Hanco” Zwaan